United Arab Emirates University
Scholarworks@UAEU

Theses | Electronic Theses and Dissertations

4-2021

DEVELOPMENT OF HEAT INSULATION COMPOSITE MATERIALS BASED ON BIO-POLYESTERS AND NATURAL FILLER

Hyder Ali Reyah Al Abdallah

Follow this and additional works at: https://scholarworks.uaeu.ac.ae/all_theses

 Part of the Engineering Commons

Recommended Citation

Al Abdallah, Hyder Ali Reyah, "DEVELOPMENT OF HEAT INSULATION COMPOSITE MATERIALS BASED ON BIO-POLYESTERS AND NATURAL FILLER" (2021). *Theses*. 818.
https://scholarworks.uaeu.ac.ae/all_theses/818

This Thesis is brought to you for free and open access by the Electronic Theses and Dissertations at Scholarworks@UAEU. It has been accepted for inclusion in Theses by an authorized administrator of Scholarworks@UAEU. For more information, please contact mariam_aljaberi@uaeu.ac.ae.

United Arab Emirates University

College of Engineering

Department of Chemical and Petroleum Engineering

DEVELOPMENT OF HEAT INSULATION COMPOSITE MATERIALS BASED ON BIO-POLYESTERS AND NATURAL FILLER

Hyder Ali Reyah Al Abdallah

This thesis is submitted in partial fulfilment of the requirements for the degree of Master of Sciences in Chemical Engineering

Under the Supervision of Professor Basim Abu-Jdayil

April 2021

Declaration of Original Work

I, Hyder Ali Reyah Al Abdallah, the undersigned, a graduate student at the United Arab Emirates University (UAEU), and the author of this thesis entitled "*Development of Heat Insulation Composite Materials Based on Bio-Polyesters and Natural Filler*", hereby, solemnly declare that this thesis is my own original research work that has been done and prepared by me under the supervision of Professor Basim Abu-Jdayil, in the College of Engineering at UAEU. This work has not previously been presented or published, or formed the basis for the award of any academic degree, diploma or a similar title at this or any other university. Any materials borrowed from other sources (whether published or unpublished) and relied upon or included in my thesis have been properly cited and acknowledged in accordance with appropriate academic conventions. I further declare that there is no potential conflict of interest with respect to the research, data collection, authorship, presentation and/or publication of this thesis.

Student's Signature:  Date: 16/5/2021

Copyright © 2021 Hyder Ali Reyah Al Abdallah
All Rights Reserved

Advisory Committee

1) Advisor: Basim Abu-Jdayil

Title: Professor

Department of Chemical and Petroleum Engineering

College of Engineering

2) Co-advisor: Muhammad Zafar Iqbal

Title: Assistant Professor

Department of Chemical and Petroleum Engineering

College of Engineering

Approval of the Master Thesis

This Master Thesis is approved by the following Examining Committee Members:

1) Advisor (Committee Chair): Professor Basim Abu-Jdayil
   Title: Professor
   Department of Chemical and Petroleum Engineering
   College of Engineering

   Signature  Date 10/5/2021

2) Member: Dr. Muhammad Zafar Iqbal
   Title: Assistant Professor
   Department of Chemical and Petroleum Engineering
   College of Engineering

   Signature  Date 16/5/2021

3) Member: Yaser E. Greish
   Title: Professor
   Department of Chemistry
   College of Science

   Signature  Date 10/5/2021

4) Member (External Examiner):
   Title: Prof. Mohammad Jawaid
   Department of Biocomposite Technology
   Institution: University Putra Malaysia, Malaysia

   Signature  Date 10/5/2021

This Master Thesis is accepted by:

Dean of the College of Engineering: Professor James Klausner

Signature James F. Klausner Date 22/6/2021

Dean of the College of Graduate Studies: Professor Ali Al-Marzouqi

Signature Ali Hassan Date 22/6/2021

Copy ____ of ____

Abstract

The increasing waste - bio or synthetic - is a critical issue, and managing this waste is a huge challenge for industry and academia. Use of biodegradable materials is sought as an eventual factor in decreasing the current level of waste generation. Therefore, one of the main research areas nowadays is to develop bio-composite materials over fuel-based materials where the bio-composites or waste-based composites serve several advantages both environmentally and economically, including the biodegradability feature of the bio fillers, and the affordability due to its abundant presence in nature. Biowaste, specifically from agricultural sources, can be used as fillers in biopolymer matrices to form true bio-composite materials for various applications. The aim of this study is to investigate the potential use of bio-composite materials in construction as heat insulators. The polymer composites in this study consisted of biodegradable polyester which is [Polylactic Acid (PLA) matrix] and a natural filler [date palm wood fibers]. Biocomposites with filler percentages ranging from 10 to 40 wt.% were prepared and characterized for their physical and mechanical properties. The composites were characterized for tensile strength, water retention, fire retardation and microstructure using Scanning Electron Microscope (SEM), and thermal properties were evaluated by thermal conductivity measurement, Thermogravimetric Analysis (TGA), and Differential Scanning Calorimetry (DSC). In addition, to increase filler/polymer compatibility, alkaline treatment as surface modification of the filler, silane treatment as coupling agent, and chemical additives were also used. Moreover, a fire retardant [Ammonium Dihydrogen Phosphate (ADP)] was added to the composites to reduce flammability of the composites.

Promising results were achieved throughout this experimental research. The silane treatment significantly enhanced the mechanical properties by increasing the tensile strength from 14 MPa for untreated fibers to 30 MPa for silane-ethanol treated composites. The silane-ethanol treatment also reduced the water retention for the 40 wt.% sample from 1.963% to 1.148%. The crystallinity for the silane-acetone samples were the highest among all the systems, reaching up to 58.8% for the 40 wt.% filler sample. The alkaline treatment significantly increased the water retention and the thermal conductivity due to the removal of impurities, leading to higher cellulose ratio.

Moreover, the Alkaline treatment heavily affected the thermal stability, leading to faster degradation of the samples when compared to neat PLA, silane treated and untreated composites. The introduction of ADP fire retardant achieved inflammable characterization of ULV-0 according to UL 94 criteria, and dropped the thermal conductivity to a value of 0.043 $\frac{W}{m.K}$, which is lower than the thermal conductivity of commercial heat insulation of such as XPS and EPS of 0.050 $\frac{W}{m.K}$.

Keywords: Bio-composites, Polylactic acid, Date palm wood fibers, Heat insulation, Silane treatment, Alkaline treatment, Thermal conductivity, Tensile strength.

Title and Abstract (in Arabic)

تطوير مواد مركبة عازلة للحرارة تعتمد على بوليستر حيوي وحشو طبيعي

الملخص

تعد النفايات المتزايدة - الحيوية أو الاصطناعية - قضية مهمة ، وتعد إدارة هذه النفايات تحديًا كبيرًا للصناعة والأوساط الأكاديمية. يُطلب استخدام المواد القابلة للتحلل كعامل نهائي في تقليل المستوى الحالي لتوليد النفايات. لذلك ، فإن أحد مجالات البحث الرئيسية في الوقت الحاضر هو تطوير المواد المركبة الحيوية على المواد القائمة على الوقود حيث تخدم المركبات الحيوية أو المركبات القائمة على النفايات العديد من المزايا بيئيًا واقتصاديًا ، بما في ذلك ميزة التحلل البيولوجي للحشوات الحيوية ، و القدرة على تحمل التكاليف بسبب وجودها الوفير في الطبيعة. يمكن استخدام المخلفات الحيوية ، خاصة من المصادر الزراعية ، كمواد مالئة في مصفوفات البوليمر الحيوي لتشكيل مواد مركبة حيوية حقيقية لتطبيقات مختلفة. الهدف من هذه الدراسة هو دراسة إمكانية استخدام المواد المركبة الحيوية في البناء كعوازل حرارية. تتكون مركبات البوليمر في هذه الدراسة من بوليستر قابل للتحلل الحيوي وهو [مصفوفة حمض عديد حمض اللبنيك] وحشو طبيعي [ألياف خشب النخيل]. تم تحضير المركبات الحيوية بنسب حشو تتراوح من 10 إلى 40٪ بالوزن وتميزت بخصائصها الفيزيائية والميكانيكية. تم إختبار المركبات من حيث قوة الشد ، واحتباس الماء ، وتأخر الحريق ، والبنية الدقيقة باستخدام مجهر المسح الإلكتروني (SEM) ، وتم تقييم الخصائص الحرارية عن طريق قياس الموصلية الحرارية ، والتحليل الحراري الوزني (TGA) ، والقياس التفاضلي للمسح الحراري. بالإضافة إلى ذلك ، من أجل زيادة توافق الحشو / البوليمر ، تم أيضًا استخدام المعالجة القلوية كتعديل سطحي للحشو ، ومعالجة سيلان كعامل اقتران ، وإضافات كيميائية. علاوة على ذلك ، تمت إضافة مثبطات الحريق [فوسفات ثنائي هيدروجين الأمونيوم (ADP)] إلى المركبات لتقليل قابلية الاشتعال للمركبات.

تم تحقيق نتائج واعدة خلال هذا البحث التجريبي. عززت معالجة السيلان الخواص الميكانيكية بشكل كبير من خلال زيادة مقاومة الشد من 14 ميجا باسكال للألياف غير المعالجة إلى 30 ميجا باسكال للمركبات المعالجة بالسيلان والإيثانول. خفضت معالجة السيلان - الإيثانول أيضًا احتباس الماء لعينة 40٪ بالوزن من 1.963٪ إلى 1.148٪. كانت درجة التبلور لعينات silane-acetone هي الأعلى بين جميع الأنظمة ، حيث وصلت إلى 58.8٪ لعينة حشو 40٪ بالوزن.

أدت المعالجة القلوية إلى زيادة كبيرة في احتباس الماء والتوصيل الحراري بسبب إزالة الشوائب ، مما أدى إلى ارتفاع نسبة السليلوز. علاوة على ذلك ، أثرت المعالجة القلوية بشكل كبير على الاستقرار الحراري ، مما أدى إلى تدهور أسرع للعينات عند مقارنتها بـ PLA الأنيق والمركبات المعالجة بالسيلان والمركبات غير المعالجة. حقق إدخال مثبطات الحريق ADP توصيفًا قابلاً للاشتعال لـ ULV-0 وفقًا لمعايير UL 94 ، وأسقط الموصلية الحرارية إلى قيمة 0.043 واط / (م ك) ، وهو أقل من الموصلية الحرارية للعزل الحراري التجاري مثل XPS و EPS البالغة 0.05 واط / (م ك).

فاهيم البحث الرئيسية : المواد المركبة الحيوية ، حمض البوليكتيك ، ألياف خشب التمر ، العزل الحراري ، المعالجة الكيميائية ، التوصيل الحراري ، مقاومة الشد.

Acknowledgements

First, I would like to thank the almighty god for giving me the opportunity and the strength to complete this work. My deepest gratitude for my beloved family for their unconditional support. I am deeply grateful and appreciative for my supervisor, Professor Basim Abu-Jdayil, who introduced me to this project and got me involved in the research, for his guidance throughout my master's degree and providing me with precious knowledge. I would like to thank Dr. Muhammad Zafar Iqbal, my co-supervisor, for his continuous help, support, and advice in this project.

I would like to thank the chairman of the department, Professor Sulaiman Al-Zuhair, and all the faculty and staff of the Chemical and Petroleum Engineering Department at the United Arab Emirates University. I would like to acknowledge the help of our lab specialist, Dr. Hussain Awad El Sayed, and Eng. Emmanuel Galiwango for their assistance in the experimental work, and all my colleagues for helping me during my studies and research. I would also like to thank the committee for their assistance and thesis evaluation.

I am deeply thankful to the United Arab Emirates University, for giving me the chance to pursue my master's degree, and for providing the fund for this research through the Emirates Center of Energy and Environment Research (grant number 31R163).

Dedication

To my beloved parents and family

Table of Contents

List of Tables

List of Figures

List of Abbreviations

ADP	Ammonium Dihydrogen Phosphate
APTES	Aminopropyl Triethoxysilane
CNT	Carbon Nanotubes
DPWF	Date Palm Wood Fibers
DSC	Differential Scanning Calorimeter
FTIR	Fourier-transform Infrared Spectroscopy
HDPE	High Density Polyethylene
IPN	Interpenetrating Polymer Network
ISBM	Injection Stretch Blow Molding
KOH	Potassium Hydroxide
NaOH	Sodium Hydroxide
PET	Polyethylene Terephthalate
PLA	Polylactic Acid
ROP	Ring-Opening Polymerization
SA	Silane-Acetone
SE	Silane-Ethanol
SEM	Scanning Electron Microscope
TGA	Thermal Gravimetric Analysis
WR	Water Retention
XRD	X-ray Diffraction

Chapter 1: Introduction

1.1 Overview

High energy consumption is one of the main contributing factors to the high levels of carbon dioxide emissions in the world. A huge amount of energy produced is supplied to buildings to maintain a suitable atmosphere within the residential and commercial buildings. In countries with extreme hot or cold weather, the portion of energy dedicated to maintaining room temperature inside buildings is relatively high. According to Our World in Data organization, UAE is among the highest energy-consuming countries per capita [1]. Nevertheless, energy supplied for residential and commercial buildings is accounted for around 70% of the total energy consumption in UAE. The harsh climate in the UAE requires the commercial and residential building to be continuously air-conditioned, which consequently demand of a high amount of energy to cool the buildings. In Table 1 below, the energy consumed by different types of buildings is showed according to each emirate.

Table 1: Electricity consumption in the major three emirates in 2018 (in GWh) per sector [2,3,4]

Authority	Residential	Commercial	Others	Total
Abu Dhabi	14,836.908	29,977.85	15,992.24	60,807
Dubai	13,429.51	21,996.456	10,534.032	45,960
Sharjah	4,582	3,921	2,715	11,218
Total	**32,848.418**	**55,895.306**	**29,241.272**	**117,985**
Percentage	**27.84%**	**46.82%**	**24.78%**	**100%**

Moreover, in the United States, energy spent on spaces heating and cooling is equivalent to 3.5 thousand kWh per household in 2019 as shown in Figure 1.

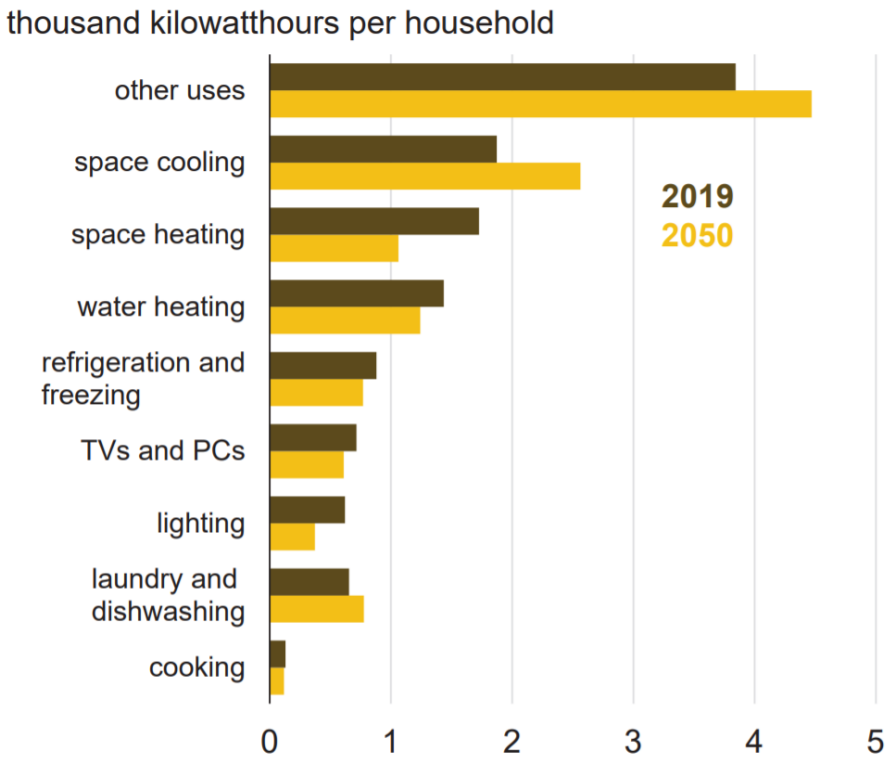

Figure 1: Residential purchased electricity intensity [5]

Heat insulation materials in construction aim to reduce the energy loss and conserve the temperature within the building, thereby decreasing the energy consumption, which leads eventually to the reduction of carbon emission. In addition, it will add economical value by reducing the costs of building materials. Several materials are used commonly as heat insulators, such as polyurethane, expanded polystyrene, cork, cellulose, and mineral wool, which are known as traditional heat insulators [6]. These common thermal insulators lack critical mechanical properties to be appropriate for construction. Therefore, developing thermal insulator material that is compatible with construction is necessary. There are ongoing research and development in the design of advanced materials for heat insulation. The current heat insulation materials in use

can be classified into five categories, which are Organic materials, Inorganic materials, Metallic or metalized reflective, Aerogels, Thermal Insulators from waste materials, Composite materials (polymer and concrete composites) [7]. For organic materials, natural fibrous such as cellulose, hemp, and cotton are studied and investigated for their appropriateness as heat insulators [7]. Cellulose has a thermal conductivity range between 0.040 and 0.050 $\frac{W}{m.K}$ [6]. However, even though natural fibers provide good alternatives for synthetic materials, they suffer from defects such as high-water absorption. These challenges are solved using various chemical treatments [8]. Other organic heat insulators include expanded polystyrene and polyurethane, which have thermal conductivity values range between 0.030 and 0.040 $\frac{W}{m.K}$, and 0.020 to 0.030 $\frac{W}{m.K}$, respectively. Moreover, inorganic materials, which are the second group of common heat insulators, contain mineral and glass wool. In Europe, these two types of wool are accounted for 60% of the total market for heat insulation materials [9]. In addition, the thermal conductivity values for glass wool and rock wool falls between 0.030–0.046 and 0.033–0.046 $\frac{W}{m.K}$, respectively [6]. Metallic materials include Vacuum Insulation Panels (VIP), Gas Insulation Panels (GIP), and Nano Insulation Materials (NIM) [10]. VIPs are homogenous materials with vacuumed voids that are distributed among the material to reduce the thermal conductivity. GIP has the same concept, except that these voids are filled with extremely low thermal conductivity gases such as Argon (Ar) and Xenon (Xe). For NIM, it is distinguished by the small volume of the pores and voids inside the homogenous materials, which is usually below 40 nm diameter. It is reported that all these materials have achieved a thermal conductivity value of 0.004 $\frac{W}{m.K}$. While for thermal insulators from waste materials, it includes coconut husk, textile waste, leather, rubber and plastic, and other natural

wastes [7]. In Table 2 below, the values for the thermal conductivity at 20℃, bulk density, maximum service temperature, and compressive strength at 10% deformation are summarized. Nevertheless, common types of insulations used in the construction are mostly derived from fossil fuel such as expanded polystyrene (EPS), extruded polystyrene (XPS) and polyurethane. Moreover, the common heat insulators possess relatively low mechanical properties, falling below 1000 KPa.

Table 2: Specifications of common heat insulators [9]

Insulation material	Type	K ($\frac{mW}{m.K}$)	ρ (kg/m^3)	Tmax (°C)	σcc (kPa)
VIP	Superinsulation	4–8	65–300	90	45–120
Silica aerogels	Superinsulation	4–20	3–350	750	0–5000
PUR-PIR	Organic, foamy	19–30	25–100	120	100–500
XPS	Organic, foamy	25–35	20–80	75	150–700
EPS	Organic, foamy	29–41	10–50	80	60–260
Glass wool	Inorganic, fibrous	30 - 46	8–150	500	15–80
Rock wool	Inorganic, fibrous	33- 46	13–240	750	15–80
Foam glass	Inorganic, foamy	38- 61	100 - 200	> 400	400- 1600

1.2 Objective of the Study

The aim of this research is to fabricate heat insulation composite materials based on biopolymers which is Polylactic Acid (PLA), and natural filler which is date palm wood fiber (DPWF). Moreover, two different chemical treatments will be applied to

the natural filler, to study the effect of them on enhancing the compatibility between the filler and the matrix. The two treatments are alkaline treatment, using NaOH and KOH solutions, and silane treatment using Aminopropyl triethoxysilane (APTES). APTES will be dissolved in two different solvents, one containing acetone, while the other contains ethanol. The effect of the treatments will be studied and compared, to determine the best treatment method.

1.3 Potential Contributions

The composite materials will be designed to be used in construction, to save the energy and cut the power lose related to cooling the buildings in UAE. Moreover, the designed composites are bio-based since both the matrix and the filler are derived from natural resources. The biodegradability feature is critical for such application because its friendly nature to the environment. Furthermore, the use of date palm wood in construction is a management to the huge agricultural waste in the country and region. It will also reduce the dependency on petroleum derived materials, since most of the common heat insulators are petroleum based. The composites are expected to have good mechanical properties that are superior to the traditional heat insulators, to be implemented and applied in the industry.

Chapter 2: Literature Review

2.1 Polylactic Acid

Due to environmental considerations, the research and development of materials is heading toward bio-based and biodegradable materials [11]. Polylactic acid (PLA) is a biodegradable, compostable, biocompatible, thermoplastic polymer with high mechanical properties. It is being heavily studied in recent years for several reasons such as its processability and relatively low price of production [12,13]. In Figure 2 below, the number of research reports related to PLA annually is showing an increase over the years. PLA was firstly discovered by Carothers (DuPont) in 1932, through heating lactic acid under vacuum [14]. PLA is extracted from natural renewable resources such as sugar cane, corn sugar, and potato [15].

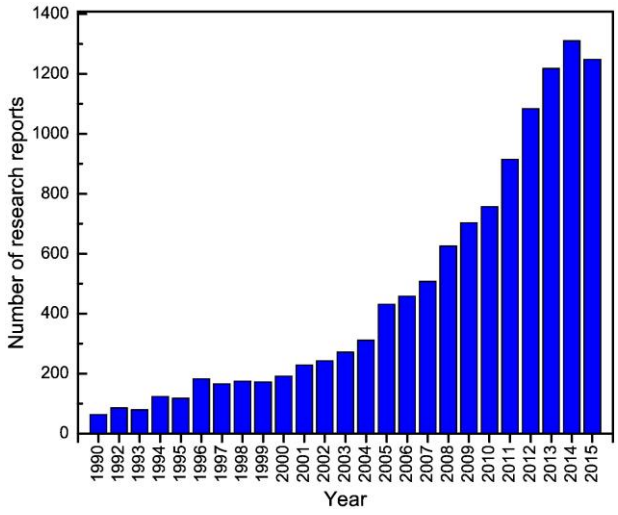

Figure 2: Number of research articles published related to PLA [15]

Moreover, PLA does not degrade under service conditions, which makes it well-suited for conventional usages and last long, while maintaining the easy disposable advantage [13]. PLA has been studied and characterized to be used for several applications, including packaging materials [16]. PLA exhibits mechanical properties that are

similar to poly(ethylene terephthalate) (PET), and better than Polystyrene (PS). Moreover, it has a lower permeability for water, oxygen, and carbon dioxide than PS, but higher than PET [16]. Therefore, PLA is being highly involved in replacing polymers derived from fossil fuels. Furthermore, PLA is also used in biomedical applications due to its compatibility with the human body [17]. The monomer for PLA, which is Lactic Acid (LA), exists in two forms, which are the stereoisomers $_{L}$-LA and $_{D}$-LA as shown in Figure 3 below [16].

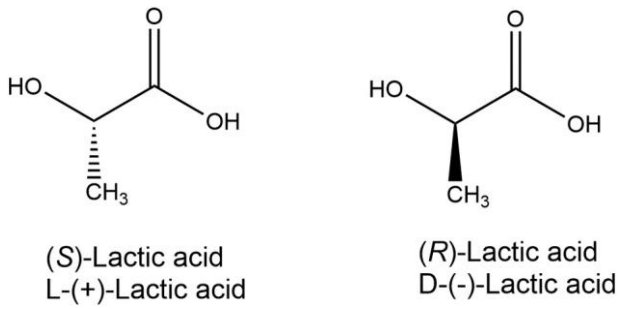

Figure 3: The stereoisomers of Lactic Acid $_{L}$-LA and $_{D}$-LA [15]

2.1.1 PLA Synthesis

LA, which is a simple chiral molecule, is the most common hydrocarboxylic acid because of its wide range of applications [14]. LA is produced whether by bacterial fermentation of carbohydrates or by chemical synthesis [15,18]. Bacterial fermentation is the method mostly used by the biggest two suppliers of PLA, NatureWorks LLC, and Corbion®, due to the high cost, and low production level of the chemical synthesis method [19]. There are two different processes within the bacterial fermentation method, which are homofermentative and heterofermentative. The two processes are categorized based on the bacteria involved in the production. For the heterofermentative process, 1.8 moles of LA are produced for each 1 mole of hexose,

with other high numbers of byproducts such as acetic acid, ethanol, and glycerol. On the other hand, for the homofermentative process, 1.8 moles LA are produced for each mole of hexose, which is identical to the heterofermentative process. However, the byproducts from the homofermentative process are insignificant, thereby making the process more efficient with around 90 g of LA generated for each 100 g of glucose [15]. The bacterial organisms that are common for the production of L(1)-isomer of LA are *Lactobacilli amylophilus, L. bavaricus, L. casei, L. maltaromicus*, and *L. salivarius*. While organisms such as *L. delbrueckii, L. jensenii*, or *L. acidophilus* produces the D-isomer or mixtures of both [12]. However, for the chemical synthesis method, LA is produced by the hydrolysis of lactonitrile using strong acids [14]. The polymerization of LA into polylactic acid is applied through two different polymerization methods, which are polycondensation or ring-opening polymerization (ROP) [14]. Polycondensation is a less costly and simpler process. However, its drawback that it results in low M_w PLA. On the other hand, ROP polymerization is more common since it produces high molecular weight PLA [14]. In ROP method, low M_w PLA is produced firstly by polycondensations. Afterward, a cyclic dimer which is known as lactide is derived from the low-density PLA by decomposition, combined with water. Distillation is applied to sperate lactide from water, and then the opened ring lactide is polymerized by adding catalyst to obtain PLA with controllable M_w [15,14,20,21].

2.1.2 PLA Processing

The processing for PLA follows the standard methods for other polymers' processing, including the polymers derived from fossil fuels, by which the polymer is melted, and then shaped into the desired dimensions according to the application [15].

2.1.2.1 Drying

The first step in the process is to dry the PLA to a water content of 0.01% w/w, due to its sensitivity to a high level of humidity and temperature, to avoid degradation [22]. However, for amorphous pellets, the drying temperature should not exceed the glass-transition temperature of PLA, which is in the range of 43℃ to 55℃, to avoid the agglomeration of pellets [22]. On the other hands, commercial PLA pellets are mostly crystallized, which allow them to be dried at higher temperature to reduce the drying duration [23]. After drying, PLA should be kept in sealed containers to avoid exposure to atmospheric conditions [22].

2.1.2.2 Extrusion

The following step is the extrusion, in which the pellets are placed inside an extruder for the phase transition from solid to liquid. Screw extruders are very common in the polymer industry. The screw extruder consists of a hopper to feed the material, one or more screws inside a barrel, an electric heater, an electric motor to rotate the screws, and a die to eject the melted material [22]. The heating temperature for the polymer inside the extruder is constrained by the degradation temperature as the upper limit and the meting point as the lower limit. For PLA, the melting point starts somewhere between 170 and 180℃, while the degradation starts at 230℃ [15,23]. An important specification for the extruder is the L/D ratio, which is the flight length of the screw to its outer diameter. Screws with high L/D ratio provide higher shear heating and better mixing for the polymer inside the extruder [22]. Figure 4 below displays the major parts of the Single-Screw extruder.

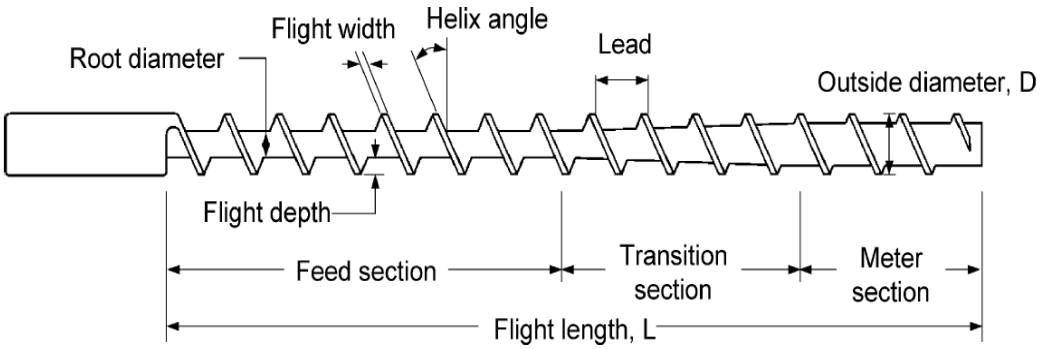

Figure 4: Single-Screw Extruder major parts [23]

2.1.2.3 Injection Molding

After the polymer is melted, it is injected inside molds with specified dimensions to produce the required shapes. the injection molding step is usually integrated with the extrusion, where two-stage equipment exists to inject the product from the melt extruder inside the attached molds, allow them to cool down and be shaped, and finally discharging the material [22]. Figure 5 below shows the components of a typical Injection Molding machine.

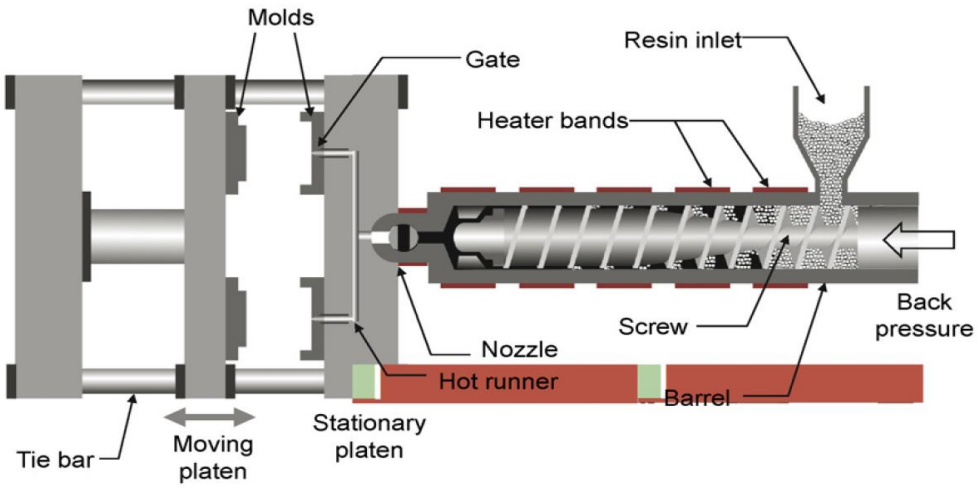

Figure 5: Major components of Injection molding machine attached to screw extruder [23]

2.1.2.4 Blow Molding

In Blow Molding, a hollow thermoplastic polymer melt is produced by extrusion, which is known as preform, is enclosed by a specific mold, then a blowing machine will inject compressed air into the hollow preform, and expand it till it fits the mold and take its shape. Finally, the final cooled object will be ejected [22,23]. There are three types of blow molding, which are Extrusion blow molding, Injection blow molding, and injection stretch blow molding (ISBM), with the latest being the most suitable for PLA bottle containers [23]. In the ISBM, a stretch rod is used to extend the preform axially, while the compressed air is expanding the preform into the mold simultaneously [23]. In Figure 6 below, the steps of ISBM are illustrated.

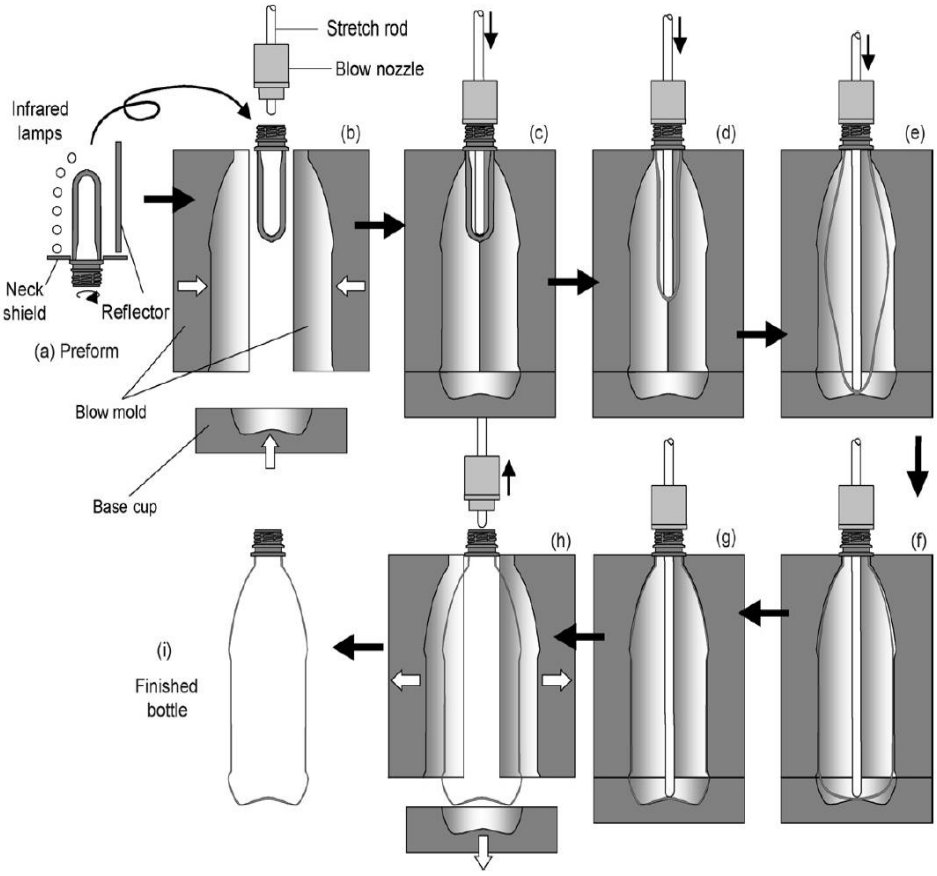

Figure 6: ISBM method with steps [23]

2.1.2.5 Cast Films and Sheets Extrusion

In cast film extrusion, the polymer melt is extruded with slit die and then rolled on more than one chilled high-speed roller that are usually chrome plated. The rollers will solidify the thin sheet and defines its thickness during their rotation [15]. Cast film extrusion is very convenient in producing sheets and thin films with good optical properties, high production rates and the desired thickness [22]. The process for cast film machine is displayed in Figure 7 below.

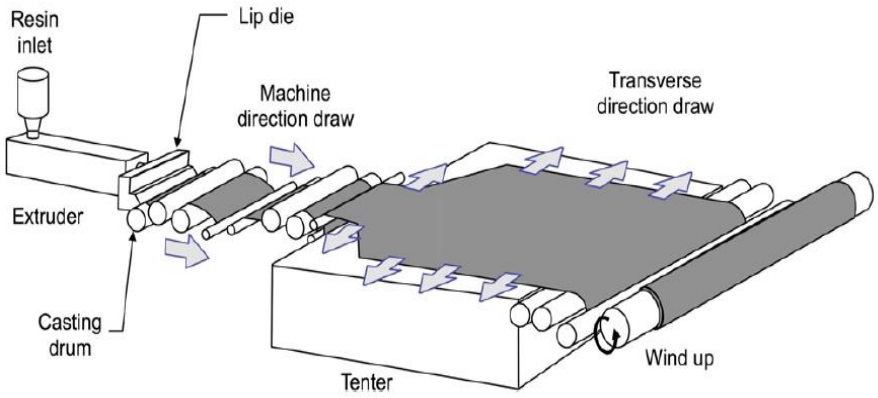

Figure 7:Extrusion cast film machine [23]

2.1.2.6 Thermoforming

In thermoforming, the plastic sheet is heated in a clap frame until it is in a rubbery form, then a vacuum is applied to remove the air below the plastic sheet, allowing it to take the form of the frame [15]. The process for the cast film machine is displayed in Figure 8 below.

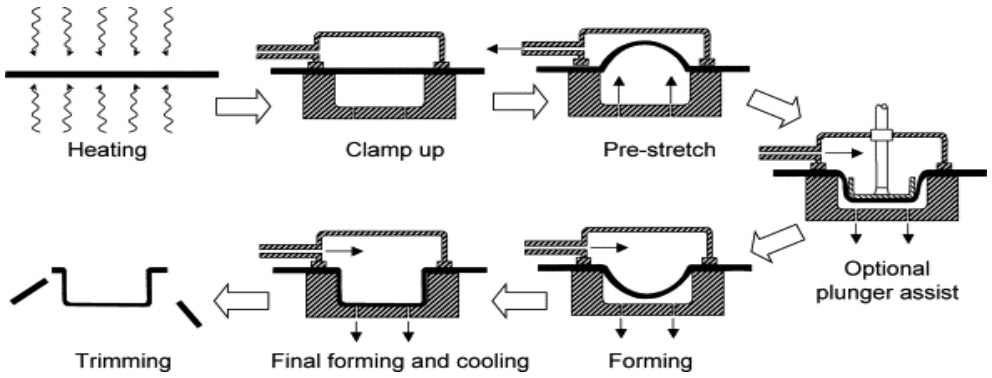

Figure 8: Vacuum Thermoforming [23]

2.1.3 PLA Degradation and End-of-life

There are three main different ways where PLA is degraded, which are hydrolysis, thermal degradation, and photodegradation. Moreover, PLA can have several end-of-life scenarios, such as reuse, recycling, and incineration for energy [15].

2.1.3.1 PLA Hydrolysis

PLA degrades by hydrolysis if it is exposed to moisture for enough time, which can take up to several months [16]. In the first stage of the hydrolysis, water absorption which lead to the cleavage and splitting of the ester bonds. The amorphous parts of the polymer will absorb water before the crystalline parts in this stage, therefore they will degrade first. This step will reduce the molecular weight of the polymer. In the second stage, low molecular weight lactic acid will be metabolized easily by microorganism due to its low density, and water and carbon dioxide will be produced [24,16]. Several factors can play a role in accelerating the degradation of PLA, such as Ph value, temperature, and UV radiation. A highly basic or acidic medium will make the degradation occurs at a faster rate. Moreover, high temperatures will also increase the rate of degradation of PLA [15].

2.1.3.2 PLA Thermal Degradation

Exposure to high temperatures can lead to the degradation of PLA chains by breaking the bonds of carbonyl carbon-oxygen [24]. Different degradation temperatures were reported by different studies. [25] reported a temperature of 270℃ at which the PLA starts to degrade. While [26] reported a temperature range of 230 – 440℃ for degradation.

2.1.3.3 PLA Photodegradation

In several applications of PLA, the polymer will be exposed to Ultra-violent light. The exposure to UV light can lead to degradation of the polymer through bulk erosion, where the light permeates through the polymer [27]. [28] studied the effect of UV light exposure on the degradation of PLA and proposed two mechanisms in which UV light-induced the degradation of PLA. The effect of range of 232 – 500 nm wavelength UV light was investigated, and it was found that the highest effect occurs between 200-300 nm. The first mechanism is the splitting of C-O bonds by photolysis, while the second mechanism involves the formation of hydroperoxide derivatives by photooxidation which are degradation compounds [28].

2.1.3.4 End-of-Life Options

PLA can be designed for long life product and reuse due to its safety and functionality. However, on the long term, the mechanical properties may decrease with time, and PLA will lose some of its functionality. Therefore, other possibilities include composting, recycling, and incineration [15]. Recycling options include chemical and mechanical recycling. For chemical recycle, the challenge is that the process is costly and complex. On the other hand, mechanical recycling also faces a serious challenge, which is the recycling infrastructure for plastics. PLA is not abundant enough to

achieve the critical mass for collecting and recycling the plastic. Moreover, the contamination of the plastics stream can affect the recycling process for PLA [29,15]. Because of this issue, only HDPE and PET are being heavily recycled because of their big market [15]. Nevertheless, there are suggestions to solve this issue. One of the resolutions is to create a special resin identification code (RIC) for PLA, which will allow the tracking and sorting for PLA among the plastic stream, and consequently facilitate the process of its recycling [15]. Presently, there are other polymers that share the same existing RIC for PLA, which is "7-OTHER", such as polycarbonate and ethylene-vinyl alcohol [15]. Moreover, another way to end the life cycle of PLA, is to use it as fuel. NatureWorks [30] and [31] reported that PLA energy content is around 19.5 MJ per KG. Using PLA as fuel will reduce the dependency on fossil fuel for energy and will create a CO_2 neutral method for energy production [31]. Finally, the least environmentally favorable option is the disposal of PLA into landfills. However, it remains the most economic option [15].

2.2 PLA Composites

Generally, a composite is a material that consists of two or more physically and chemically distinct synthetic/natural components. The first component is a selected filler for reinforcing purpose (discontinuous phase) while the other component is a compatible matrix binder (continuous phase) [32]. This combination makes the composite materials special when compared to individual components since it will possess hybrid qualities of the primary materials. Composite materials differ from solutions in such that the primary individual components do not dissolve and lose their structure, but rather they are combined to form the final material while maintaining their original identity [33]. Composite materials occur naturally in many

environments, such as wood in plants, and bones in human bodies [33,34]. Nevertheless, PLA has disadvantages such as sensitivity for water, high stiffness, and lack of durability [16]. Consequently, several adjustments are applied to enhance its features and provide them with appropriate properties. These adjustments include plasticization, impact modification, and the introduction of fillers [11]. Combining PLA with different types of fillers, whether natural or synthetic, can improve the performance of the polymer [11]. There are several types and classifications for composite materials, depending on the filler or matrix types. Based on the matrix type, there are three different types of composite materials, which are polymer composite materials, ceramic matrix composites, and metal matrix composites. Moreover, based on the filler types there are also three categories, which are fiber, particle, and sheet filler composites. Examples for polymer, ceramic, and metal composite materials can be Polylactic Acid based polymers, silica carbide, and aluminum oxide composite ceramics, Aluminum, Copper, Magnesium, and Titanium metals, respectively [33,35]. Furthermore, based on the scale, there can be nanocomposites, or bio-composites [33]. Glass fibers (GF) and carbon fibers (CF) are very common reinforcements in the composites industry. It is reported that PLA-GF composites are also fabricated, and they have shown a greater mechanical properties when compared to neat PLA [36]. PLA-CF were also investigated for biomedical applications [36]. Moreover, due to their unique characteristic, carbon nano tubes (CNT) are commonly investigated as filler for PLA composites. It was shown that the addition of CNT to the PLA increases its thermal conductivity [37]. CNT was also added up to 2 wt.% to PLA to investigate the mechanical properties, and it showed an increase in the tensile strength, with the maximum strength achieved at 0.5 wt.% [38]. Due to the ability of Hydroxyapatite to bond with the bone structure. Composites of PLA with Hydroxyapatite at different

loading levels ranging from 10 to 50 wt.% are studied by [39] for biomedical applications. two different preparation methods were studied, and silane surface treatment was applied to test the effect of the coupling agent. The composites showed good mechanical properties, reaching 39 MPa yield stress, and a young modulus value of 1400 MPa. The best results achieved were using silane treatment at 0.5 and 1 wt.%, with 30 wt.% filler loading. However, the mechanical properties for PLA-HA composites still fails to meet the requirement for the application of bone replacement [36]. Another filler material for PLA composites is Barium Sulphate. PLA-$BaSO_4$ composites were studied as Bioabsorbable Radiopaque Stent Material in the rat pancreas by [40]. The results showed that the material is not more toxic and harmful when compared to the standard steel material. Moreover, PLA–calcium carbonate, PLA-β-tricalcium phosphate, and PLA-Calcium Sulfate composites were all studied and investigated for different biomedical applications [36].

2.2.1 PLA-Natural Filler Composites

According to the above-mentioned classifications, the composites prepared in this research falls under polymer matrix composites in terms of matrix classifications. In addition, it is classified as fiber composites based on the filler classifications, and bio-composites based on the scale. Therefore, the composite is a bio-filler based polymeric composite material. Considering environmental and sustainability issues, Bio-composite materials that consist of biopolymer matrices and bio filler materials are preferred because of their biodegradability feature. Therefore, using material from agricultural resources as natural filler is a treatment for these biowastes. Natural fillers also have light weights, low density, recyclable, and lack of health hazards [41,42].

Natural-filler based polymers are being heavily studied for a variety of applications such as automobiles, buildings and construction, and airplanes interiors [43]. Several natural fillers such as hemp, flax, jute, sisal, henequen, wood, coconut coir, pineapple leaf fiber, kenaf, bamboo fiber, are studied as reinforcements for polymeric matrices [43,44]. The most polymer matrices used are petroleum-based polymers such as polypropylene and polyethylene. In addition, bio polymers such as PLA are also being studied as matrices for natural filler reinforcement. Moreover, natural fibers are attempting to replacing synthetic fillers such as glass and carbon fibers, due to sustainability concerns [43,44].

Composite of PLA reinforced with flax was studied for the application of automotive industry by [45]. The composite was fabricated by incorporating scattered flax with up to 30 vol.% using film stacking techniques. The results found out that the PLA-Flax composites have higher tensile strength and young's modulus compared to PP-flax, and close to Polyester-glass fibers, which is very promising. Kenaf fibers were also studied as reinforcement to PLA matrix by [46]. It was found out that the glass transition temperature decreased slightly compared to pure PLA, while the melting point increased. The water retention increased as the filler percentage increased, and the same trend was noted for the mechanical properties. Due to its abundant presence, cellulose, the most common biomass material in nature, is also a subject for study in bio composites. Cellulose has many advantages such as low cost, non-toxic structure, low weight, and biodegradable. However, because of its hydrophilic nature, cellulose lead to weak adhesion in the matrix, which lowers the mechanical properties significantly. Another type of natural filler that is widely studied as filler for PLA is talc. Talc addition to PLA showed a significant increase in the crystallinity, even at low percentages such as 1%. Moreover, it enhances the stiffness and reduces the

processing time. It also worthy to mention that lower sizes of talc leads to slightly higher crystallinity [36]. Another common type of filler for PLA matrices is wood, whether in fiber or powder form. It was found that the introduction of wood powder at 5% loading slightly decreased the tensile strength of the material, compared to pure PLA [47]. Wood fibers can be easily obtained from agricultural wastes, which makes them available at low costs [48]. In UAE, palm trees are widespread and planted. Palm trees produce around 15 kilograms of wood annually, which makes the date palm fiber (DPF) abundant. These fibers consist mainly of cellulose, hemicelluloses, lignin, and pectins, with a minor quantity of extractives [49].

Nevertheless, natural fibers has also disadvantages such as high moisture absorption, inadequate dispersion and adhesion with the polymer matrix, and low thermal stability [50]. The addition of Flax natural filler to PLA and Polypropylene was studied by [51]. The thermal and mechanical properties of neat PLA/PP, 30%, and 40% were investigated. Moreover, 5%, 10%, and 15% of triacetin plasticizer were added to the 40% flax content to enhance the poor elasticity and reduce stiffness. Recycled wood fiber was incorporated into PLA matrix to form biodegradable matrix was done by [50]. In addition, 0.5% of (gamma-methacryloxypropyltrimethoxysilane) was added as coupling agent to enhance the surface adhesion between the filler and the matrix.

2.3 Chemical Treatments

Nevertheless, experimental studies found some drawbacks in natural fiber composites such as poor wettability, incompatibility of fibers with some polymeric matrices, and high moisture absorption of fibers [41]. Research suggests chemical treatment for the bio-filler, before introducing it to the polymer matrix. Chemical treatments showed good results for enhancing the properties of bio-composites when compared to composite material with the untreated filler of the same type [52]. Chemical treatments can alter the behavior of fiber cell walls permanently by three different approaches; The use of coupling agents, crosslinking of the fibers, and grafting polymers onto the fibers [49]. These chemical modifications can promote the adhesion between fiber and matrix, and reduce water retention, but may reduce the strength since it makes the composite brittle. Coupling agents are chemicals that function at the interface to link the polymer matrix with the filler cell walls [49]. Alkaline treatment, Silane treatment, Acetylation, and Benzoylation treatments for filler were mentioned by [53]. Moreover, A combination of Silane and Alkaline treatment was examined by [54]. Alkaline treatment is effective in removing surface impurities, such as wax and oil covering materials from the fiber [55]. On the other hand, Silanes are well-known and highly effective coupling agents that improve the compatibility between the filler and the matrix [49]. Several other treatments to various types of natural fillers were reviewed and mentioned by [32] such as Peroxide treatment, Sodium chlorite treatment, Acrylation, and acrylonitrile grafting Isocyanate treatment, and many others. Chemical treatment to natural filler is applied by immersing them in solutions with different concentrations of the treatment and coupling agents for different periods. For Alkaline treatment, solutions with concentrations of NaOH ranging between 0.5% to 10%, for

a period between 1 hour to 72 hours were used in the treatment process [32]. For Silane treatment, the solvent of Acetone, Ethanol, or water is prepared first, and then Silanes are added to prepare the final solution for the filler to be immersed in. Ratios of Ethanol/Acetone to water ranges from 1:1 to pure Acetone solvents [54,52,53]. Moreover, the concentration of Silane in the final solution ranges between 0.1% and 3%, with different types of Silane material used, such as Aminopropyl Triethoxy Silane (APTES) and Vinyl Trimethoxy Silane (VTS) [32,52,53,49]. Another unique treatment was the hydrothermal carbonization of rice husk to use it as a filler for PLA matrix [56]. In this research, APTES was used in concentrations ranging from 1% to 3%, in solvent of Ethanol/Acetone and water.

2.3.1 Alkaline Treatment

Alkaline treatment, which also known as mercerization is one of the most common chemical treatment of natural fibers that are used as reinforcement for polymer matrices. The alkaline treatment removes a certain amount of lignin, wax, and oils covering the external surface of the fiber cell wall, which increases the cellulose ratio and exposure to the surface of the filler [53]. Alkaline treatment is done using NaOH and KOH solution. The concentration of the alkaline solution, the time of immersion, and the temperature varies based on the study. D. Bachtiar et. al. studied the effect of 0.25 and 0.5M NaOH concentration, for soaking time of 1, 4, and 8 hours on sugar palm fiber reinforced epoxy composites. It was found out that for 1-hour immersion, the tensile strength increased for 0.25M concertation, and then decreased for 0.5M concentration. For 4, and 8 hours immersion, both 0.25M and 0.5M concentration decreased the tensile strength when compared to the untreated filler [57]. It was explained that high exposure time or relatively high concentration of alkaline can

damage the structure of the fiber [57]. Alvarez et. al. studied the alkaline treatment for different immersion times that varied between 25, 48, and 72 hours for a composite of biodegradable matrix with Sisal Fibers. Moreover, the temperature was also varied between 5℃, room temperature, and 40℃. It was found out that the combination to enhance the tensile strength was at 5℃ for 48 hours [58]. Several other combinations decreased the tensile strength compared to untreated samples, such as at room temperature for 48 and 72 hours. Although it is generally mentioned in the literature, that alkaline treatment enhances the mechanical properties due to removal of impurities and increasing the surface roughness, it was found out that different combinations of time, concentration, and temperature conditions resulted in decreasing the mechanical properties, due to damaging the structure, or the resulted form of fibers was not compatible with the matrix as the untreated one.

2.3.2 Silanes Treatment

APTES is one of the most used coupling agents for polymer composites [59]. In natural filler, the main components are cellulose, hemicellulose, and lignin. The primary component of natural fiber, which is cellulose, has a polar nature that limits the compatibility with the non-polar polymer matrices [60]. Moreover, even in polar matrices, natural fibers' hydrophilic nature causes adhesion problems because of the moisture intake in a highly humid atmosphere [61]. For PLA, which is a non-polar hydrophobic polymer, chemical treatment is essential to enhance the adhesion with natural filler such as date wood fibers. Furthermore, hydrogen bonds could form between the polar filler, causing the filler to agglomerate and unevenly being distributed inside the non-polar matrix [59]. Another factor that contributes to the poor compatibility is the lack of wetting for the filler by the non-polar matrix [59]. Silanes,

as coupling agents, acts as a bridge that alters the surface nature of fiber to make it compatible with the polymer matrix.

The structure of APTES consists of $(RO)_3Si\_(CH_2)_3\_NH_2$ in which R is alkoxy group (Methyl or Ethyl), and the functional group is the amino group NH_2. Alkoxy group in silanes, which is in the case of APTES is Ethoxy, can be hydrolyzed off by the reaction with water to form the more reactive silanol groups. Silanol groups will also attract each other and form $\_Si\_O\_Si\_$ bonds, generating a siloxane network in the solution in a step called self-condensation. Furthermore, the silanol molecules will attach to the surface of fibers and form hydrogen bonds with the hydroxyl groups of the cellulose in the step of adsorption, generating a monolayer of polysiloxane on the surface of the fibers. This process will result in a coating of fiber surfaces. Finally, drying the sample and the removal of water/solvent will initiate the dehydration step, in which the covalent bonds of $\_Si\_O\_C\_$ between the filler and the silane occur [59]. The four steps are illustrated in Figure 9 below:

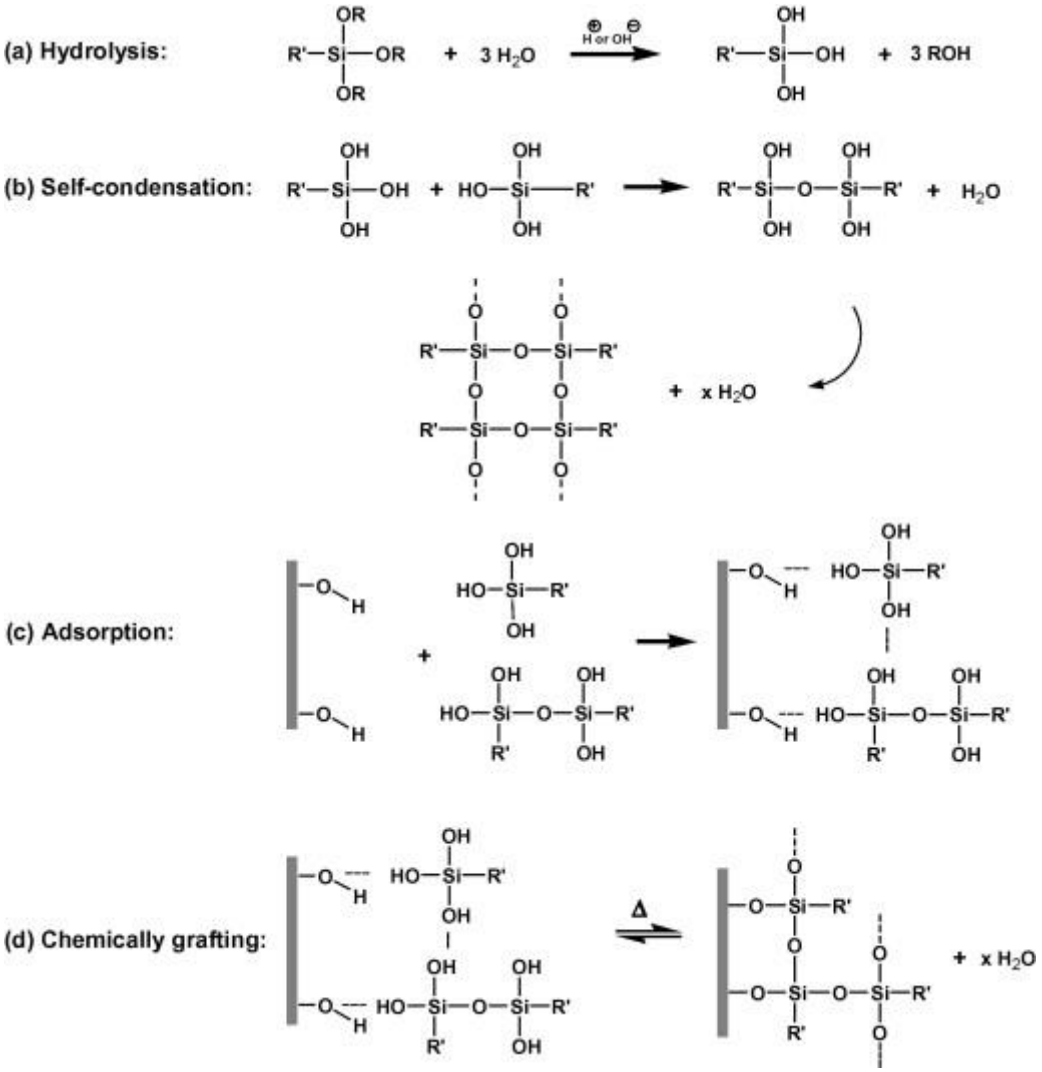

Figure 9: The steps of Silane treatment for natural fibers [59]

Nevertheless, it is reported that the silane does not react with the hydrocarbon backbone of thermoplastic polymers. However, the enhancement in the mechanical properties after silane treatment is due to the coating of fibers with a polysiloxane layer. The polymer molecules may diffuse into the polysiloxane monolayer, forming Interpenetrating Polymer Network (IPN) that enhances the compatibility between the treated filler and the thermoplastic polymer matrix. Thereby, achieving better dispersion of filler into the polymer matrix.

Chapter 3: Materials and Methodology

3.1 Materials

3.1.1 Polylactic Acid

The PLA used in this study was purchased from Zhejiang Zhongfu Industrial Limited, Zhejiang, China in pellets form. It has the following specifications: L-lactide: D-lactide ratio from 24:1 to 32:1, pellet diameter of 3.5 mm, and a molecular weight 2.41 x 10^5 g/ mol. It is labeled as PLA (4032D). Moreover, the melting point is between 155 to 170 ℃. The PLA is semi-crystalline, with a specific gravity of 1.24. The pellets used in the research are captured closely in Figure 10.

Figure 10: Polylactic Acid pellets used in the research

3.1.2 Date Palm Wood Fibers (DPWF)

The palm date wood studied in this research was obtained from the UAE University farm in Al Foah. It consists of wood waste of palm trees, collected from different parts in the tree such as leaf, branches, and base. Figure 11 below shows the wood waste generated from palm trees in the farm.

Figure 11: Palm trees wood waste

Moreover, the wood is dried, then its size was reduced by grinder, and ultimately sieved through sieving trays with aperture size of 212 micrometers. The final form of the wood is displayed in Figure 12.

Figure 12: Size reduced Date wood fiber below 212 micrometers

3.1.3 Treatment Chemicals

For the alkaline treatment, NaOH and KOH in the pellet form provided by Sigma Aldrich were used. For the silane treatment, two solvents used were Acetone and Ethanol, both supplied by Sigma Aldrich. (3-Aminopropyl) Triethoxysilane (APTES) was used as a coupling agent to enhance the compatibly between the filler and the polymer matrix as a form of chemical treatment for composites. It is supplied by Sigma Aldrich, with a volume of 100 ml, and a concentration of 97%. Ammonium Dihydrogen Phosphate (ADP) was purchased for fire retardancy from Pure Chempur in powder form.

3.2 Sample Preparation Methodology

3.2.1 Chemical Treatment

Alkaline treatment was applied to the wood fiber by immersing the filler in the treatment solution. In the treatment solution, NaOH and KOH were dissolved in

distilled water at 2 wt.% concentration. The mixture was stirred using a magnetic stirrer under room temperature, and the filler was added and kept inside the beaker for two hours.

Figure 13: Alkaline Treatment process

Silane treatment was applied to the filler to test its effect. Initially, two different solvents were prepared, which are Acetone-Water, and Ethanol-Water. The ratios of Acetone and Ethanol to water were 50:50, and 90:10, respectively. The two systems are referred to in this research as Silane-Ethanol (SE), and Silane-Acetone (SA), Accordingly. For the Silane-Ethanol system, APTES was hydrolyzed in 3 different percentages, which are 1, 2, and 3%. Nonetheless, for the Silane-Acetone system, APTES was added with a 3% concentration only. The solution was stirred at room temperature for 1-hour. After preparing the solution with APTES in it, the filler was

immersed for two hours, then filtered out from the solution, and finally dried in the oven at a temperature of 95℃ for 24 hours.

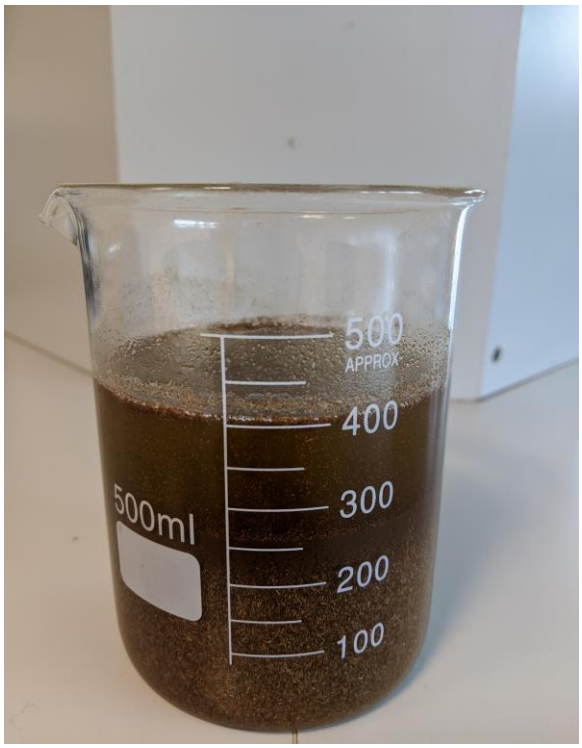

Figure 14: Treatment solvent with filler immersed inside

For the fire-retardant addition, ADP was dissolved in distilled water with 5, 10 and 20 wt.% of the solution. The previously silane-ethanol treated filler was immersed in the solution for 4 hours and kept at room temperature of 50℃. The fibers were then filtered and dried at 50℃ for 12 hours.

3.2.2 Fabrication of Samples

Samples were prepared with 4 different filler concentrations, which are 10, 20, 30, and 40 wt.%. The five composite systems prepared are untreated Date palm wood fibers with PLA (PLA-UTDPWF), fibers treated with NaOH with PLA (PLA-NaOH), fibers treated with KOH with PLA (PLA-KOH), fibers treated with Silane-Acetone with PLA (PLA-SA), and fibers treated with Silane-Ethanol with PLA (PLA-SE). The

pellets were mixed with the filler using a double screw melt extruder. Moreover, the conditions were as follows; a temperature of 190℃, a torque of 140- and 3-minutes retention time inside the extruder. Furthermore, the extruded product was placed inside different molds designed for different tests. The three molds are the square mold, which was used for the thermal conductivity test, the cylindrical mold, which was used for water retention, and for measuring the density. Finally, the dog-bone shape was used for the tensile strength test. The three molds are displayed in Figure 15.

A B

Figure 15: (A) Square (Plate) mold and Cylindrical mold, and Tensile dog bone shape (B)

Afterward, the square and dog bone molds are placed inside a hot press machine, to smooth the surface of the samples and make the samples take the shape of the molds. The hot press occurred at 3 stages. In the first stage, a pressure of 0.50 tons was applied, accompanied by a temperature of 180℃ for 5 minutes and 20 seconds. In the second stage, the pressure was increased to 0.52 tons, and the temperature was also increased to 185℃. In the third stage, the pressure was increased to 3 tons, and the temperature was reduced to 100℃ for 3:30 minutes. For the cylindrical molds, the same pressure and temperature conditions are applied. However, the periods for the three stages are

16 minutes, 10 minutes, and 3:30 minutes, respectively. The final step in sample preparations was the annealing, which took place inside an oven for 3 hours at a temperature of 95℃. The final sample shapes are displayed in Figure 16.

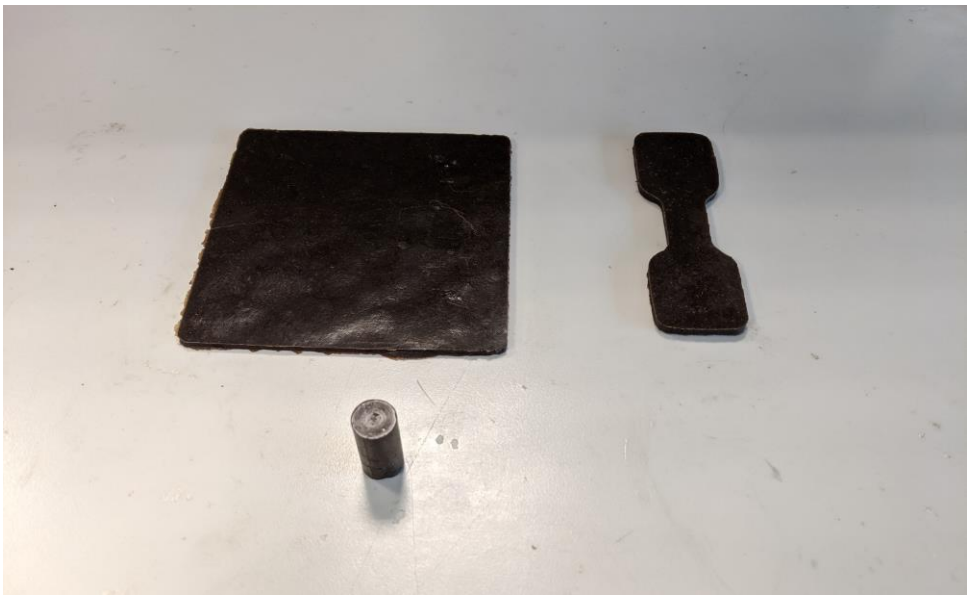

Figure 16: The plate, dog-bone shape, and cylindrical samples

3.3 Experimental Tests

3.3.1 FTIR

Fourier Transform Infrared test is used to determine the functional groups that are present in our composite materials, and whether chemical reaction occurred due to the addition of the filler. The test was done using FT/IR-4700 by JASCO.

3.3.2 SEM

The morphology of samples was investigated by scanning electron microscopy. SEM machine NeoScope provided by JOEL was used in this experiment. This test gives a clear image of the arrangements of the filler particles within the polymer matrix and shows the amorphous phase and the pores in the prepared composite as well. All the samples were mounted on aluminum stubs and coated with a layer of gold. The gold coating is performed before conducting the test to avoid electrostatic charges and ensure the maximum magnification of the textural and morphological characteristics of the composite sample. All samples for SEM were taken from fractured tensile samples.

3.3.3 XRD

XRD test was done to untreated filler, NaOH treated, and silane-acetone treated to investigate the effect of the treatment on the crystalline structure. The equipment used was Malvern Panalytical X-ray diffractometer.

3.3.4 Thermal Conductivity

The thermal conductivity test was done using Lasercomp FOX-200 by TA Instruments with the plate-sample, which has the dimensions of 110mm X 110mm X 3mm. The sample is placed between two plates that have two different temperatures, and the heat

flow occurs due to the difference in temperature between the two plates, with the heat flowing from the hotter plate to the cooler plater, until it reaches equilibrium.

3.3.5 Differential Scanning Calorimeter

The DSC test was run using a Differential Scanning Calorimeter Analyzer by TA Instruments (25DSC). The concept of DSC involves the continuous supply of heat to samples with a weight of milligrams inside Aluminum vessels, to investigate the thermal sensitivity. The DSC will explore properties such as glass transition temperature (T_g), crystallization temperature, melting point, enthalpy of melting, and specific heat capacity (Cp). Samples with weights ranging between 5 and 10 mg were placed inside aluminum crucibles and then placed inside the instrument. An identical procedure was followed for all samples, which include a first heating cycle from 20℃ to 200℃, with a ramp of 10℃/min. Followed by an isothermal for 2 minutes. Consequently, it is cooled down by 10℃/min. to 95℃, and then isothermal for 180 minutes to simulate the annealing inside the DSC. The sample is then cooled by 10℃/min to 20℃. The final cycle is a second heating cycle from 20℃ to 200℃, with a ramp of 10℃/min. For the Cp test, the temperature range was from 0 to 60℃, and the Cp considered in this research is at 25℃.

3.3.6 Density

Density measurement was also taken using the cylindrical sample. Due to its concise size and defined shape. The volume was calculated after measuring the dimensions of the sample, and the sample was weighed on a scale, to measure the density by dividing the mass over volume.

3.3.7 Specific Heat Capacity (Cp) and Thermal Diffusivity (α)

Specific heat capacity was found using the Differential Scanning Calorimeter Analyzer by TA Instruments (25DSC). Afterward, the diffusivity was found by dividing the thermal conductivity over the density and the thermal conductivity.

3.3.8 TGA

TGA test provides data regarding thermal degradation and thermal stability. The test was done using TGA Q500 by TA Instruments. Samples of weight ranging from 5 to 10 mg were placed in the instrument, and the temperature was raised from 40 to 600℃. The TGA data can be interpreted in two graphs, which are weight percentage versus temperature, and derivative weight versus temperature.

3.3.9 Mechanical Properties

Tensile test was applied for dog-bone shape to determine several important mechanical properties such as stress, strain, and modulus of elasticity. The test was done using AG-X, by Shimadzu. The rate was 10mm/s. The tensile was done to neat PLA, untreated, Silane-Ethanol, and Silane-Acetone treated samples. When the test was applied to Alkaline treated samples, the samples broke just after the test started due to high brittle nature.

3.3.10 Water Retention

For the water retention test, the cylindrical sample was weighed firstly, and then immersed fully in water, for 48 hours. The test was carried under room temperature, which is labeled as cold-water retention, and under 50℃ in a water bath, which is labeled as hot-water retention. Several readings were taken during the 48 hours, mostly

we will mark the reading at 24 hours and 48 hours. While taking the readings, the sample was removed from the water, dried using cloth, and then weighed again to investigate the water absorption by the sample. The following equation was used to calculate the water retention relevant to the initial reading, which is for the dry sample.

$$WR\% = \frac{\text{weight of equilibrated sample} - \text{weight of dry sample}}{\text{weight of dry sample}} \quad (1)$$

3.3.11 Fire Test

The fire test was carried before and after incorporating the ADP fire retardant into the composite material. UL 94 fire testing standard was applied, with samples of the following dimensions 127 mm x 12.7 mm x 3 mm. Samples are shown in Figure 17.

Figure 17: Fire test specimen, with three replicates for each sample

The setup for the test is illustrated in the figure below. Methane gas was used, and a stand with a clamp to hold the sample above the fire source. The distance between the bottom of the held sample and the fire source is 10 mm, while the fire flame is 20 mm in height. Cotton batting was placed below the sample to indicate the specimen fire dripping.

Chapter 4: Results and Discussion

4.1 PLA-UTDPWF, PLA-NaOH, and PLA-KOH systems

4.1.1 FTIR

FTIR test was done on untreated filler, NaOH treated, and KOH treated, and it is displayed in Figure 18 below. While for composites, FTIR test was done on neat PLA, PLA with 20 wt.% untreated filler, NaOH treated, and KOH treated filler. For the date wood fibers, the FTIR results show the presence of the C-O functional group at a wavelength of 1000, C=O group at around 1750, and C—H bonding at around the wavelength of 3000. Moreover, the O—H group is present at 3300 wavelengths [62]. No major change in the functional groups due to the treatment. The alkaline treatment removes the impurities such as wax and dust from the surface of the treatment and does not form any new bonding. Thereby, it is expected that there are no new functional groups.

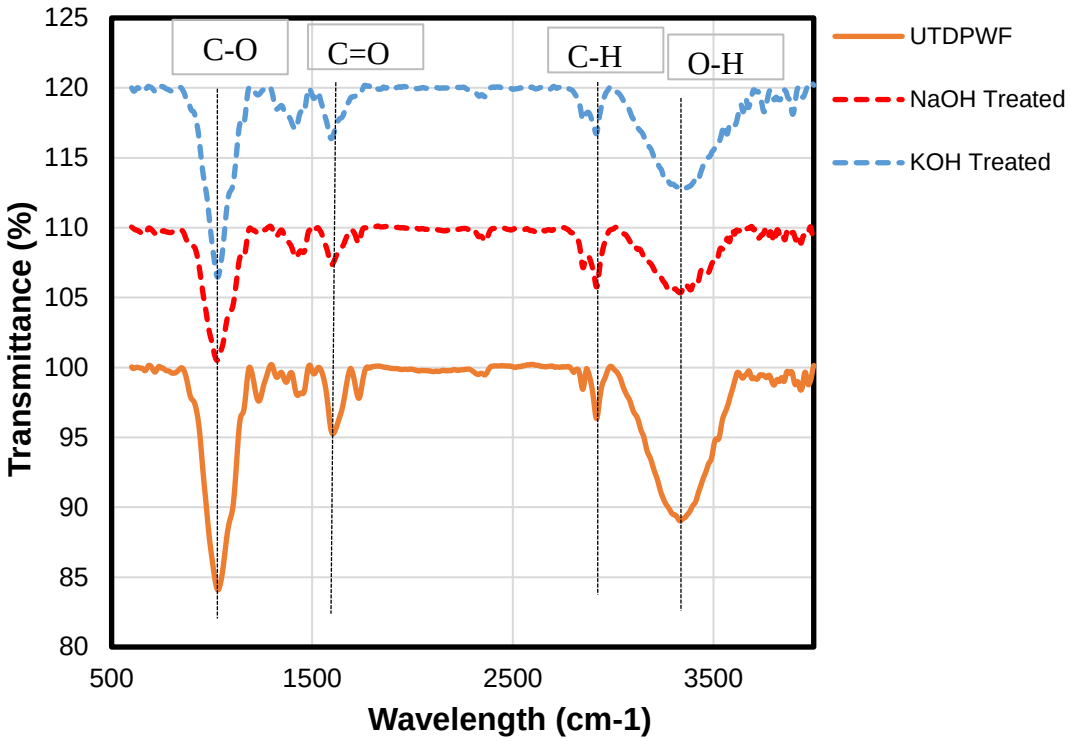

Figure 18: Untreated filler, compared to KOH and NaOH treated

However, for the composites, the introduction of the untreated filler exhibited the functional group O—H at around a wavelength of 3000 as shown in Figure 19 below. This peak is due to the water absorption that occurred because of the filler's hydrophilic nature. Since the alkaline treatment removes the lignin and the hemicellulose from the natural fiber, the cellulose ratio is higher in the alkaline treated samples. Thereby, the O—H functional group is sharper in the treated samples due to the structure of cellulose illustrated in Figure 20 below.

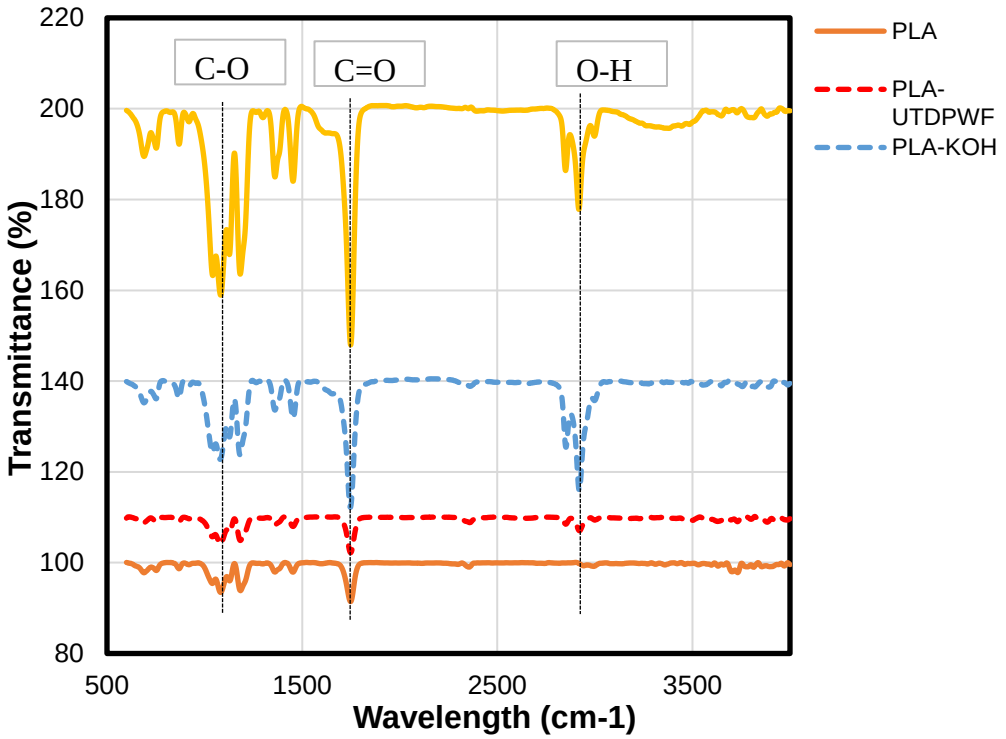

Figure 19: FTIR for PLA, and 20 wt.% of PLA-UTDPWF, PLA-KOH, and PLA-NaOH treated composites

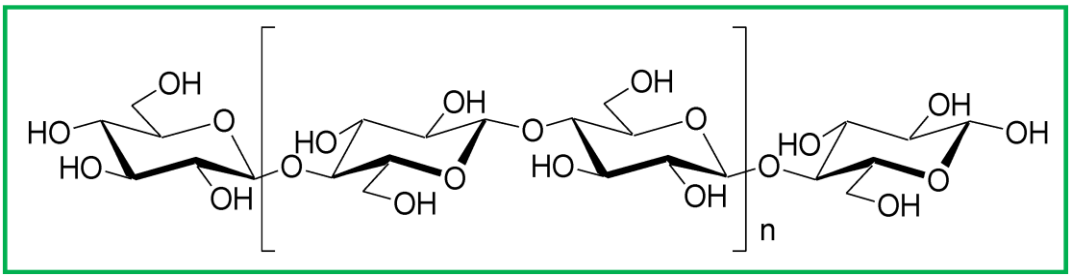

Figure 20: The structure of Cellulose [63]

4.1.2 SEM

SEM test was done to the filler particles before and after the treatment to investigate the effect of the impurities' removal. In pictures a and b in Figure 21, particles and impurities on the surface of the filler are clear and visible. However, after the treatment, it is noticeable that the surface became much smoother with few particles

remained. This is mostly because of the particles' solubility in the treatment solution that caused the particles to be removed.

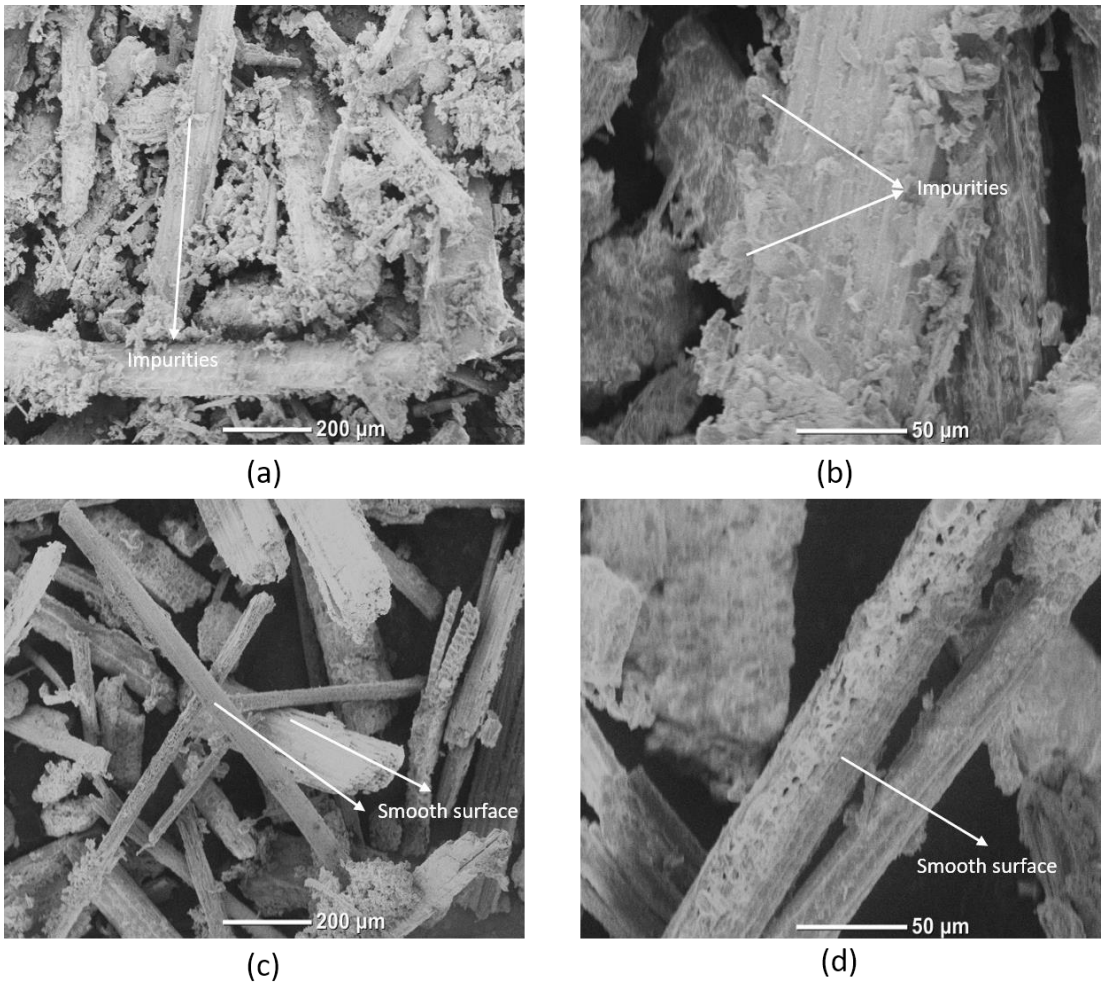

Figure 21: SEM for UTDPWF (a and b), and NaOH treated fibers (c and d).

Although the alkaline treatment was successful in removing the impurities and particles from the surface of the filler, it did not enhance the compatibility between the filler and the matrix. As it can be seen in Figure 22 below, there are obvious hollow spaces and voids that lead to poor mechanical properties.

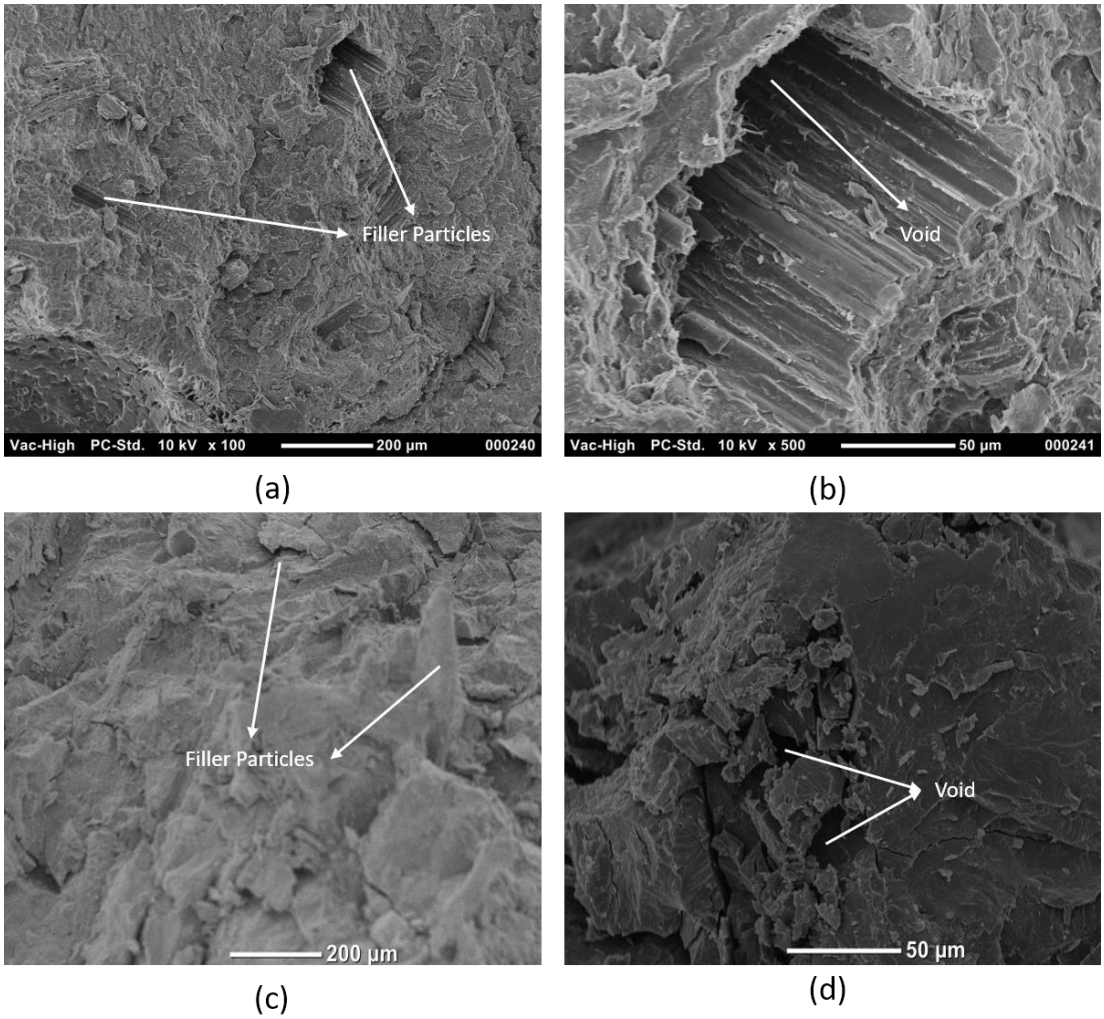

Figure 22: SEM for PLA-UTDPWF (a and b), and PLA-NaOH (c and d)

4.1.3 XRD

XRD analysis is shown in Figure 23 below. It indicates two major peaks, which lie between 20 and 30 degrees. These two peaks correspond to the cellulose component in the wood [64,65]. The peak is sharper for the treated sample, which indicates the removal of impurities that resulted in a higher cellulose ratio in the wood.

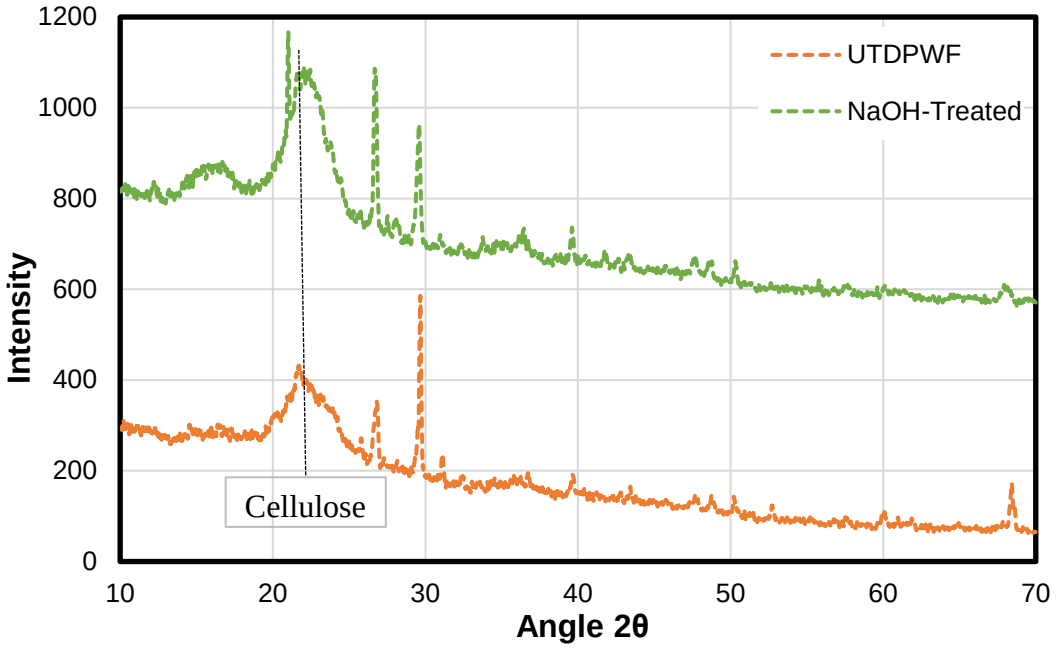

Figure 23: XRD for UTDPWF and NaOH-Treated fibers

4.1.4 Thermal Conductivity

A thermal conductivity test was done on the three systems, PLA-UTDPWF, PLA-NaOH, and PLA-KOH. For thermal conductivity of the untreated system, the values decreased with the introduction of the filler up to 20 wt.%, then it increased slightly. The minimum value for the thermal conductivity achieved was around 0.07642 $\frac{W}{m.K}$, at 20 wt.% loading, while the maximum value was around 0.0841 $\frac{W}{m.K}$, which is for the pure PLA. The thermal conductivity for the pure wood was measured to be 0.06806 $\frac{W}{m.K}$. This explains the drop in the thermal conductivity when the filler is added. Since the thermal conductivity of the date wood fiber is lower than the thermal conductivity of the polymer, the introduction of the filler into the matrix reduced the thermal conductivity. [66] indicated that adding filler will create hollow spaces, due to the interruption of the polymer matrix by the filler particles, which reduced the thermal

conductivity. Therefore, the excess filler material incorporated into the matrix can lead to the filling of these hollow spaces, and thereby increasing the thermal conductivity again as the trend shows for the 30 and 40 wt.%. This is due to the relatively high thermal conductivity of the filler compared to the air voids. The results are shown in Figure 24 below.

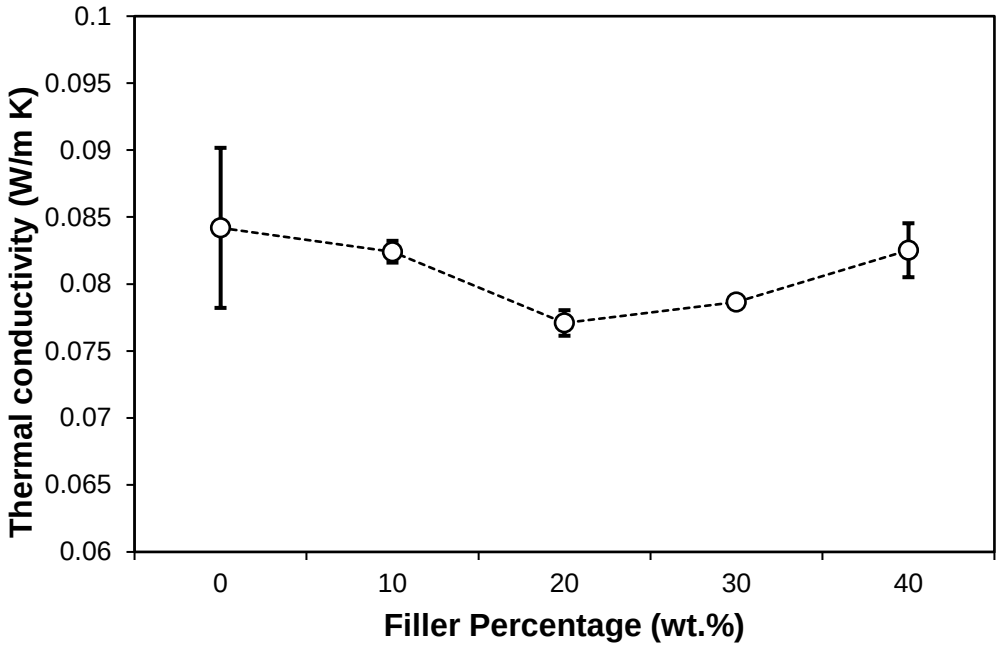

Figure 24: Thermal Conductivity for neat PLA and Untreated samples

For the treated samples, both systems showed an increase in the thermal conductivity values as the filler percentage increases as shown in Figure 25. This can be explained by the role of the cellulose inside the polymer matrix, which acts as a nucleating agent that increases the crystallinity of the samples as its percentage increases. The crystallinity is directly proportional to the thermal conductivity, which explains the increasing trend for the thermal conductivity of this system [67]. The KOH-treated system showed relatively higher values than the NaOH, which illustrates that it is more effective in the removal of the wax, lignin, and other components in the natural filler.

This matches another study for the alkaline treatment where KOH treatment effect surpassed NaOH, and it was more effective in removing the lignin by alkaline cleavage and hydrolyzing the hemicellulose [68]. Moreover, the high moisture content as noted in the FTIR lead to an increase in the thermal conductivity when compared to the PLA-UTDPWF composites. This is because water has relatively high thermal conductivity when compared to air voids.

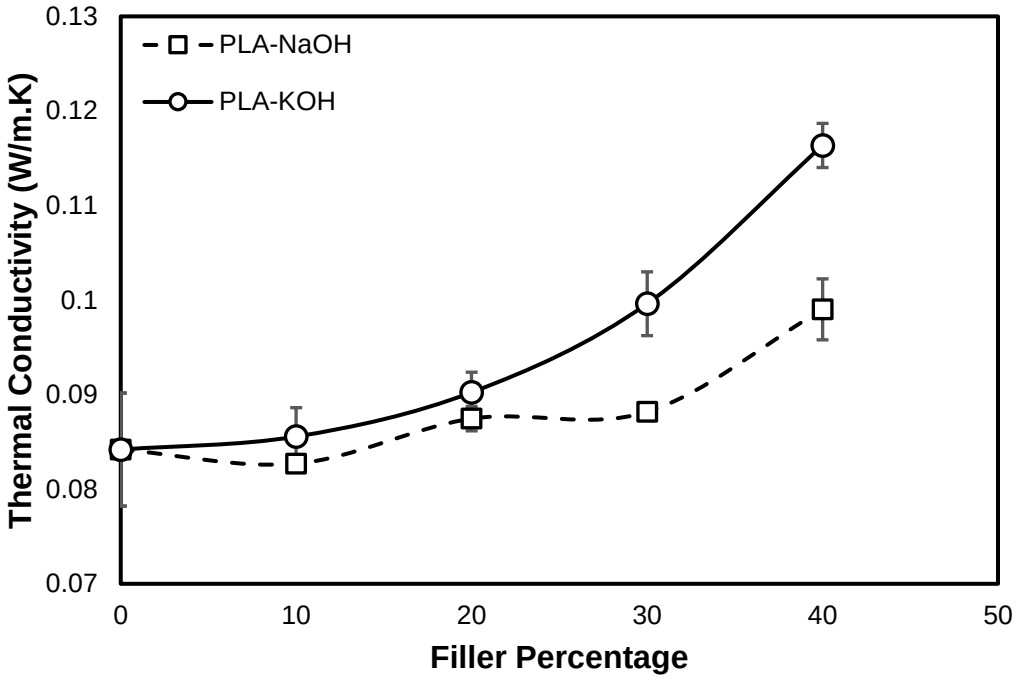

Figure 25: Thermal conductivity for PLA-NaOH and PLA-KOH

4.1.5 DSC

DSC test was done for all the samples from the three systems, which are PLA-UTDPWF, PLA-NaOH, and PLA-KOH. In Figure 26 and Figure 27, the two heating cycles are plotted, with the glass transition (T_g) region bracketed in the box. The thermal characters are presented in Table 3 below for the PLA-UTDPWF. The T_g fluctuates with the maximum value reaching 60.38, at 30 wt.% loadings. For the

melting point T_m, it varies slightly among the composites, in the range between 168 and 170 °C. The crystallinity for the 1st heating cycle increases as the filler percentage increase, except for the 30 wt.%, where it drops significantly. An identical trend is noticeable for the 2nd heating cycle, with a slight decrease in the values. The crystallization was calculated using the following equation:

$$\frac{\Delta H_m}{\varphi_{PLA} \cdot \Delta H_m^0} \qquad (2)$$

Where φ represents the PLA fraction, while ΔH_m^0 represents the standard enthalpy of PLA at 100% crystallinity, which is equivalent to 93.7 J/g [69].

Table 3: Results for thermal characterization of PLA-UTDPWF system

DWF wt.%	**T_g (°C)**	**T_m 1st (°C)**	**T_m 2nd (°C)**	**ΔH_m 1st (J/g)**	**ΔH_m 2nd (J/g)**	**X_c 1st (%)**	**X_c 2nd (%)**
0%	60.72	168.23	168.36	37.28	34.77	40.09	37.39
10%	57.9	169.62	168.2	36.78	34.33	43.94	41.01
20%	56.19	170.41	167.86	40.47	37.91	54.40	50.95
30%	60.38	168.48	170.92	29.63	25.89	45.52	39.77
40%	57.82	168.22	166.97	35.30	29.70	63.26	53.23

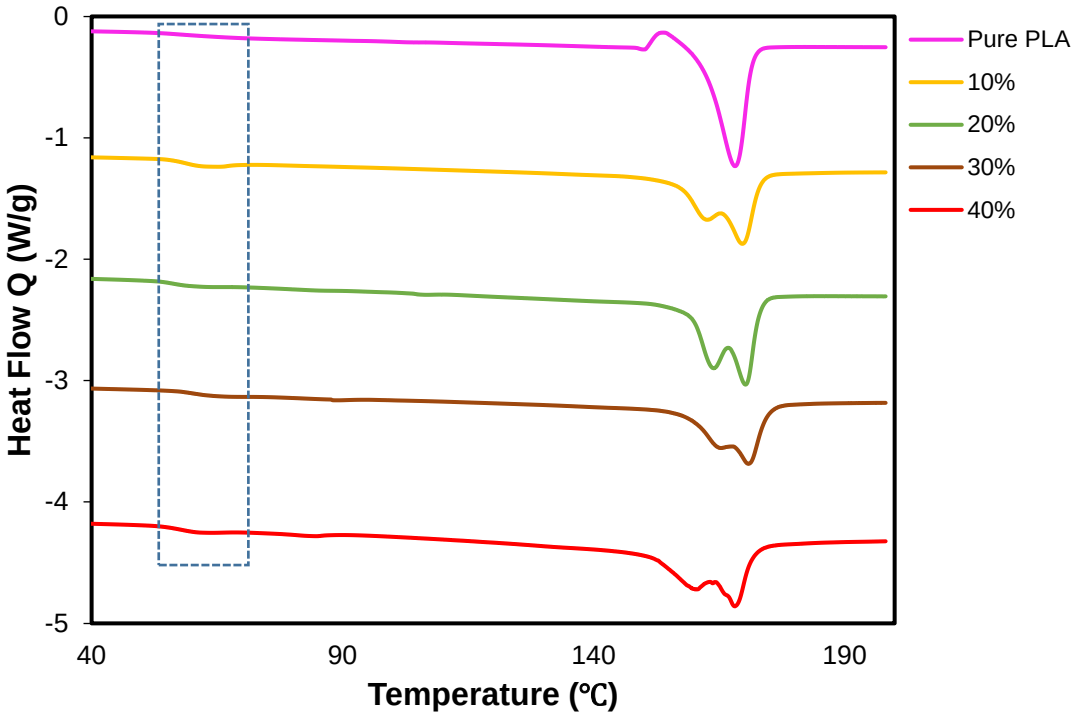

Figure 26: DSC graphs for PLA and PLA-UTDPWF 1st cycle

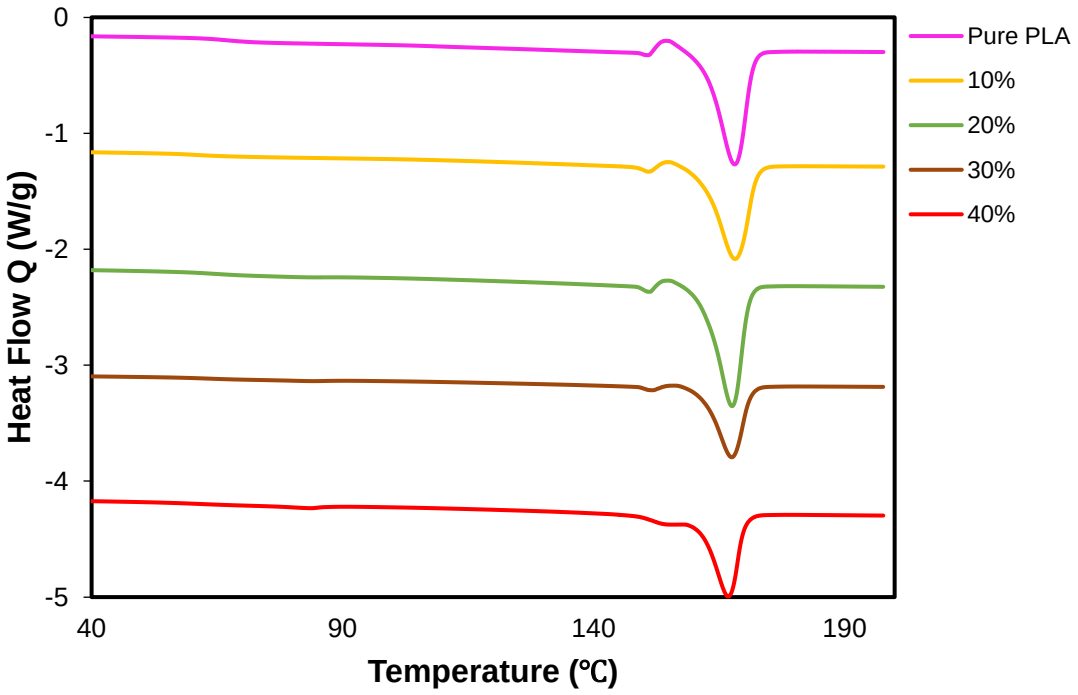

Figure 27: DSC graphs for PLA and PLA-UTDPWF 2nd cycle

For the PLA-KOH system. The T_g increases slightly with the introduction of the filler at 10 wt.% to 62.07℃, when compared to pure PLA which has a T_g of 60.72℃. However, it then drops for the 20 and 30 wt.%, and then slightly increase for the 40 wt.%. For the crystallinity, it follows a clear trend where the crystallinity increases as the filler percentage increase in the first heating cycle. In the second heating cycle, the crystallinity varies from the 1st and fluctuates with no clear trend. The graphs for the 1st and 2nd heating cycles of PLA-KOH system are presented in Figure 28 and Figure 29 below, and the results are summarized in Table 4.

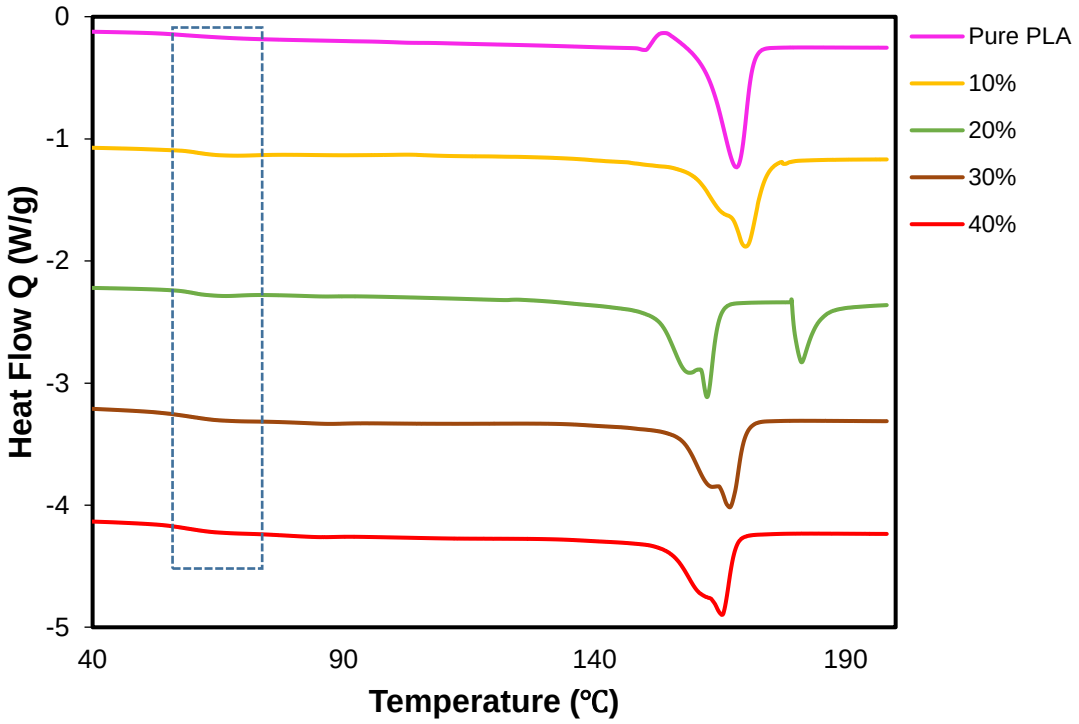

Figure 28: DSC graphs for PLA and PLA-KOH 1st cycle

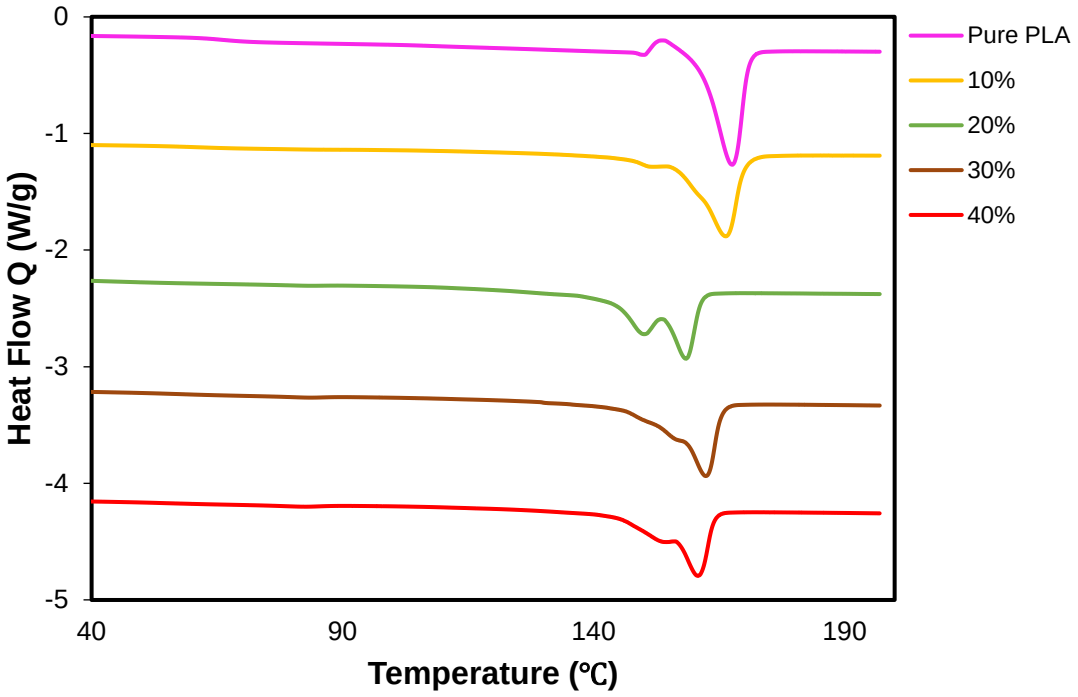

Figure 29: DSC graphs for PLA and PLA-KOH 2nd cycle

Table 4: Results for thermal characterization of PLA-KOH system

DWF wt.%	T_g (℃)	T_m 1st (℃)	T_m 2nd (℃)	ΔH_m 1st (J/g)	ΔH_m 2nd (J/g)	X_c 1st (%)	X_c 2nd (%)
0%	60.72	168.23	168.36	37.28	34.77	39.79	37.12
10%	62.07	170.12	166.96	39.71	38.77	47.09	45.97
20%	60.76	162.36	159.11	40.29	32.36	53.75	43.16
30%	58.52	166.78	162.98	38.79	33.77	59.14	51.48
40%	58.55	165.33	161.53	34.56	28.54	61.47	50.77

The results for the PLA-NaOH system show a fluctuation in the glass transition temperature and the melting point from both heating cycles, the first and the second. For the crystallinity, it increases as the filler weight percentage increase up to 20 wt.%

filler content, reaching around 61%, for the first heating cycle. Later, it drops for the 30 and 40 wt.%. In the second heating cycle, there is a slight drop in the crystallinity at 20 wt.%. However, the trend is similar. The increase in the crystallinity for the composites is due to the filler acting as a nucleating agent. Moreover, in both heating cycles, the T_g does not appear, except for the 10 wt.% sample in the first heating cycle, besides the pure PLA. The graphs for the 1st and 2nd heating cycles of PLA-NaOH system are presented in Figure 30 and Figure 31 and summarized in Table 5.

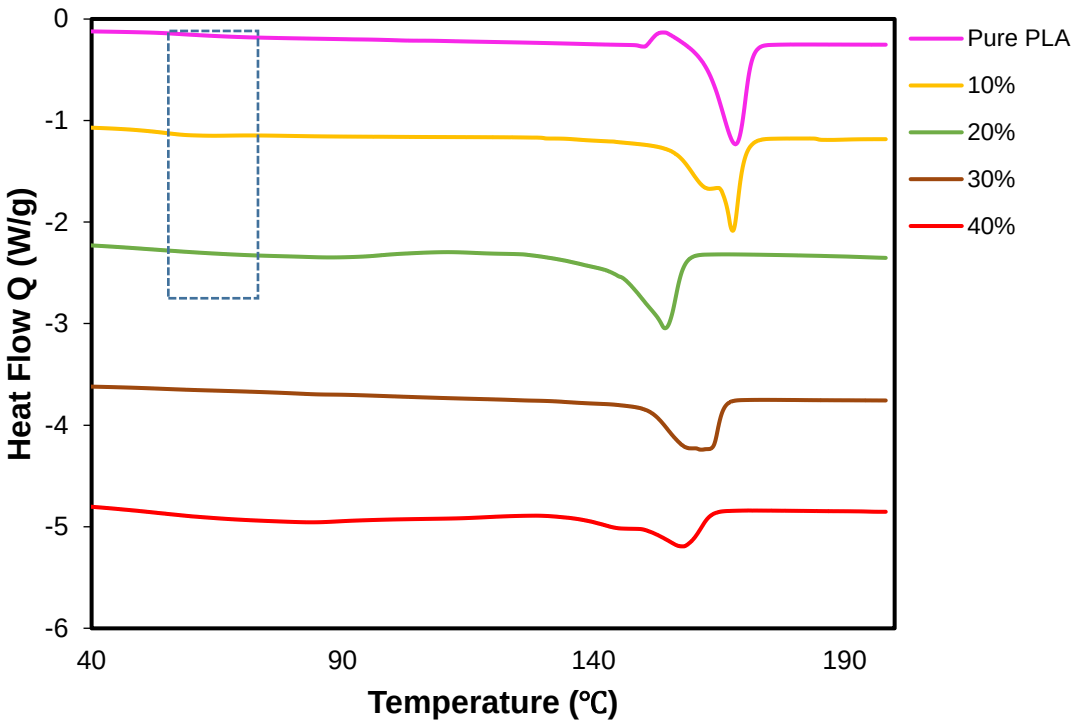

Figure 30: DSC graphs for PLA and PLA-NaOH 1st cycle

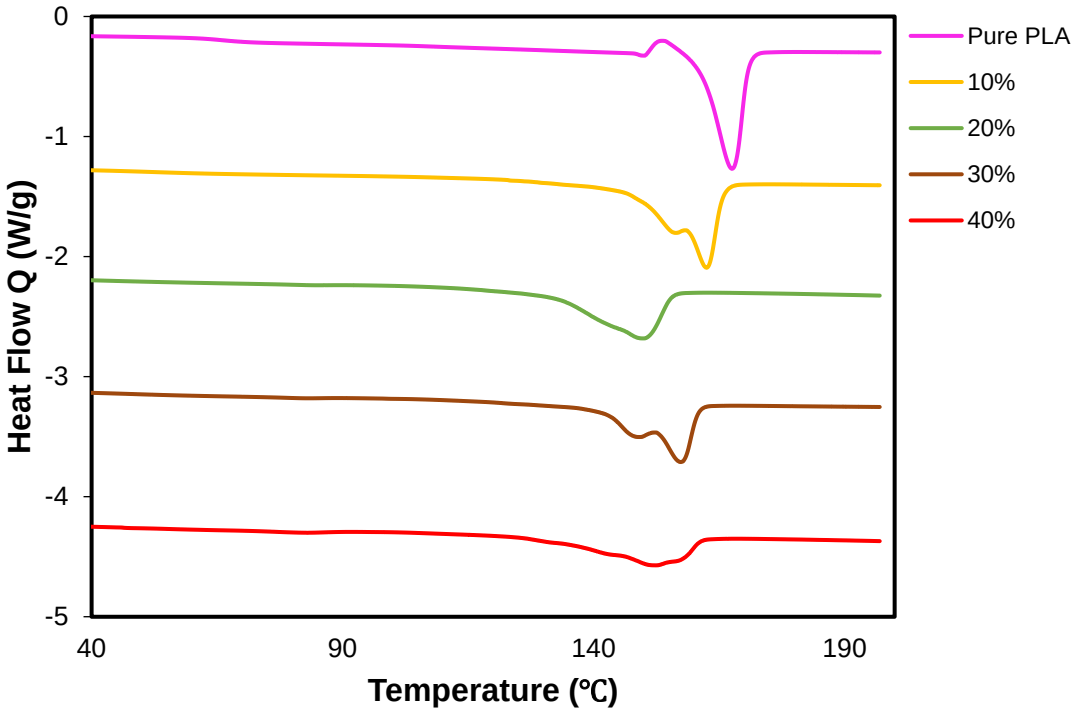

Figure 31: DSC graphs for PLA and PLA-NaOH 2nd cycle

Table 5: Results for thermal characterization of PLA-NaOH system

DWF wt.%	T_g (℃)	T_m 1st (℃)	T_m 2nd (℃)	ΔH_m 1st (J/g)	ΔH_m 2nd (J/g)	X_c 1st (%)	X_c 2nd (%)
0%	60.72	168.23	168.36	37.28	34.77	39.79	37.11
10%	54.06	167.37	162.97	43.64	43.48	51.75	51.56
20%		154.07	150.48	45.42	32.52	60.59	43.38
30%		161.56	158.07	37.84	30.24	57.69	46.1
40%		157.82	153.09	29.16	23.19	51.86	41.24

4.1.6 Density

The density was measured for the samples with different percentages and the results are shown in Figure 32 below. For the PLA-UTDPWF, there is a clear trend where the

density increases as the filler increase. This can be associated with the fulfillment of the air voids in the PLA by the fibers.

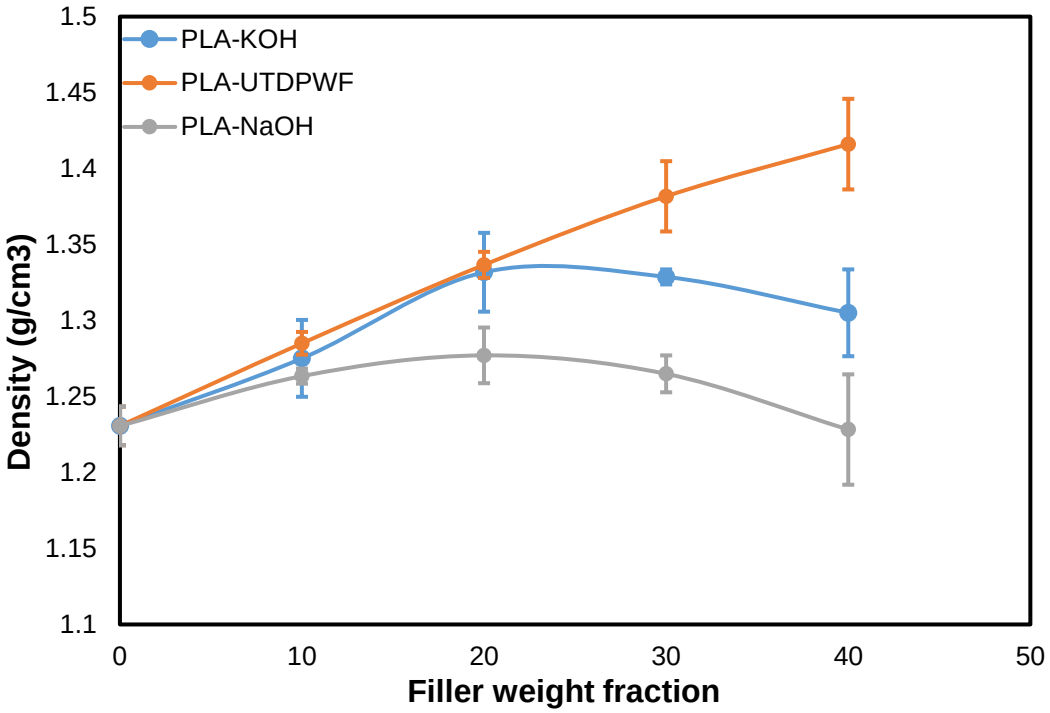

Figure 32: Density for PLA-UTDPWF, PLA-KOH, and PLA-NaOH

On the other hand, the density for the PLA-KOH and PLA-NaOH decreased after the 20 wt.% filler. This may happen because of the higher ratio of cellulose which made the treated filler less dense when compared to the untreated samples. After the 20 wt.%, the effect of the fulfillment of air voids in the composite was overwhelmed by the effect of the relatively low-density treated filler, which leads to lower density for the 30 wt.% and 40 wt.%. This is because the filler started to take huge portion of the volume of the composite, and the density of the filler is lower than the density of the matrix.

4.1.7 Specific Heat Capacity (Cp) and Thermal Diffusivity (α)

For the diffusivity, it was calculated using the following equation:

$$\alpha = \frac{k}{\rho . C_p} \quad (3)$$

The trend for the C_p was inversely proportional to the thermal conductivity. While the diffusivity, it increased with the addition of the filler to the polymer for both PLA-KOH and PLA-NaOH as displayed in Figure 33 and Figure 34 and summarized in Table 6 and Table 7.

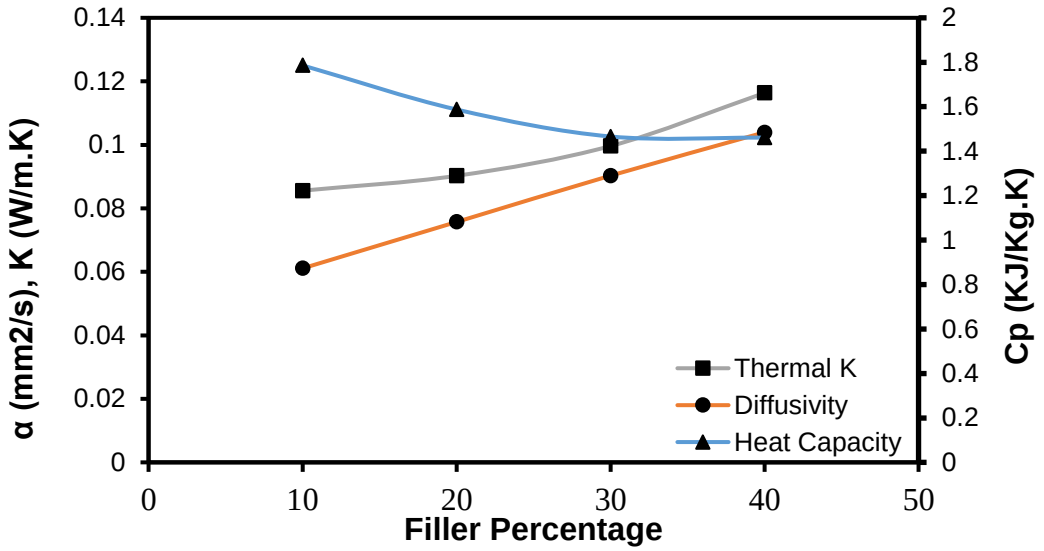

Figure 33: K, Cp, Density and α for PLA-KOH system

Table 6: K, Cp, Density and α for PLA-KOH

DWF wt. %	K (W/m.K)	Cp (J/g.K)	ρ (g/cm^3)	α (mm^2/s)
0	0.084	1.333	1.231	0.0778
10	0.086	1.786	1.275	0.061
20	0.090	1.588	1.332	0.076
30	0.10	1.466	1.329	0.090
40	0.116	1.461	1.305	0.104

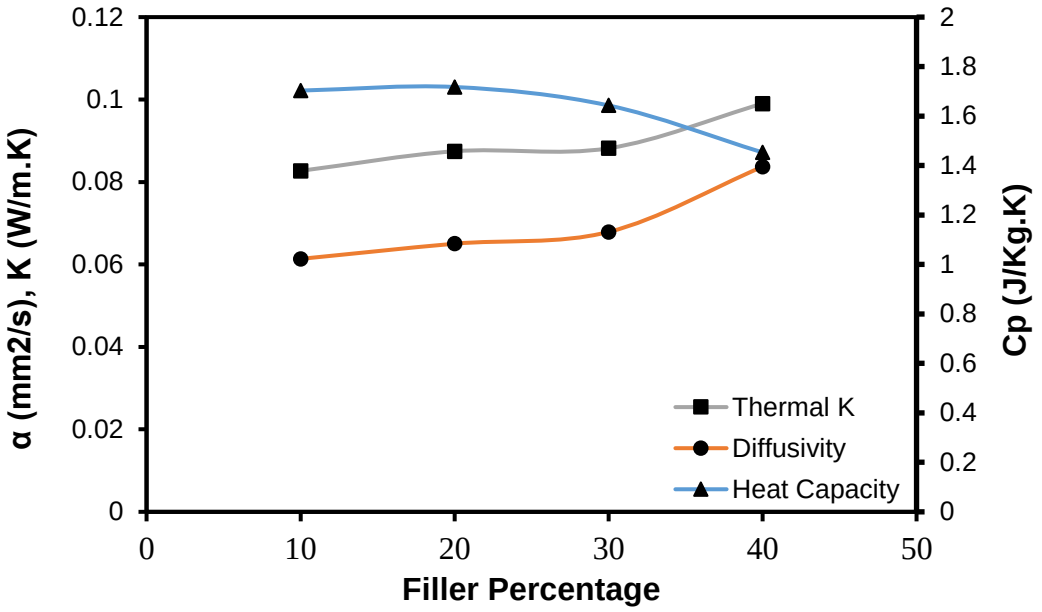

Figure 34: K, Cp, Density and α for PLA-NaOH system

Table 7: K, Cp, Density and α for PLA-NaOH

DWF wt. %	K (W/m.K)	Cp (J/g.K)	ρ (g/cm^3)	α (mm^2/s)
0	0.0841	1.333	1.231	0.078
10	0.083	1.703	1.263	0.061
20	0.087	1.718	1.277	0.065
30	0.0881	1.643	1.265	0.068
40	0.099	1.453	1.228	0.084

4.1.8 TGA

For the Thermogravimetric analysis, it was found that the PLA-NaOH with 20 wt.% filler sample degrades first when compared to other tested samples. The PLA-NaOH starts degrading at a temperature of 226℃ and loses 80% of its weight at a temperature of 295℃. PLA-KOH with the same filler content degrades at a higher temperature,

starting from around 250°C, and losses 80% of its total weight at around 333°C. The neat PLA and PLA-UTDPWF both start degrading at around 280°C, and losses 80% of its total weight at around 350°C. It is obvious that the treatment caused removal of particles and impurities that were dissolved in the treatment solution. Thereby, the treated samples started degradation at lower temperatures. The results are displayed in Figure 35 below.

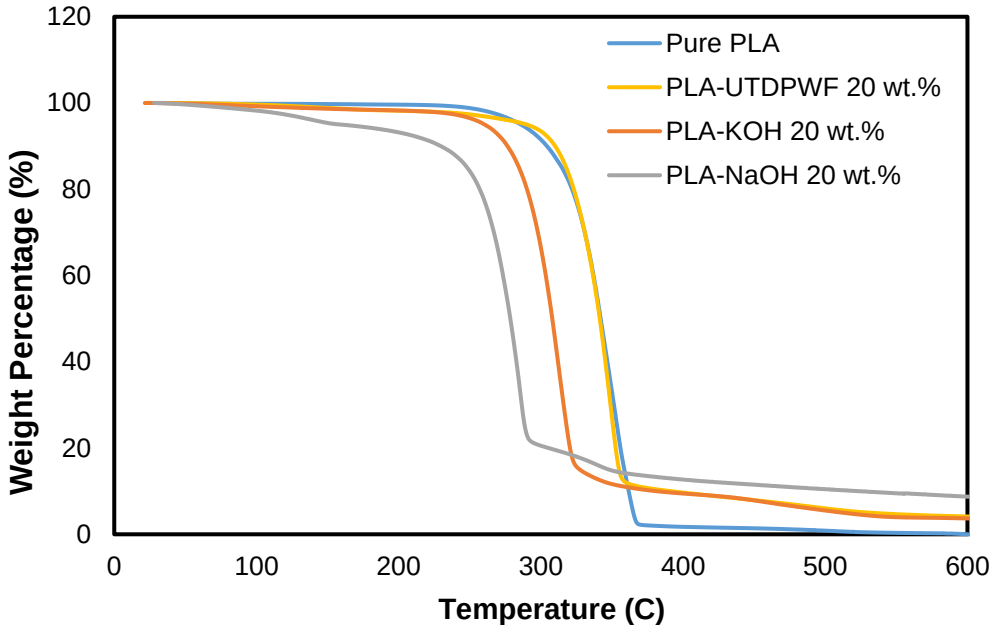

Figure 35: TGA graphs for neat PLA and composites with 20 wt.% filler

For the DTG, it shows that pure PLA losses the maximum weight at around 350°C, which amounts to 43% of its initial weight. At the same temperature, the maximum weight loss takes place for PLA-UTDPWF. However, it is accounted for only 27% of the total weight. For PLA-NaOH, it losses a maximum of 26%, at around 268°C. Lastly, PLA-KOH losses at 315°C around 25% of its weight. The results are displayed in Figure 36 below.

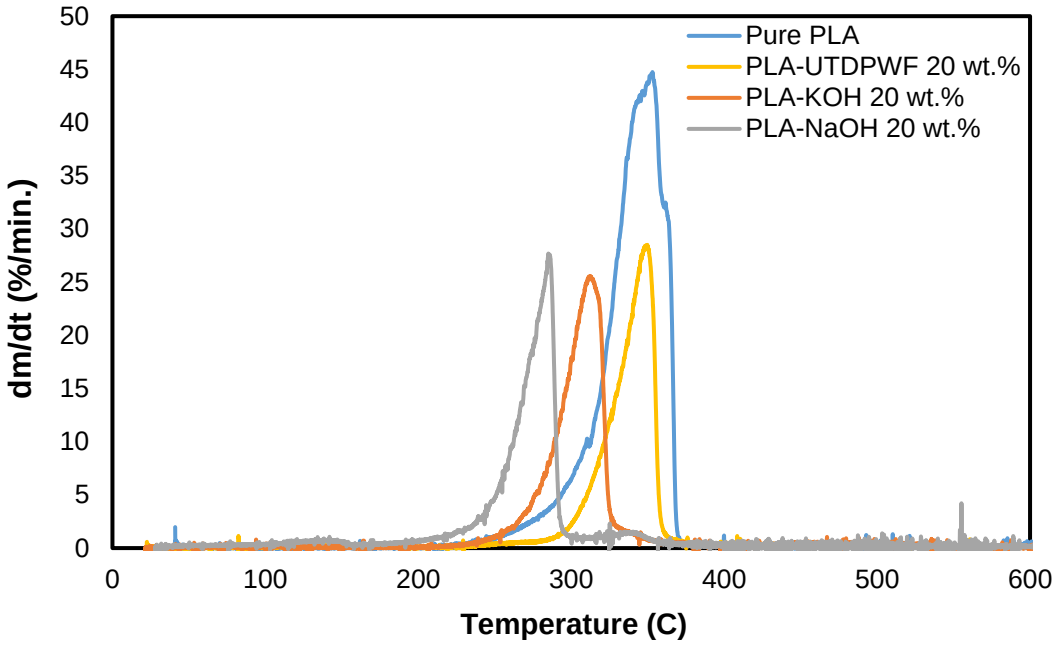

Figure 36: DTG graph for neat PLA and composites with 20 wt.% filler

For the fiber material, the test was taken to a temperature of 800℃ since the material did not show high degradation at 600℃. All the three fille material starts losing mass at around 217℃. However, the NaOH and KOH treated samples degrade at a faster rate than untreated date wood fiber, with NaOH achieving the lowest final residue with around only 13% at 800℃. The results are displayed in Figure 37.

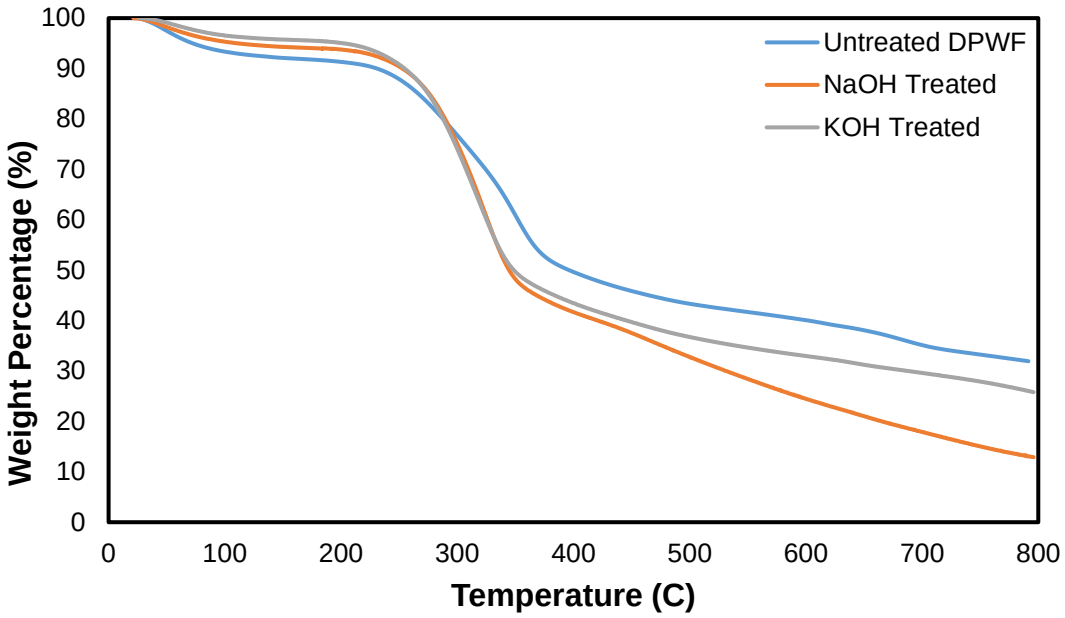

Figure 37: TGA for untreated, KOH, and NaOH treated fiber

For the DTG, it shows that the highest degradation occurs at around 350℃ for raw filler, with only 8% mass loss. For alkaline treated samples, the maximum degradation takes place at around 320℃, with only 6% mass loss. Moreover, there is a very high noise noted in the treated filler samples at high temperatures. The results are presented in Figure 38 below.

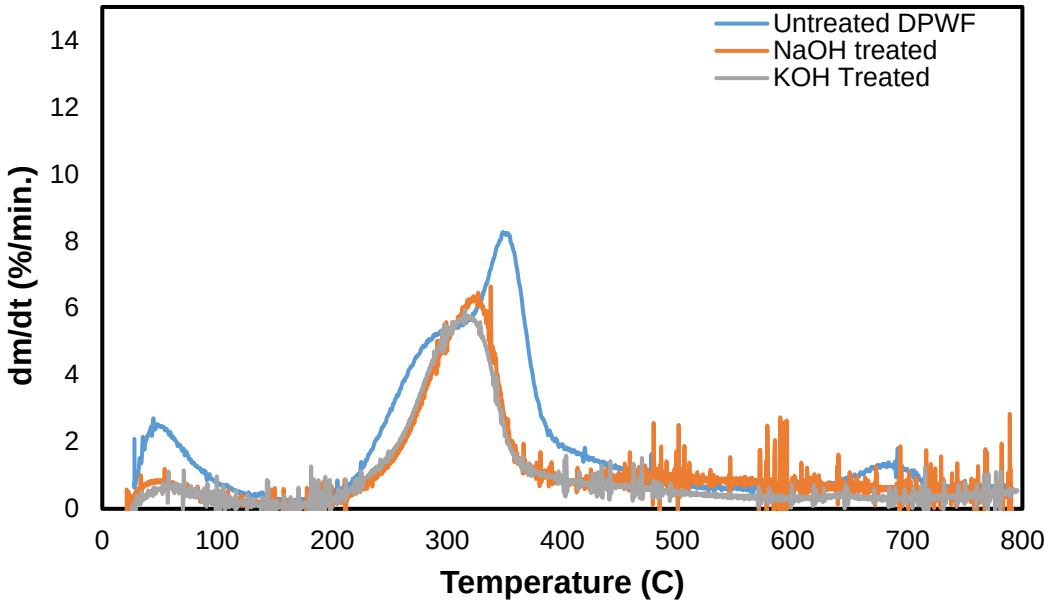

Figure 38: DTG for untreated, KOH, and NaOH treated fiber

4.1.9 Mechanical Properties

For the compression strength in the untreated system, it decreases at 20 wt.% compared to 10 wt.%. Nevertheless, it increases at 30 wt.% and then slightly declines at 40 wt.% filler material. However, for the KOH system, the strength decreases as the filler percentage increases until the 30 wt.%, then it slightly increases for the 40 wt.% loading. On the other hand, the NaOH treated samples compression strength decreases at 20 wt.% compared to the 10 wt.% and then it keeps increasing until 40 wt.% filler. In all the percentages, PLA-KOH achieved higher compression strength than the PLA-NaOH samples as shown in Figure 39 below. There is a correlation between this trend and the density trend, in which they are inversely proportional. At filler percentage exceeding 20 wt.%, samples had lower density, which was linked to higher cellulose content. The increase in the mechanical strength can be associated with the cellulose acting as reinforcement for the composite.

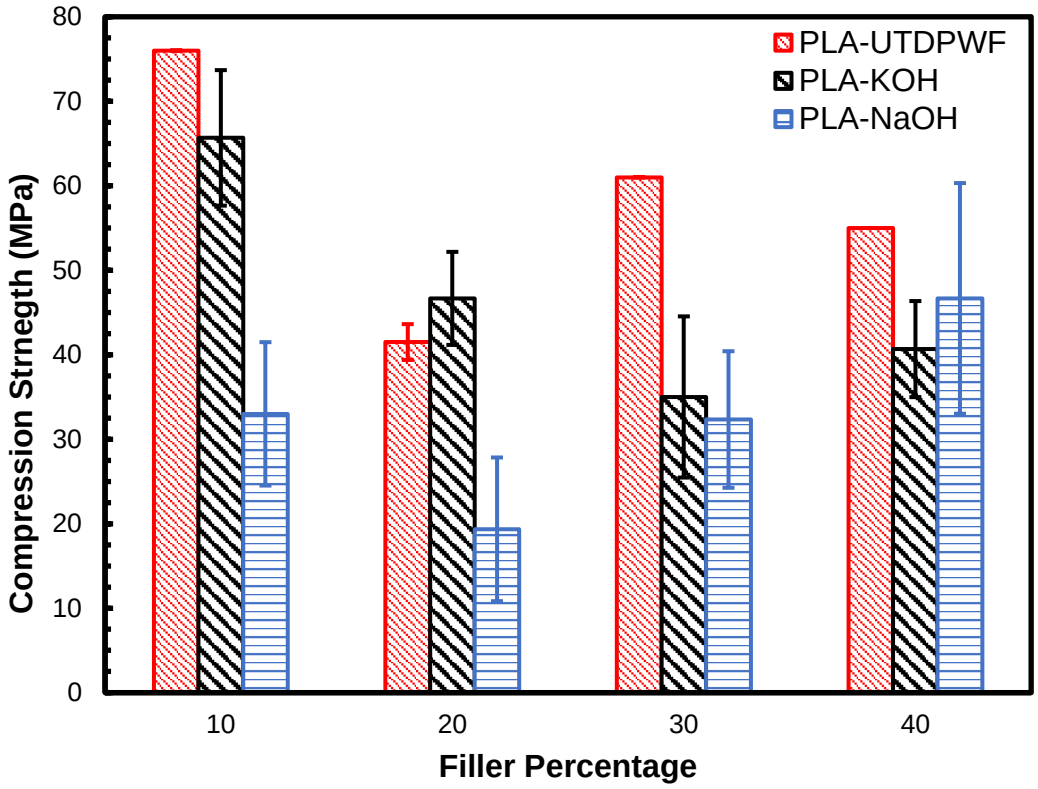

Figure 39: Compression strength versus filler percentage for PLA-KOH and PLA-NaOH

For the compression strain, it was noted that the strain is almost consistent, except for a slight increase at the 30 wt.% filler as illustrated in Figure 40 below. PLA-KOH exhibited higher strength than PLA-NaOH and the untreated samples across all filler wight fractions. Finally, for the young modulus, the trend is similar to the trend of the compression strength, due to the consistent strain property Figure 41 below.

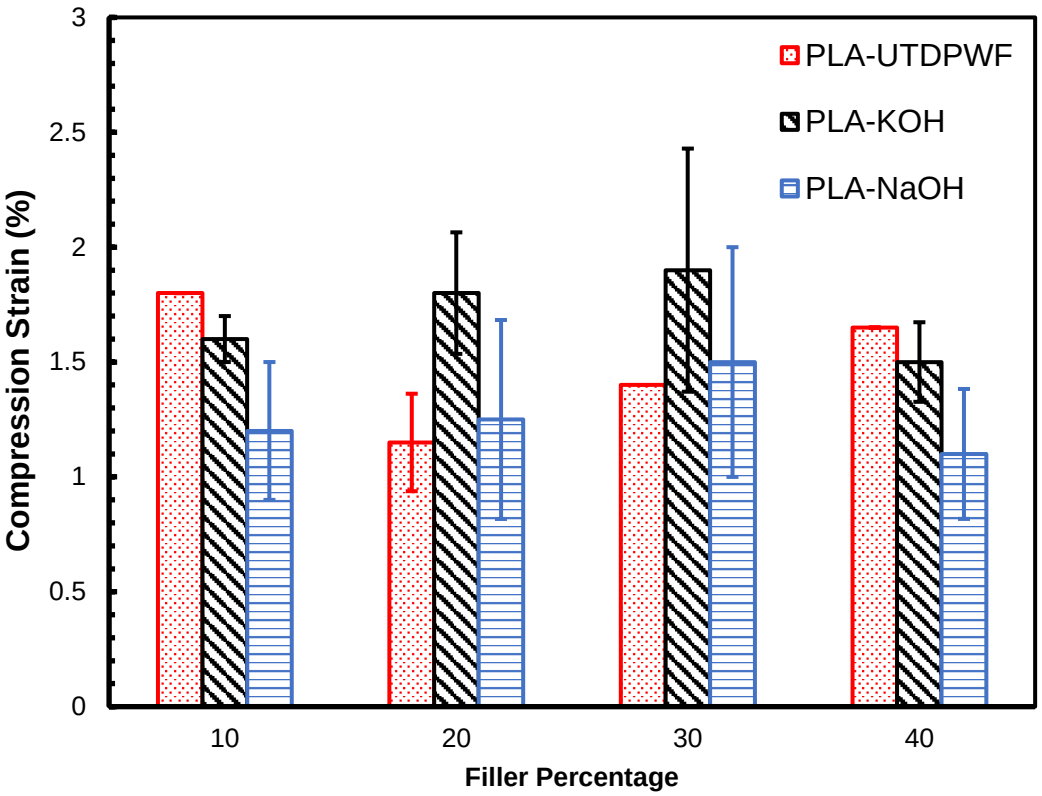

Figure 40: Compression strain versus filler percentage for PLA-KOH and PLA-NaOH

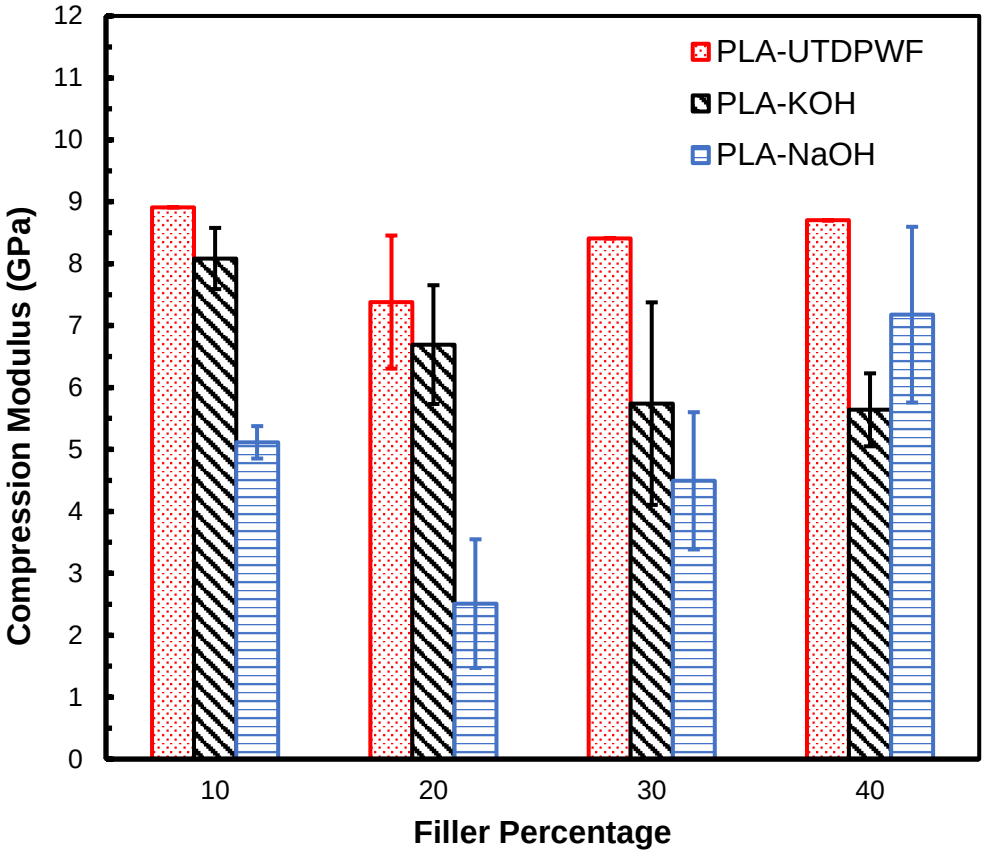

Figure 41: Young modulus versus filler percentage for PLA-KOH and PLA-NaOH

4.1.10 Water Retention

Water retention was applied for the samples, to investigate the absorption capability of the composites. Because of the hydrophilic nature of the filler, as the filler increased, the water retention increased as well. A similar trend is found for both hot and cold-water immersion. For the cold-water retention, Figure 42 below shows that the PLA-KOH samples had water retention after 48 hours ranging from 0.5%, to 4.5%, for the 10 wt.%, and 40 wt.% filler content, respectively. On the other hand, hot-water retention at 50℃ resulted in higher absorption as illustrated in Figure 43 below, ranging from 2.5% to 12.5%, for the 10 wt.% and 40 wt.% filler content, accordingly.

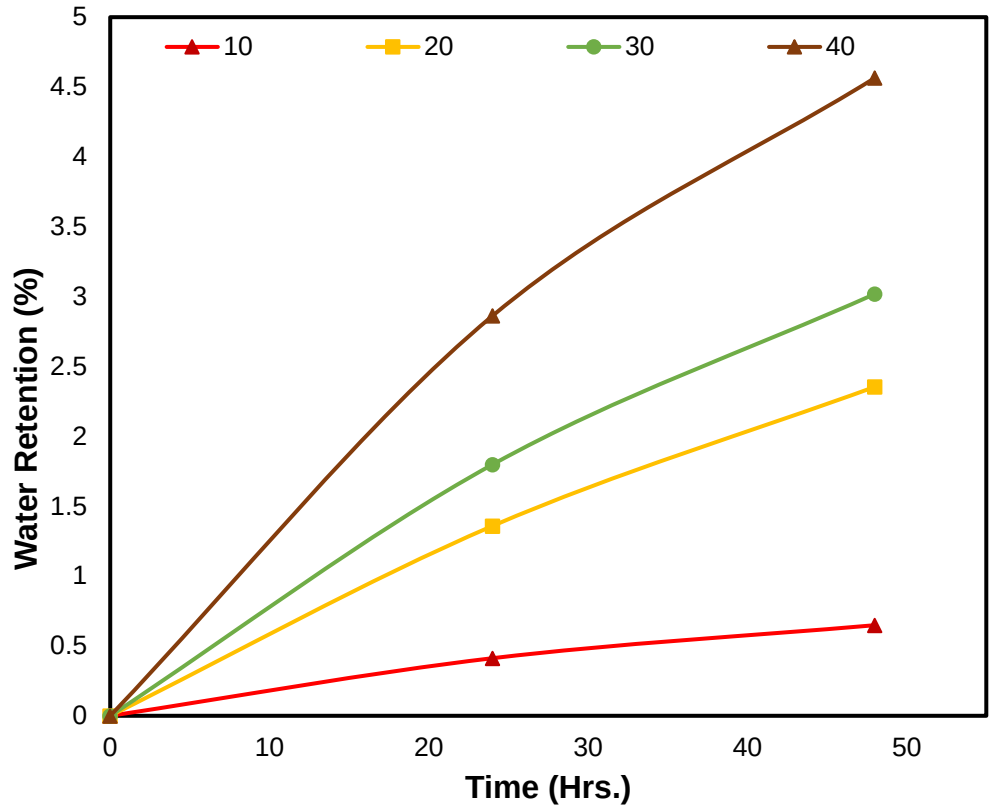

Figure 42: Cold Water Retention for PLA-KOH system

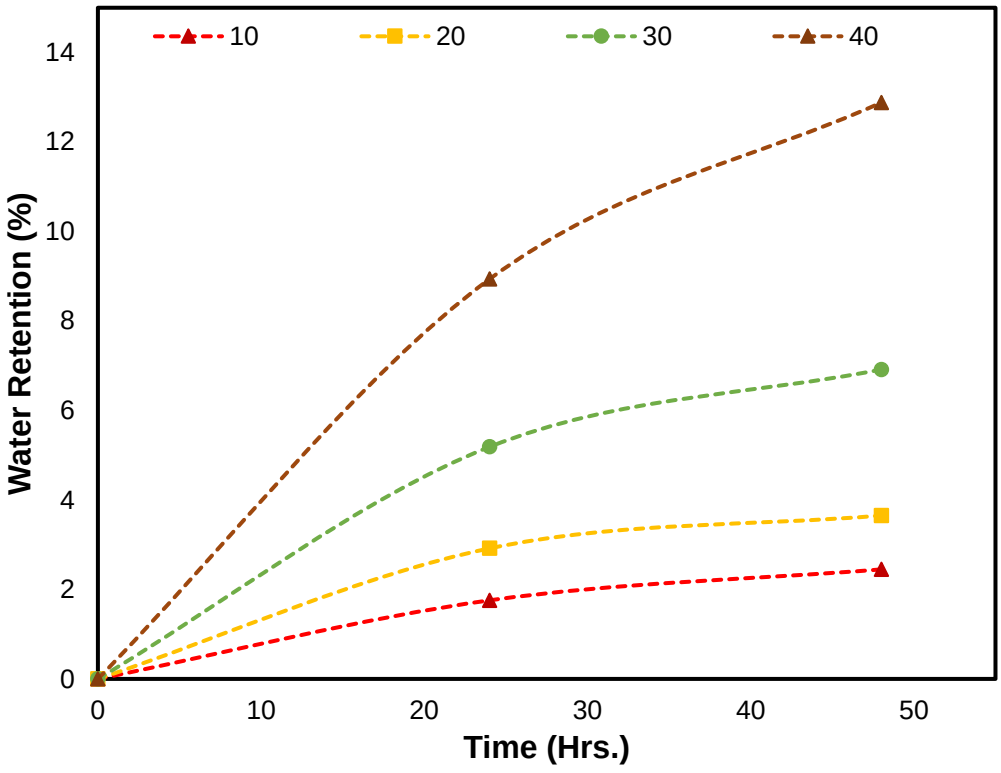

Figure 43: Hot Water Retention for PLA-KOH system

For PLA-NaOH composites, the samples showed extremely high-water intake, when compared to untreated and PLA-KOH composites. For cold-water retention, the water intake after 48 hours was ranging from 2.35% to 22.2%, for 10 wt.% and 40 wt.%, respectively, as shown in Figure 44 below. Moreover, hot-water retention was more extreme, with water intake ranging from around 14% for the 10 wt.% filler, up to 42% for the 40 wt.% filler as Figure 45 illustrates below. Figure 46 shows the effect of the treatment on the 20 wt.% sample.

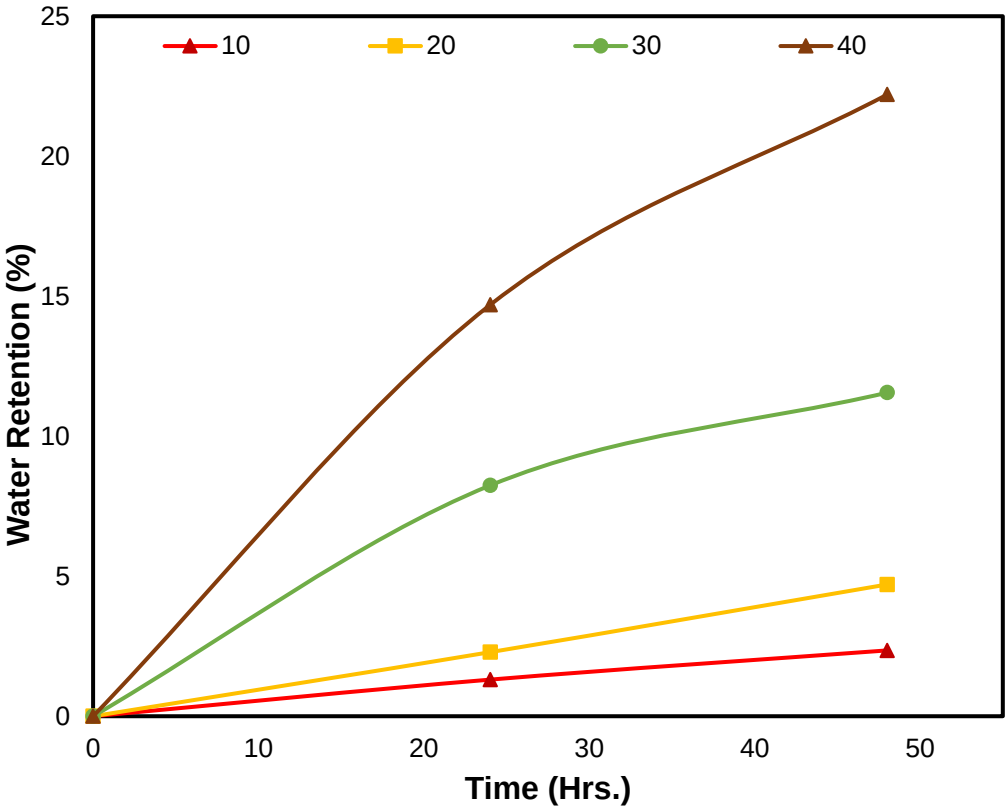

Figure 44: Cold Water Retention for PLA-NaOH system

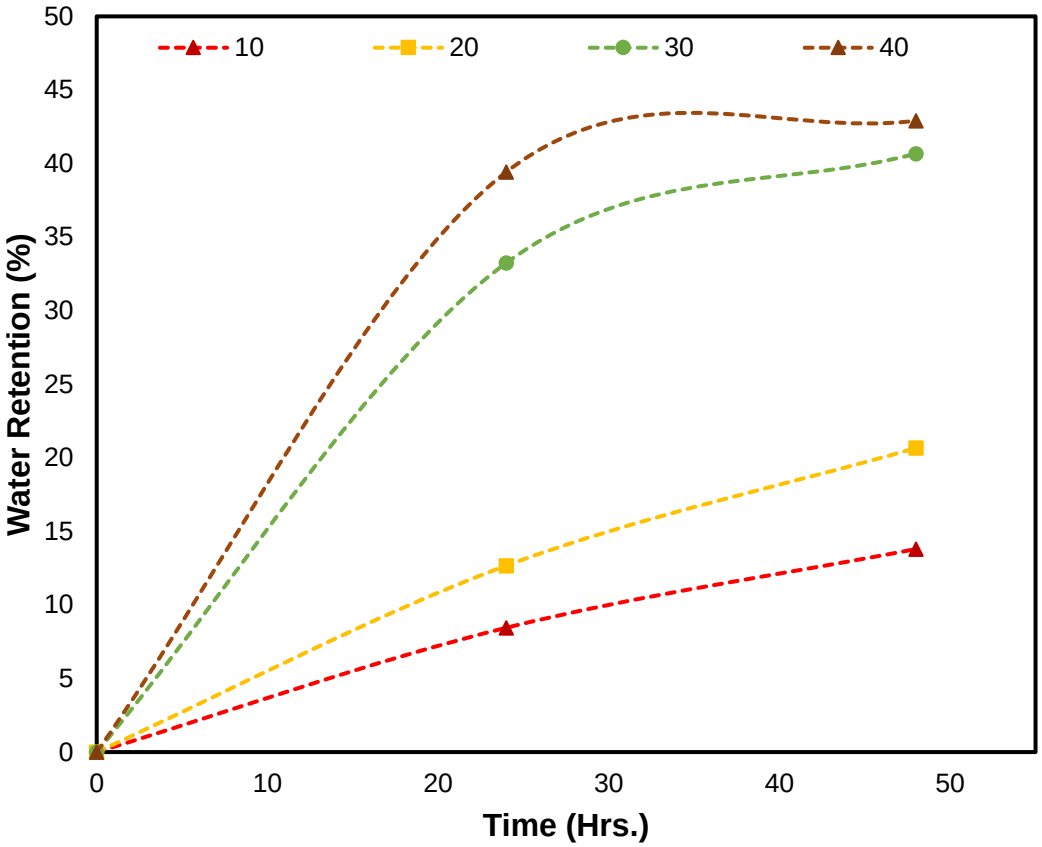

Figure 45: Hot Water Retention for PLA-NaOH system

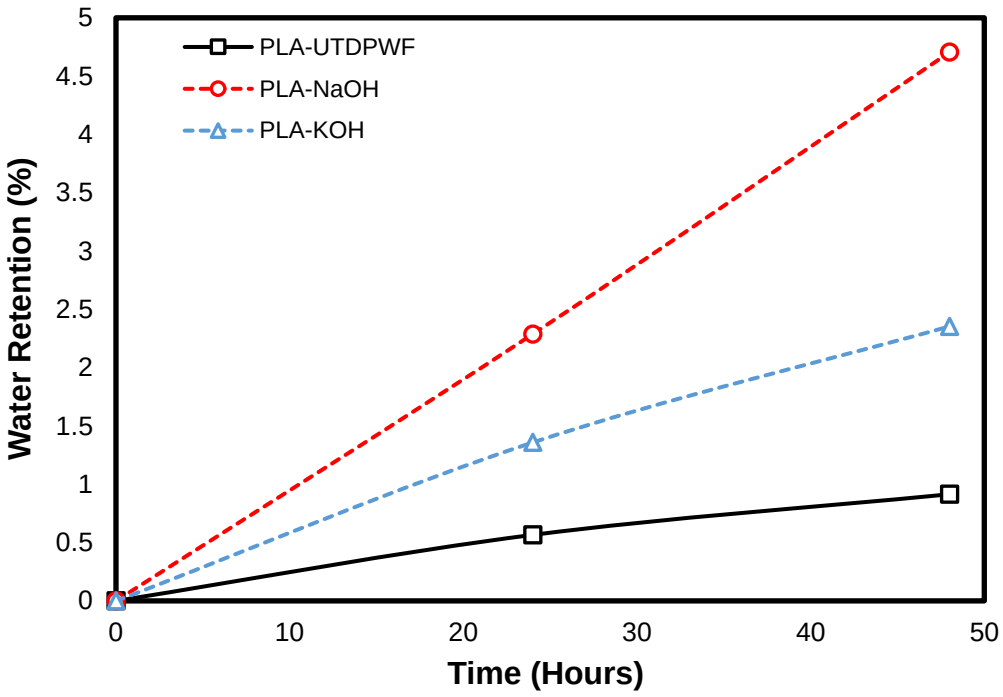

Figure 46: Effect of Treatment on the 20 wt.% samples

4.2 PLA-UTDWF, PLA-SA, and PLA-SE systems

4.2.1 FTIR

Fourier Transform Infrared test was done on the untreated filler, and SE treated. Moreover, it was also done to the 20 wt.% filler samples of the 3 systems, PLA-UTDPWF, PLA-SA, PLA-SE, and pure PLA. For pure PLA, the peaks in the range between 1163-1210 are associated with the C—O stretching. Moreover, the peak within the 1715-1730 wavelength represents the C=O carbonyl group. The peaks in the range of 2840-3000 wavelengths are associated with C—H stretching. Finally, the beaks within 3330-3500 are linked to O—H carboxylic acid functional group [70]. For the silane-treated filler, it is noticeable that the O—H functional group intensity is lower when compared to untreated filler as demonstrated in Figure 47 below. This indicates that the treatment was successful in lowering the moisture intake in the filler, which will lead to better compatibility with the PLA matrix.

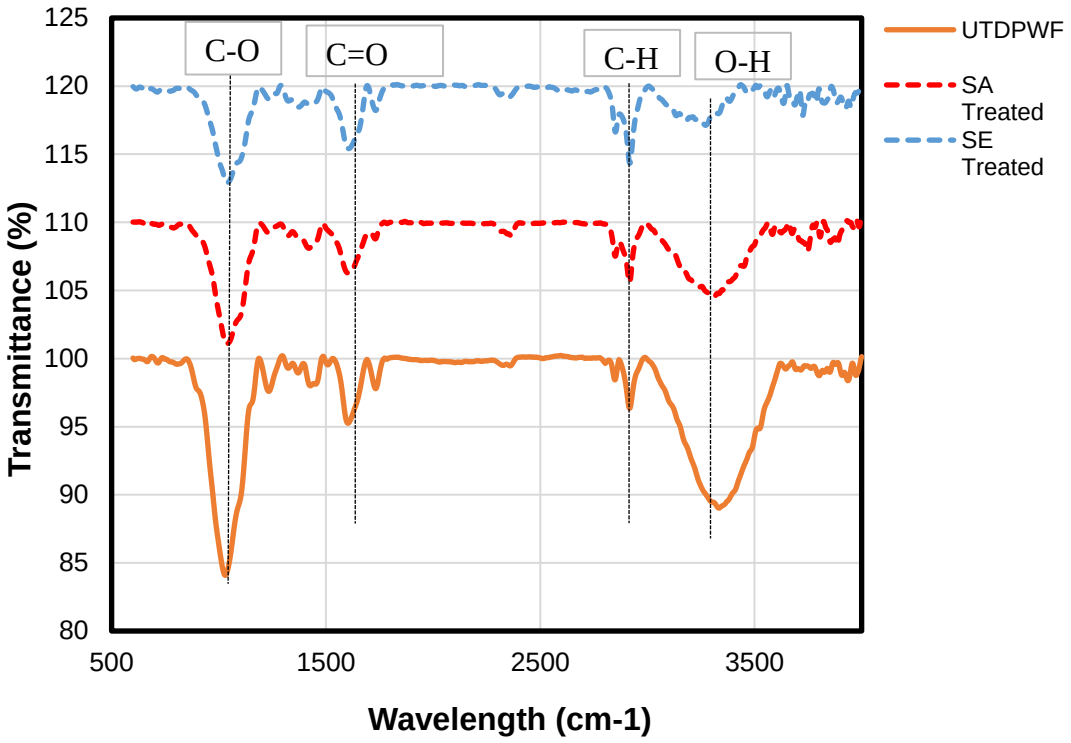

Figure 47: FTIR for UTDPWF, SE and SA treated

Given the structure of PLA below in Figure 48, all the above-mentioned functional groups are typical and expected.

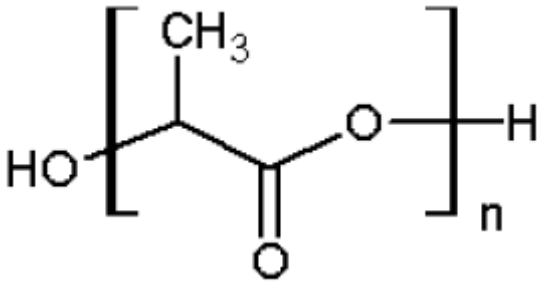

Figure 48: PLA Structure

For the composites, [71] noted a small peak in the range between 1000 and 1300 cm^{-1} in his work for the cellulose samples treated with APTES, when compared with the untreated samples, which corresponds to C-N functional group, due to the amino group

in the APTES. This peak is obvious also in our composites. Moreover, [71] asserts that the peak at around 1730 cm^{-1}, which reflects the C=O functional group, is associated also with hemicellulose. It is noted in our composites that this peak has a higher intensity in untreated and Silane-Ethanol treated composites, compared to Silane-Acetone, which indicates higher removal of hemicellulose in the SA treatment. While cellulose is crystalline, hemicellulose is amorphous. Thereby, reducing the content of hemicellulose increases crystallinity, which will be illustrated later in section 4.2.5. moreover, the O—H functional group is more intense in the PLA and PLA-UTDPWF compared to treated samples as demonstrated in Figure 49 below, which indicates lower moisture intake and better compatibility. this led to higher thermal conductivity and better mechanical properties as will be shown in the following sections.

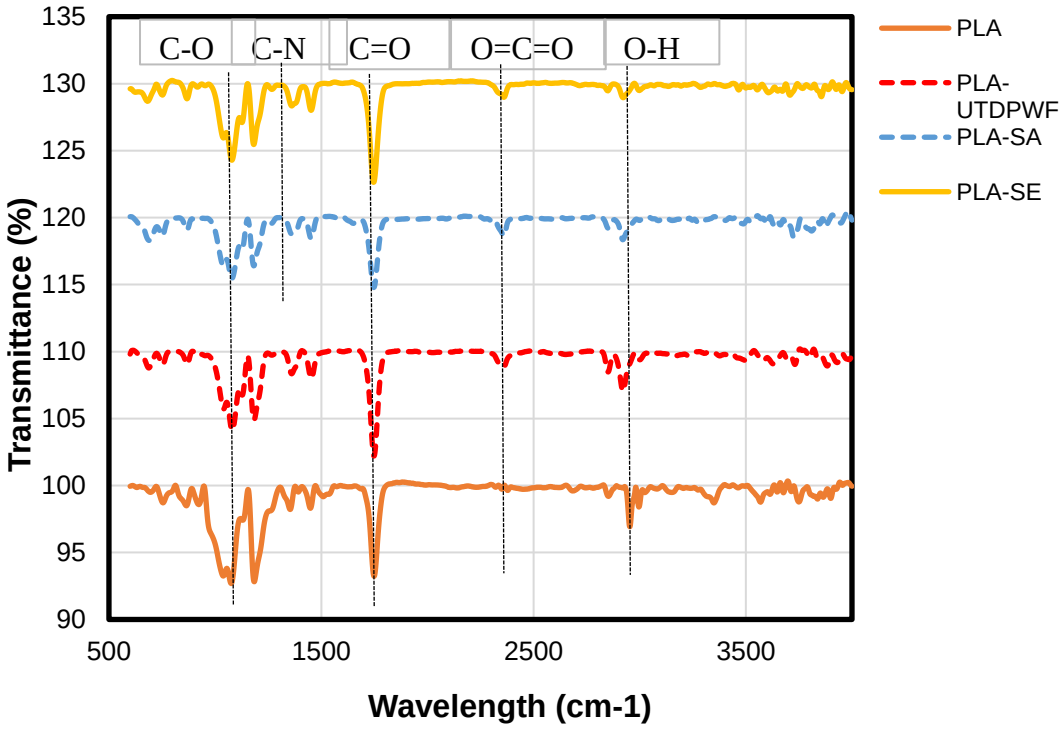

Figure 49: FTIR for Pure PLA and 20 wt.% of PLA-SE, PLA-SA, and PLA-UTDPWF

4.2.2 SEM

SEM displayed in Figure 50 below, shows the silane coating stains of the surface of the wood particles, compared to untreated filler. Moreover, particles and impurities were also partially removed due to the presence of silane and ethanol solvents.

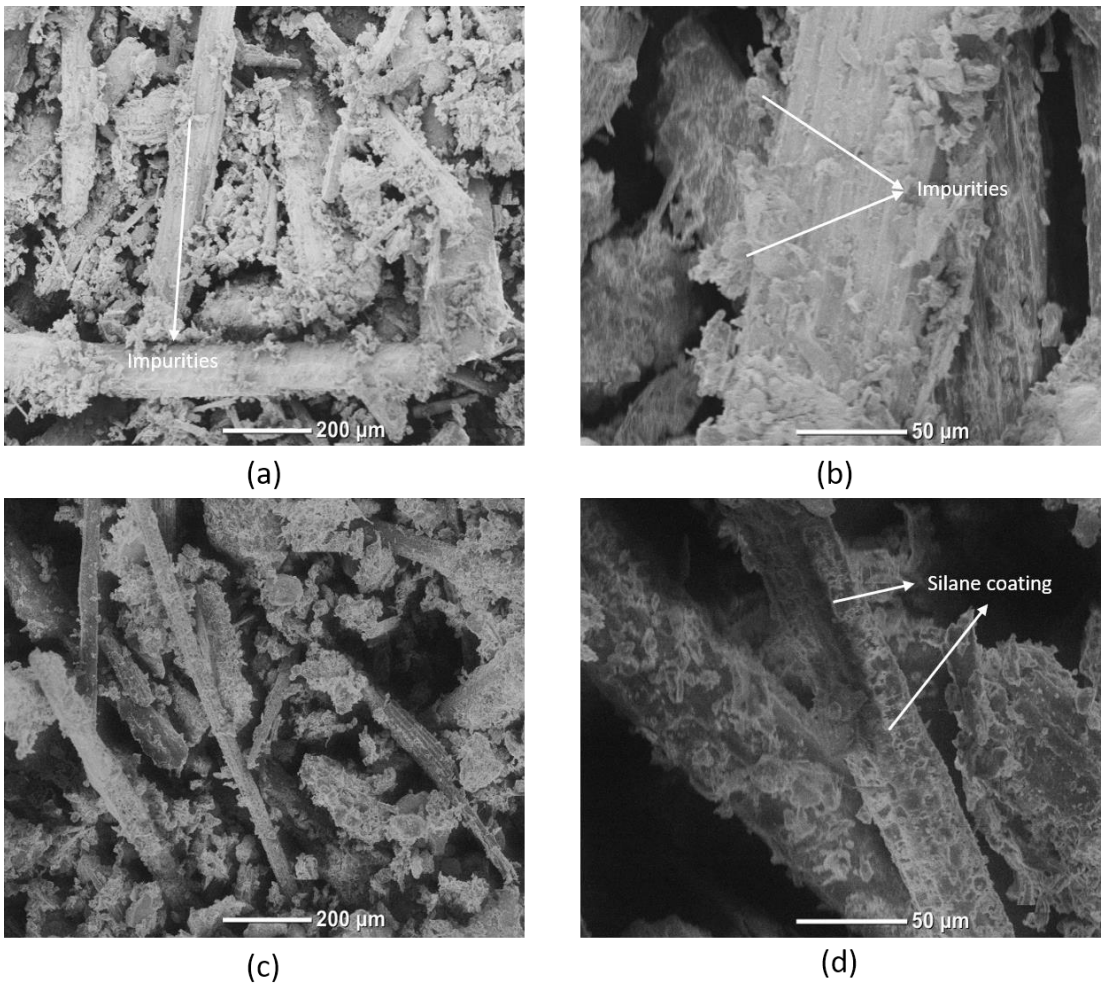

Figure 50: SEM for UTDPWF (a) and (b), SE treated fiber (c) and (d)

The SEM exhibited in Figure 51 below is for the 20 wt.% filler sample, with two magnifications which are x 100 and x 500. The roughness and poor compatibility between the filler and the matrix are obvious when at x 500 magnification. For the PLA-SA sample, it is noticeable that the compatibility is enhanced in the third picture,

in which there is no huge gap or void between the matrix and the filler particle. A similar observation is found for the PLA-SE sample in the fourth picture, where the crack is not very huge.

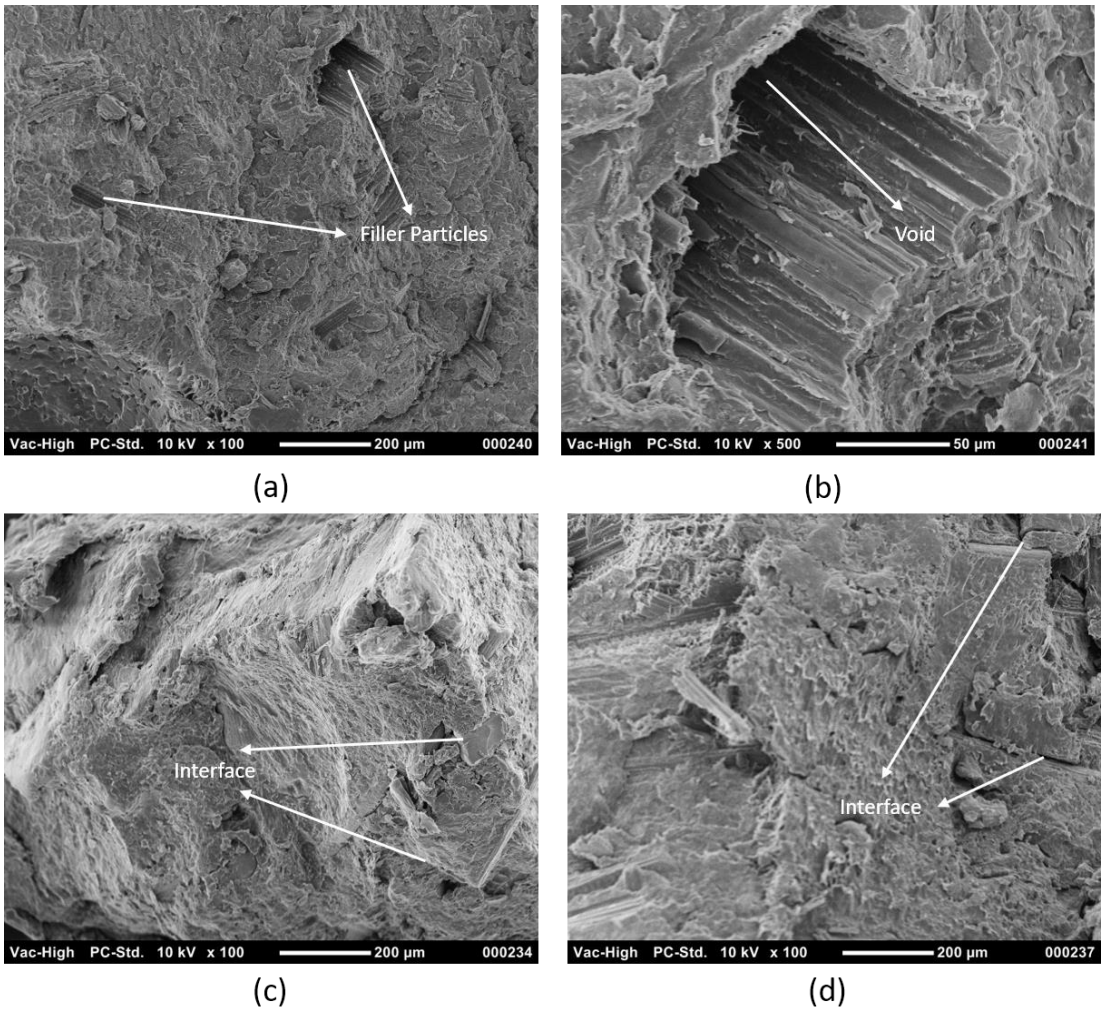

Figure 51: SEM for PLA-UTDPWF (a) and (b), PLA-SA (c), and PLA-SE (d)

4.2.3 XRD

XRD analysis is presented in Figure 52 below. SA-treated filler was chosen since the PLA-SA composites exhibited the highest crystallinity as will be shown later in the DSC analysis. Like the NaOH-treated and UTDPWF, there are two major peaks, which lie between 20 and 30 degrees. These two peaks correspond to the cellulose component

in the wood [64,65]. It is also noted that the peaks are much sharper in the SA-treated sample compared to the UTDPWF, which reflects higher crystallinity and higher cellulose ratio in the filler particles.

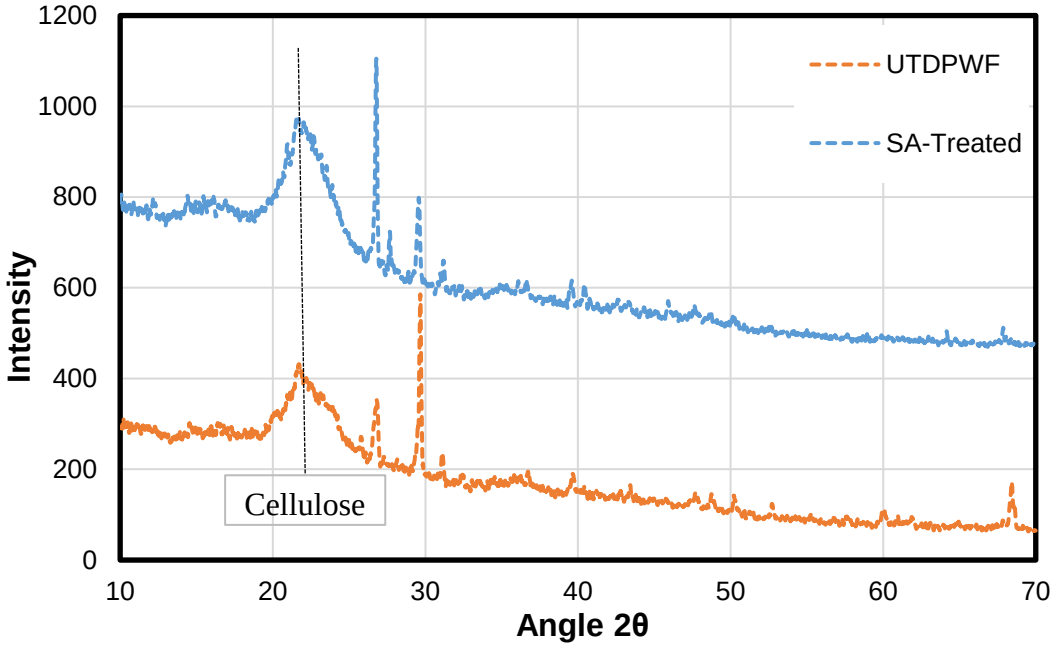

Figure 52: XRD for UTDPWF, and SA-Treated fibers

4.2.4 Thermal Conductivity

The results for the thermal conductivity at 25°C for the three systems, which are Silane-Ethanol treated samples, Silane-Acetone treated samples, and untreated samples with filler content from 0 to 40 wt.% are displayed in Figure 53 and Figure 54. For the Silane-Acetone samples, it increases as the filler content increase. The values for thermal conductivity are ranging from 0.0842 $\frac{W}{m.K}$ for pure PLA, to 1.05 $\frac{W}{m.K}$ for 40 wt.%. This increase can be explained by the removal of hemicellulose because of the acetone as mentioned in section 4.2.1. Moreover, the addition of filler material acts as a nucleating agent for the polymer, which increases the crystallinity

and leads to higher thermal conductivity. The crystallinity has a directly proportional correlation with the thermal conductivity, as mentioned by [67]. Nevertheless, the results show that the thermal conductivity of PLA-SA is higher than PLA-UTDPWF samples. This is due to better compatibility between the filler and matrix, and the reduction of the air voids that are caused by the silane coupling agent.

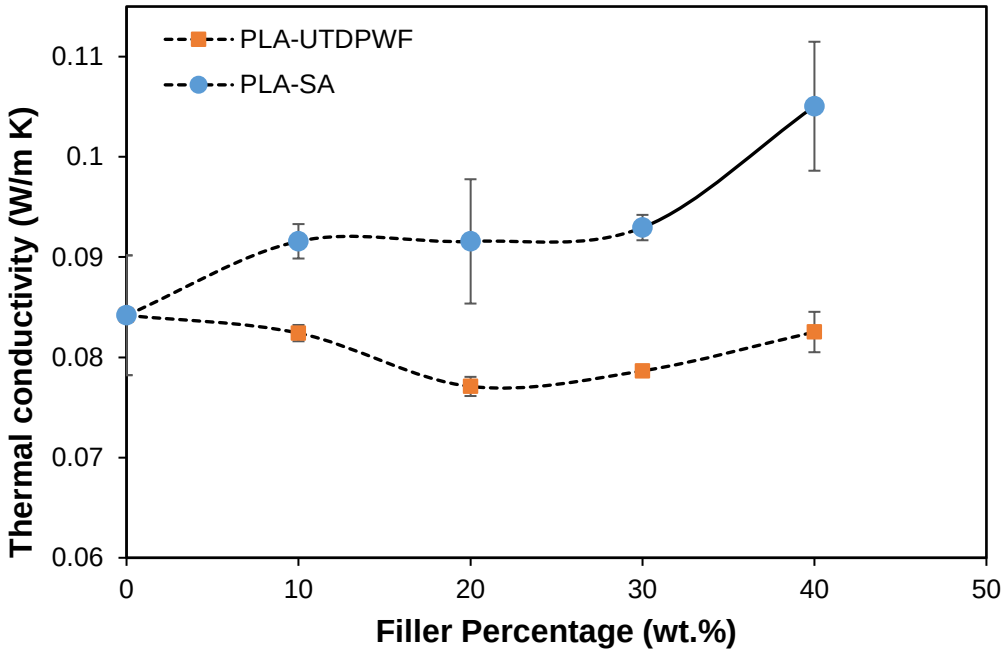

Figure 53: Thermal Conductivity values at 25℃ for PLA-UTDPWF and PLA-SA

For the PLA-SE system, the thermal conductivity also increases in a slight pattern, with values ranging from 0.0842 $\frac{W}{m.K}$ for pure PLA, and 0.0878 $\frac{W}{m.K}$ for the 40 wt.% sample. The results show that the thermal conductivity values are relatively consistent for PLA-SE compared to other systems in this work, which indicates higher homogeneity for the samples. Similarly, the PLA-SE system also showed higher thermal conductivity for all the samples when compared to untreated samples due to the enhancement interface between the polymer and the date wood.

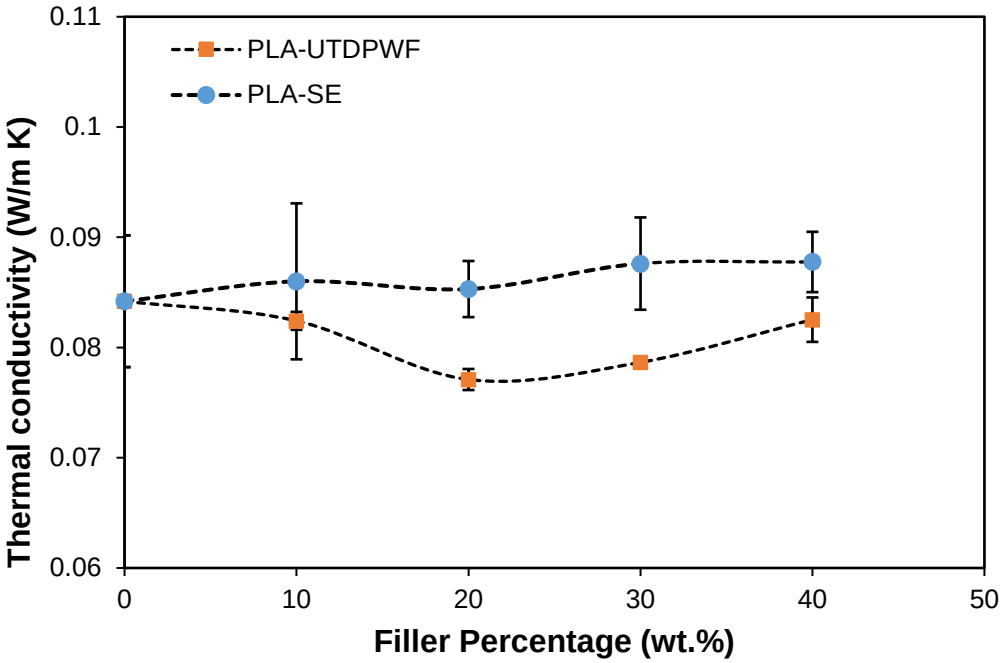

Figure 54: Thermal Conductivity values at 25℃ for PLA-UTDPWF and PLA-SE

Generally, the thermal conductivity values for the three systems are lower than other insulation materials such as wood and plywood, which are above 0.1 $\frac{W}{m.K}$ [72]. Moreover, it is lower than the thermal conductivity values for construction building materials such as perlite concrete and wood fiber concrete, which have values ranging between 0.15-0.31, and 0.09-0.16 $\frac{W}{m.K}$, respectively [72].

4.2.5 DSC

For the Differential Scanning Calorimeter, all the samples for the two systems were tested. The first and second heating cycles for the Silane-Ethanol samples, in addition to pure PLA, are presented in Figure 55 and Figure 56 below, respectively. Moreover, the results for thermal characterization are summarized in Table 8 below.

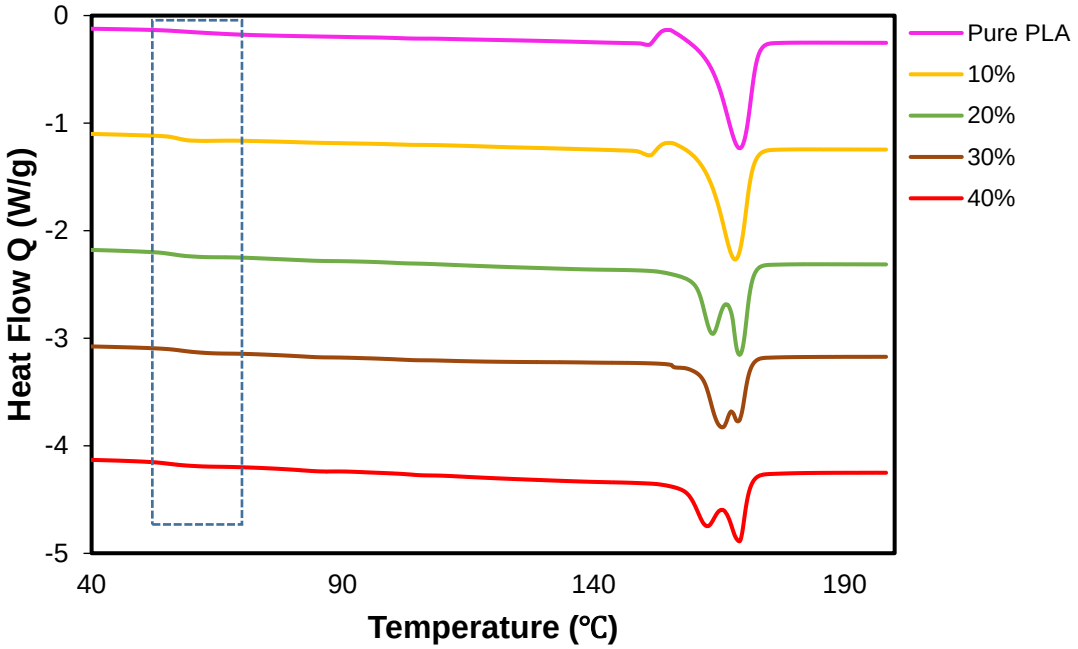

Figure 55: 1st Heating cycle for PLA-SE

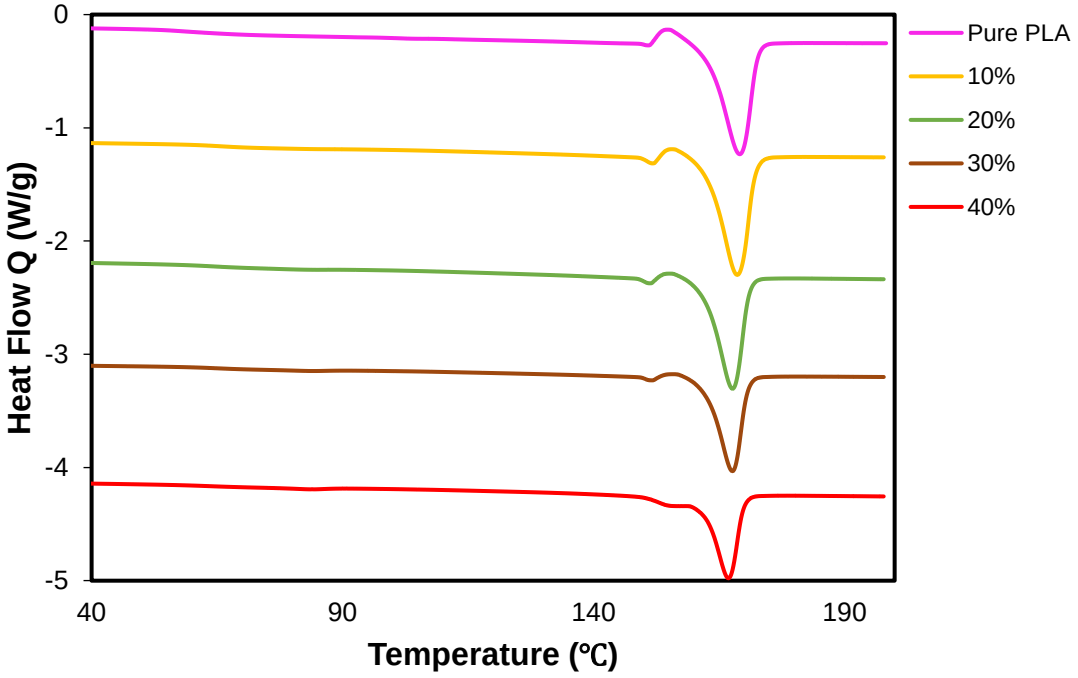

Figure 56: 2nd Heating cycle for PLA-SE

Table 8: Results for thermal characterization of PLA-SE system

DWF wt.%	**T_g (℃)**	**T_m 1st (℃)**	**T_m 2nd (℃)**	**ΔH_m 1st (J/g)**	**ΔH_m 2nd (J/g)**	**X_c 1st (%)**	**X_c 2nd (%)**
0	60.72	168.23	168.36	37.28	34.77	39.79	37.11
10	57.5	168.23	168.53	39.42	39.51	46.75	46.85
20	56.24	168.95	167.63	37.41	35.22	49.90	47.0
30	58.28	165.64	167.66	29.0	28.45	44.21	43.38
40	55.1	168.99	166.82	29.40	28.90	52.30	51.4

The results show that the glass transition (T_g) for PLA-SE samples decreases as the filler percentage increases. The crystallinity also increases. However, there is no clear pattern for crystallization. The reduction of the T_g is due to the addition of the filler, which reduced the homogeneity of the material. The melting point is almost stable at around 167 ± 1. The T_g was taken from the first heating cycle, while the melting point and its enthalpy are shown for both heating cycles. The Tc was not observed in either of the heating cycles for PLA-SE and pure PLA. This indicates the absence of forming a crystalline structure in the second heating cycle since it was formed during the annealing process for 3-hours at 95℃ [73].

However, for PLA-SA, the enthalpy of melting increases as the filler percentage increases. similarly, the crystallinity also increases, which explains the sharp increasing trend for the thermal conductivity of this system [67]. The clear pattern for the crystallinity can be attributed to the removal of the hemicellulose as shown in the FTIR analysis. The melting point, glass transition (T_g), and the cold crystallization decreases as the filler percentage increases. The results are summarized in Table 9 and

presented in Figure 57 and Figure 58 below. The T_g and the T_c were taken from the first heating cycle, whereas the melting point and its enthalpy for both heating cycles are represented.

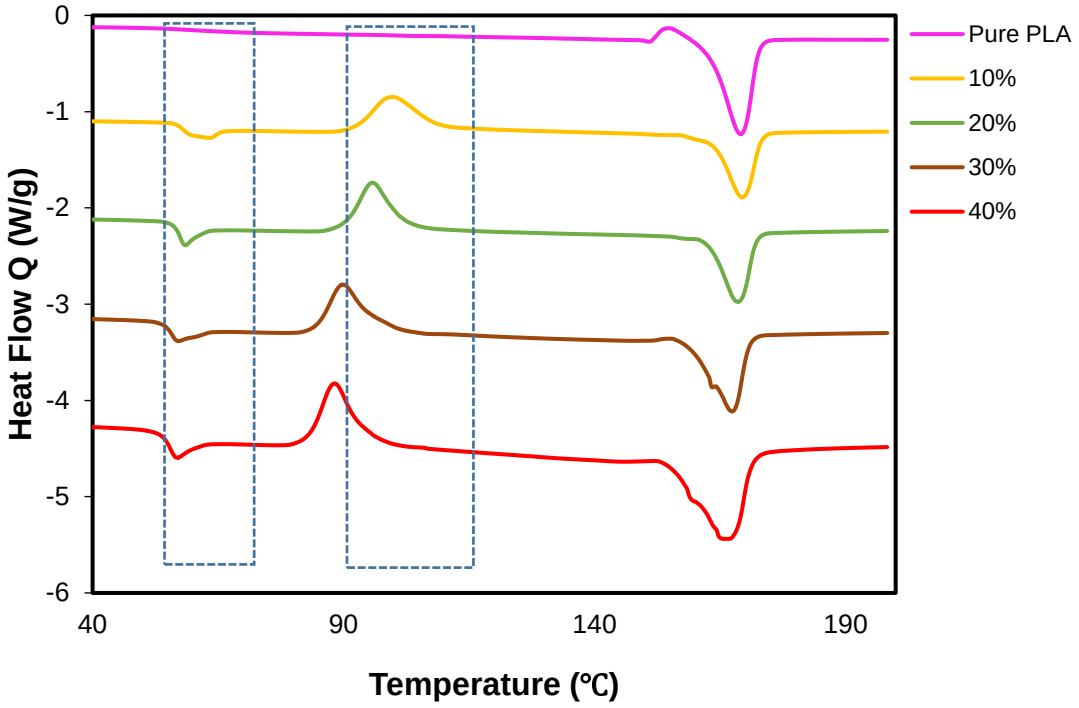

Figure 57: 1st Heating cycle for PLA-SA system

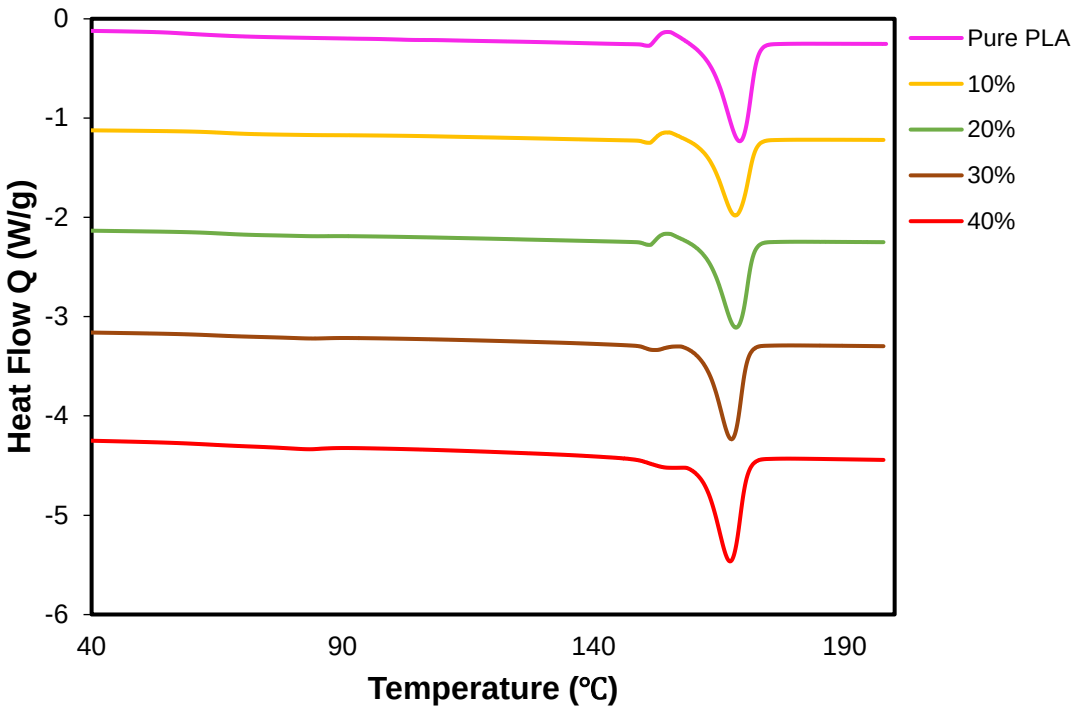

Figure 58: 2nd Heating cycle for PLA-SA

Table 9: Results for thermal characterization of PLA-SA system

DWF wt.%	T_g (℃)	T_c (℃)	T_m 1st (℃)	T_m 2nd (℃)	ΔH_m 1st (J/g)	ΔH_m 2nd (J/g)	X_c 1st (%)	X_c 2nd (%)
0	60.72		168.23	168.36	37.28	34.77	39.79	37.11
10	57.22	98.92	168.79	168.31	25.408	29.291	30.13	34.73
20	55.81	95.01	167.69	168.39	26.346	31.085	35.15	41.47
30	54.27	89.13	166.45	167.54	34.539	31.77	52.66	48.44
40	54.32	87.55	166.03	167.19	53.69	33.046	95.50	58.78

4.2.6 Density

The densities for all samples were measured. Density values increases as the filler percentage increase, which is a similar conclusion to the work of [74]. The results for the 3 systems are presented in Figure 59 below.

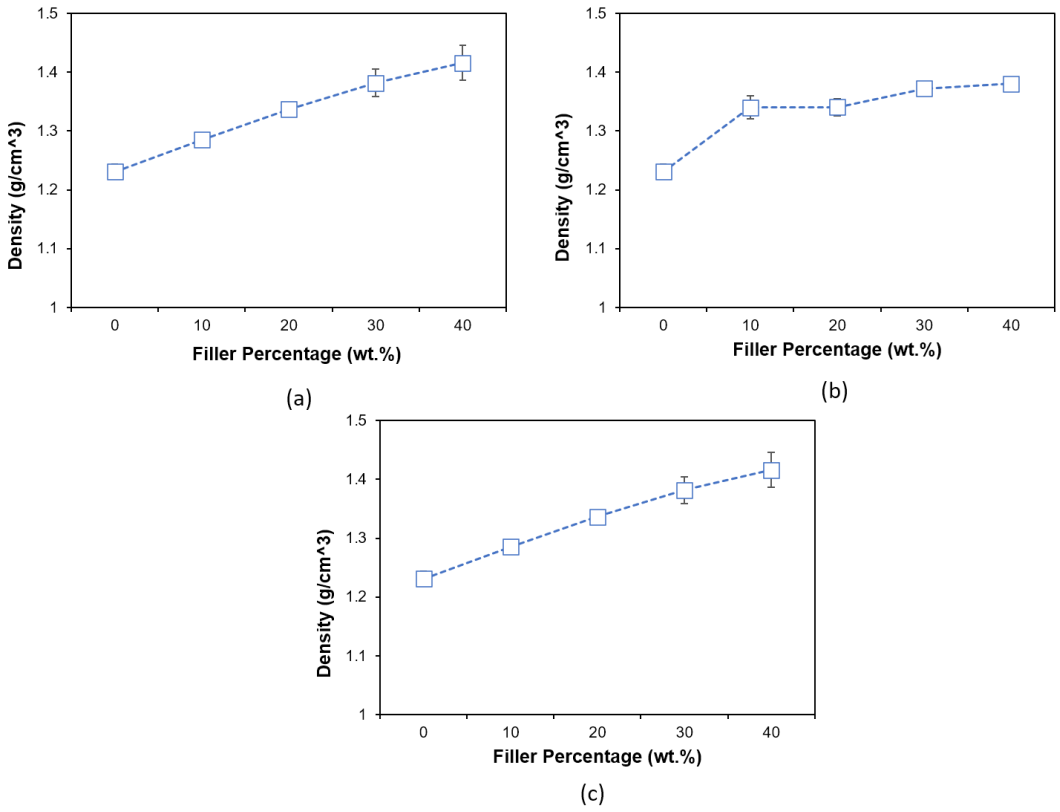

Figure 59: Densities for PLA-UTDPWF (a), PLA-SA (b), and PLA-SE (c)

The trend can be explained by the filling of the air voids of the polymer by the filler in the composite.

4.2.7 Specific Heat Capacity (Cp) and Thermal Diffusivity (α)

The specific heat capacity (Cp) was calculated using the same instrument, to find the thermal diffusivity (α). Using the thermal conductivity, Cp, and density, we can obtain the diffusivity. It is noted that the Cp has a negative correlation to thermal conductivity

as indicated in Figure 60 below. This is because the specific heat capacity for amorphous phases is larger than the Cp for crystalline [67]. Hence, as the thermal conductivity decreases, the Cp increases. Diffusivity results are presented in Table 10 below for PLA-SE.

Table 10: K, Cp, Density and α for PLA-SE

DWF wt. %	**K (W/m.K)**	**Cp (J/g.K)**	**ρ (g/cm^3)**	**α (mm^2/s)**
0	0.0842	1.624	1.231	0.064
10	0.0853	1.62	1.345	0.071
20	0.0858	1.543	1.348	0.075
30	0.0876	1.31	1.377	0.092
40	0.0878	1.33	1.398	0.092

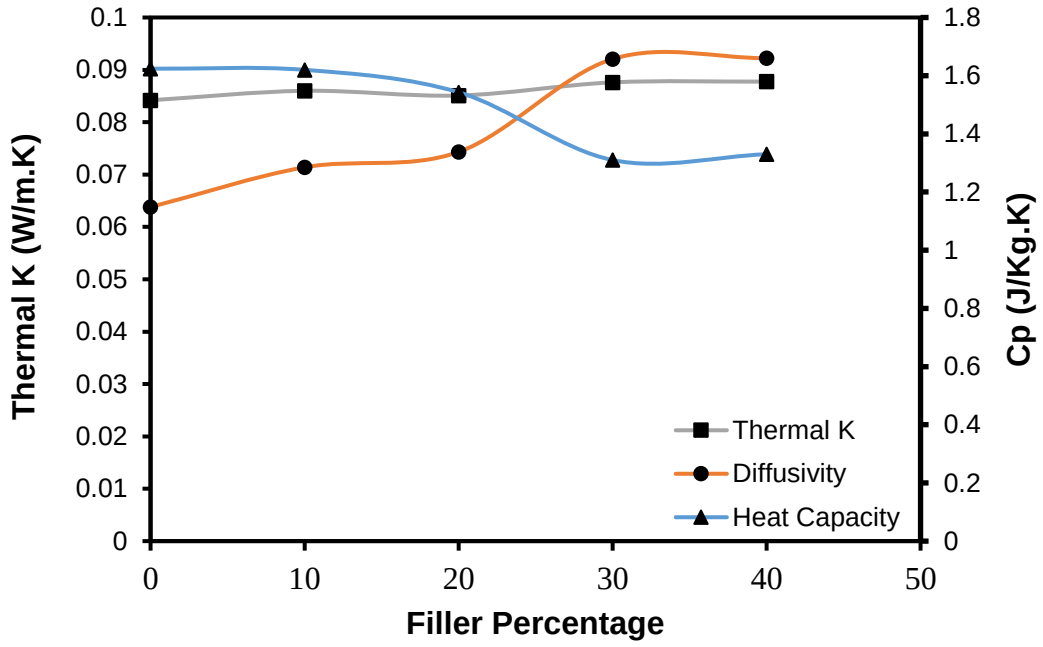

Figure 60: K, Cp, Density and α for PLA-SE

For silane acetone system, the thermal conductivity increases as the filler percentage increase, thereby the Cp decreases accordingly. A shows a similar behavior for the thermal conductivity for this system as well. The results are presented in Table 11 and Figure 61.

Table 11: K, Cp, Density and α for PLA-SA

DWF wt. %	**K (W/m.K)**	**Cp (J/g.K)**	**ρ (g/cm^3)**	**α (mm^2/s)**
0	0.0842	1.333	1.231	0.078
10	0.092	1.129	1.34	0.109
20	0.092	1.026	1.34	0.12
30	0.093	0.938	1.372	0.136
40	0.105	0.864	1.38	0.168

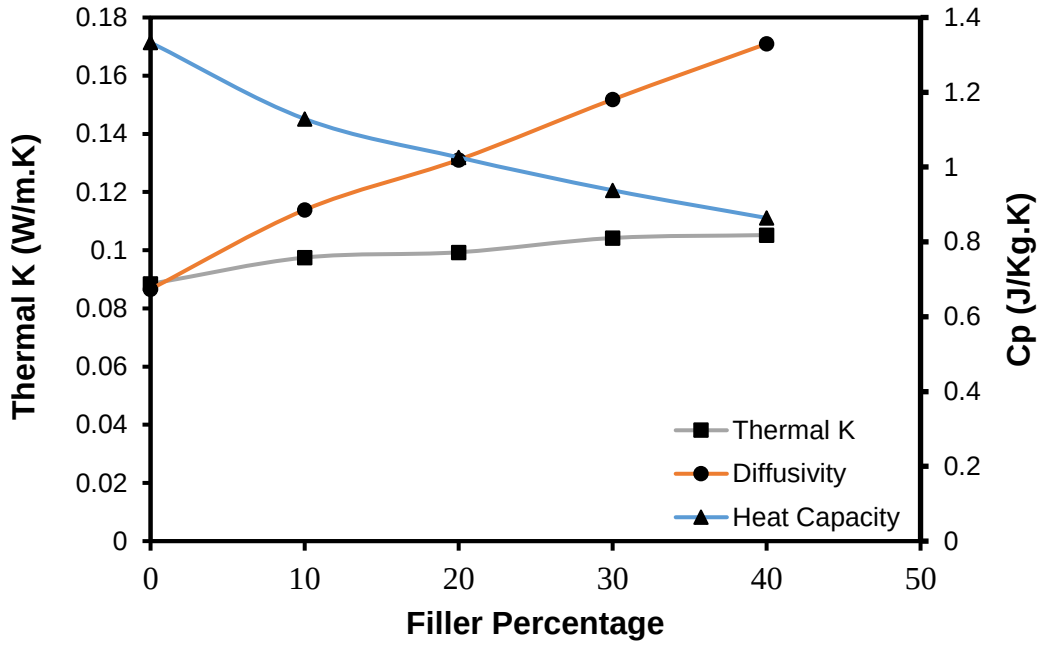

Figure 61: K, Cp, Density and α for PLA-SA

4.2.8 TGA

The TGA test results for the untreated fiber besides the SA treated and SE treated show that there is no huge difference in the thermal stability, since all three samples start degrading at the same temperature. However, the final residue for the SE-treated samples is relatively lower than the untreated and SA-treated samples. The samples start degrading at a temperature of 255℃. At around 375℃, the untreated and SA treated samples reach around 50% of their initial weight. On the other hand, SE treated sample reaches 40% of the initial weight at the same temperature. The results are displayed below in Figure 62 below.

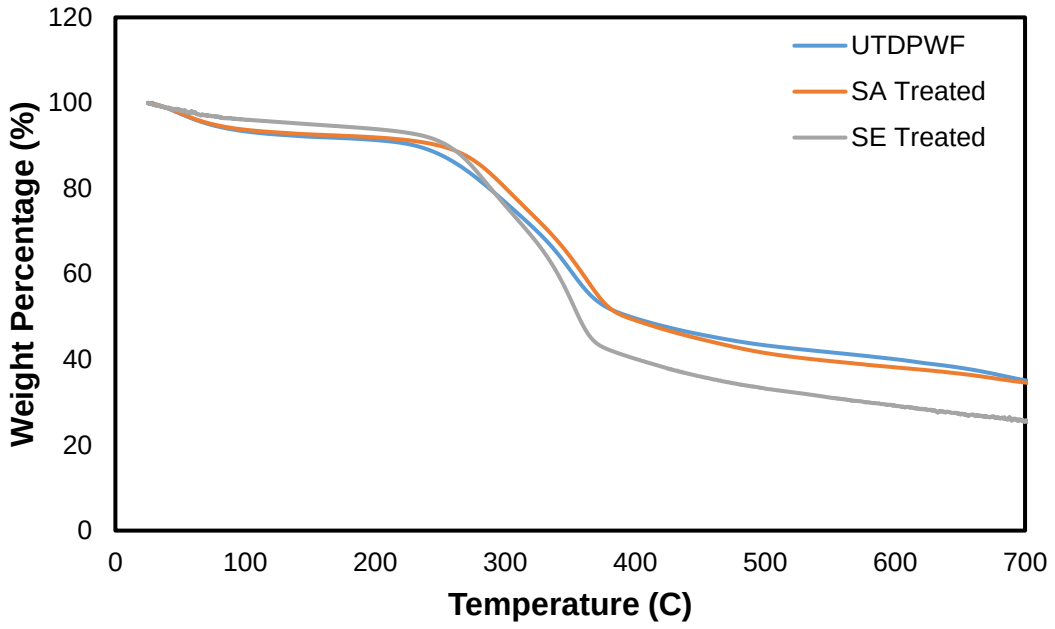

Figure 62: TGA for untreated filler, SA treated, and SE treated

In Figure 63 below, the TGA analysis of pure PLA, in addition to the 20 wt.% samples of the three systems are shown. it is observed that the samples start degradation at around 320℃. For neat PLA, the sample almost fully degrades at around 370℃. For PLA-UTDWF and PLA-SE, 90% of the sample degrades at around 360℃, then the

rest degrades slowly. However, for the silane acetone system, the sample degrades fully at a similar temperature to the neat PLA, at around 370℃, possibly due to better removal of impurities in the filler during the treatment.

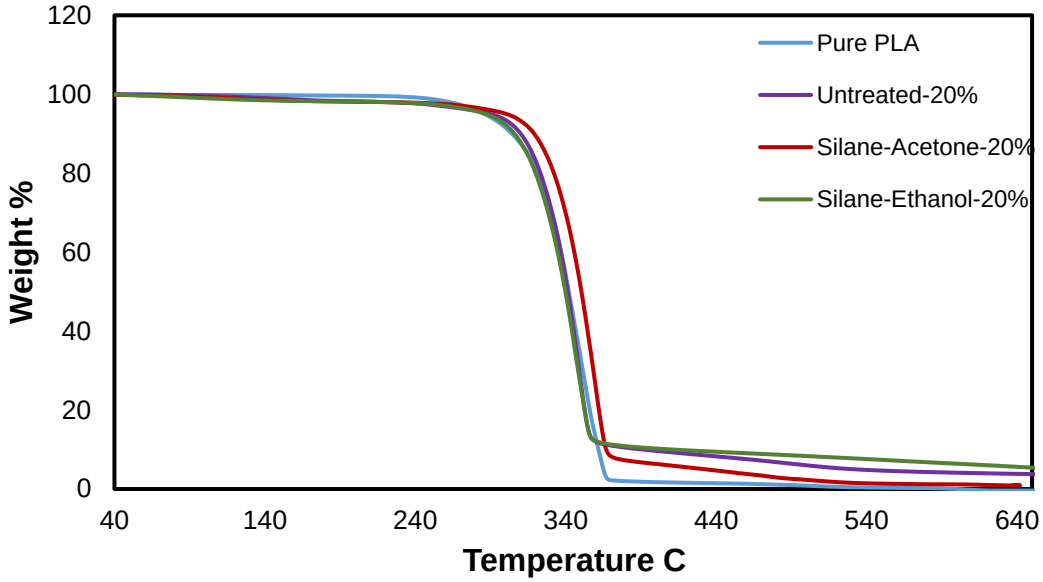

Figure 63: TGA for pure PLA and 20 wt.% samples of the three systems

For the DTG, the same conclusion is reached as the maximum degradation for neat PLA and PLA-SA samples is shown to be at around 360℃, while for PLA-UTDPWF and PLA-SE at around 350℃.

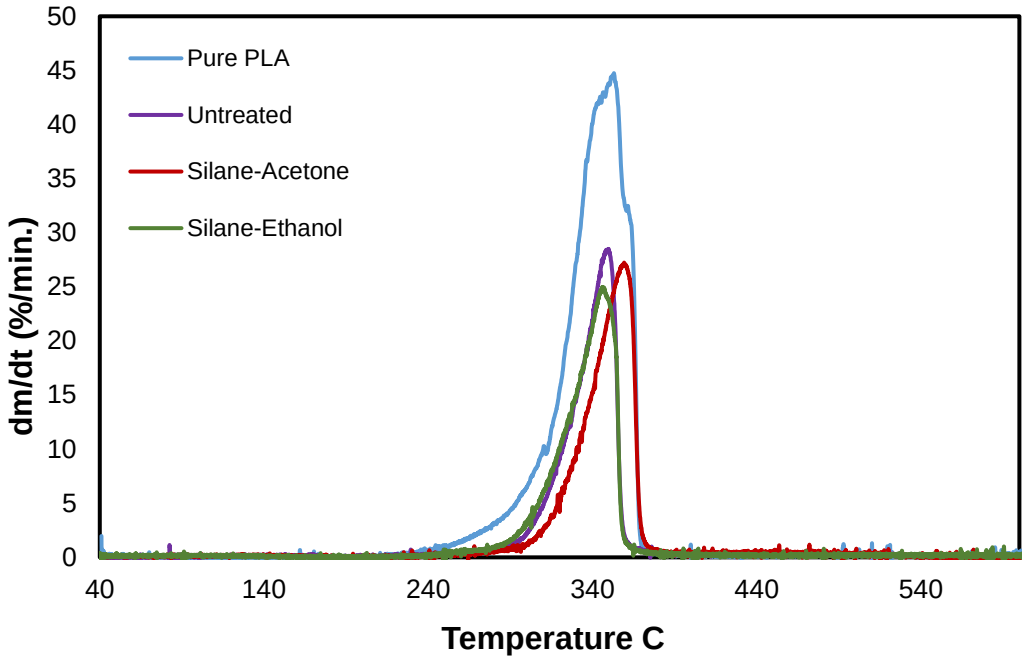

Figure 64: DTG results for Pure PLA and 20 wt.% samples of the three systems

4.2.9 Tensile Properties

The tensile test was applied to all the samples of the three systems, in addition to pure PLA. The results are presented in Figure 65 below.

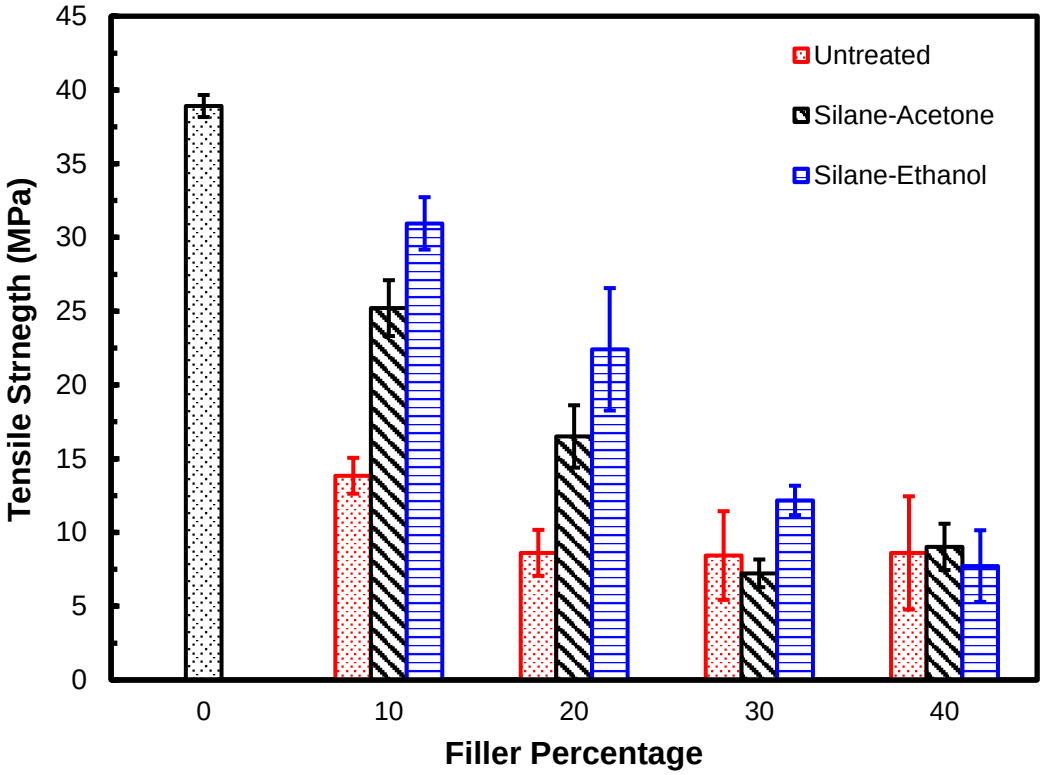

Figure 65: Tensile Strength for pure PLA and the three systems

As the filler percentage increases, the material becomes weaker and breaks at lower forces for all the systems. The highest tensile stress achieved, after pure PLA, was at 10 wt.% loadings for the Silane-Ethanol treated samples, with an average of 31 MPa. The 20 wt.% samples were also good and achieved relatively high tensile strength with an average of around 23 MPa. For low percentages such as 10 and 20 wt.%, the effect of the treatment is obvious for both Silane-Acetone and Silane-Ethanol. However, as the filler percentage increases, the effect of the treatment diminishes, since it is overwhelmed by the effect of the filler added to the matrix. It is also noticeable that the treated sample achieved better consistency since their standard deviation is lower for higher percentages of 30 and 40 wt.%.

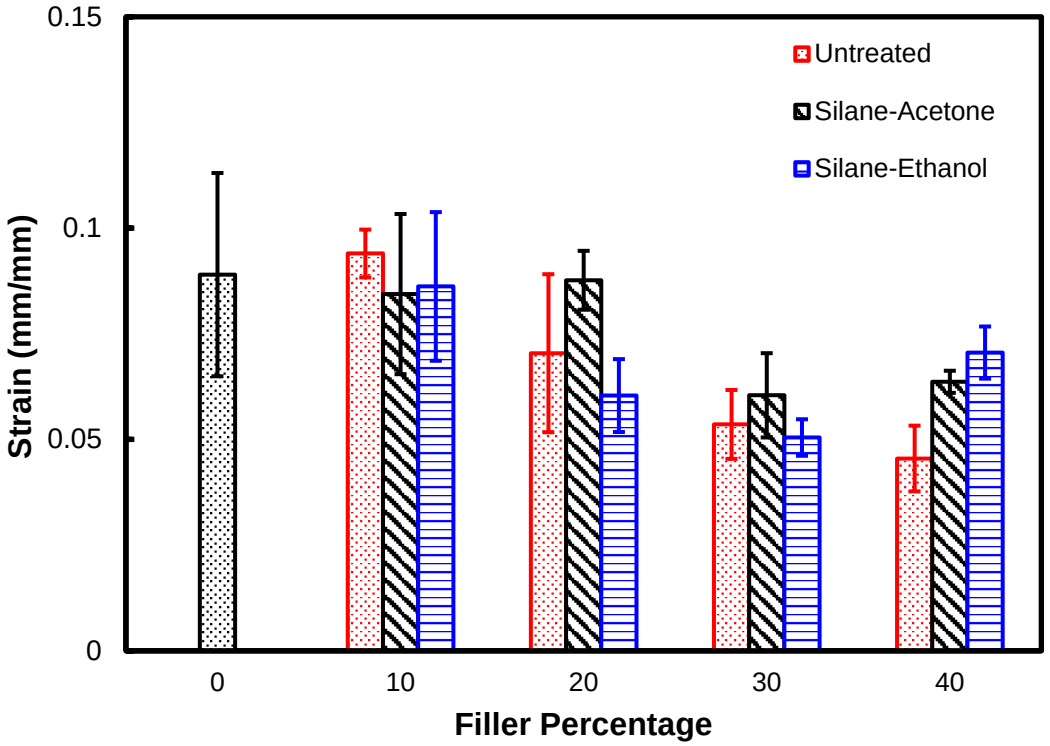

Figure 66: Strain for pure PLA and the three systems

For the strain curves, the percentage of maximum elongation at the breaking point with respect to the original length was taken. The pattern here is that the strain decreases with the filler percentage up to 30 wt.%, then it rises again slightly for the PLA-SE samples for the 40 wt.% as displayed in Figure 66 above. Nevertheless, the error is the strain curve is relatively high for some samples. The maximum average strain was 9.4% and around 8.7%, for the untreated 10 wt.%, and SA treated 20 wt.% samples, respectively. Considering the error margin, the pure PLA can go up to 10.5%, which is the highest strain observed. The most brittle samples were the untreated 40 wt.%. For the young modulus, it was the highest at pure PLA sample, ranging from 400 to 700 MPa, and then it decreases as the filler percent increases for the rest of the samples, except for untreated, where it increases slightly for 30 and 40 wt.% as displayed in Figure 67.

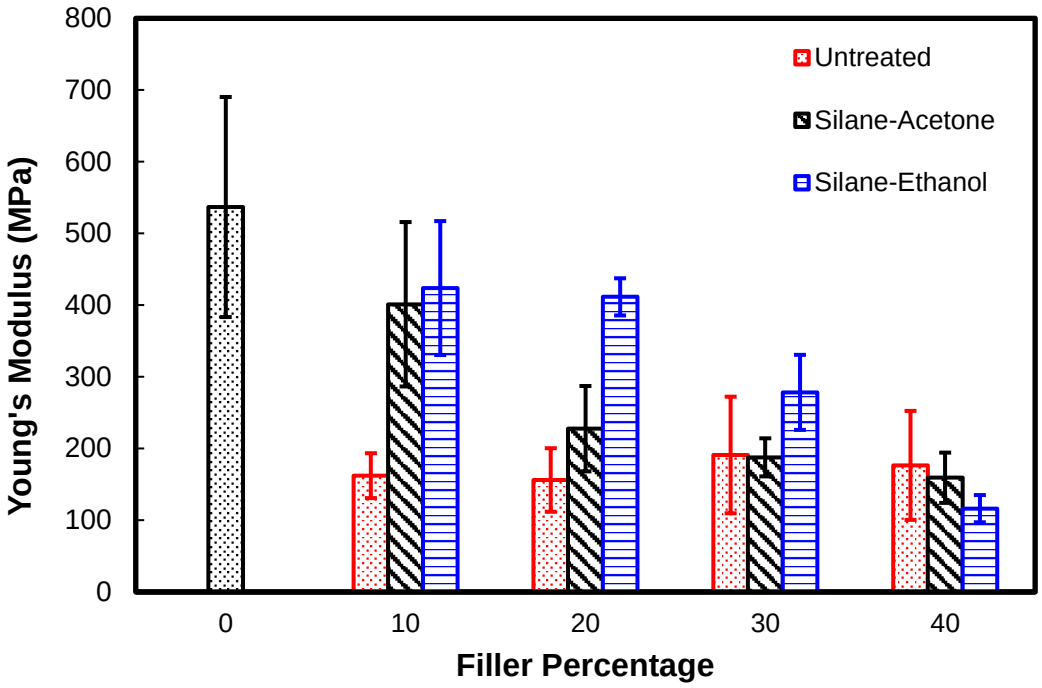

Figure 67: Young's Modulus for pure PLA and the three systems

For the tensile properties, the results are similar to previous works in which the filler material decreases the tensile strength and strain, while the modulus fluctuates sightly [75,76]. For the 20 wt.% PLA-SE sample, which achieved the lowest thermal conductivity, the tensile strength of 23 MPa is still very high, compared with other insulation materials. Polyurethane foam has a tensile strength of only 0.77 MPa [77]. While expanded polystyrene has a maximum tensile strength of 1.2 MPa [78].

4.2.10 Water Retention

The water retention is measured using equation 1 for 24 hours and 48 hours at room temperature and hot water temperature at 50℃. Figure 68 and Figure 69 below represent the data collected, which indicate that as the filler percentage increases, the water retention increases. Moreover, hot water retention has a higher percentage than room temperature water retention. This behavior is expected since the filler is

hydrophilic. Similar results were obtained for various composites such as PLA-Date Pits [75], Polyester-Scrap Tires [79], and Polyester-Date Pits [76]. The WR% after 48 hours submerging in room temperature ranges from around 0.14% to around 1.14%, for 10-40 wt.%. However, for hot water submerging, it ranges from 0.9% to 4%, for 10-40 wt.%.

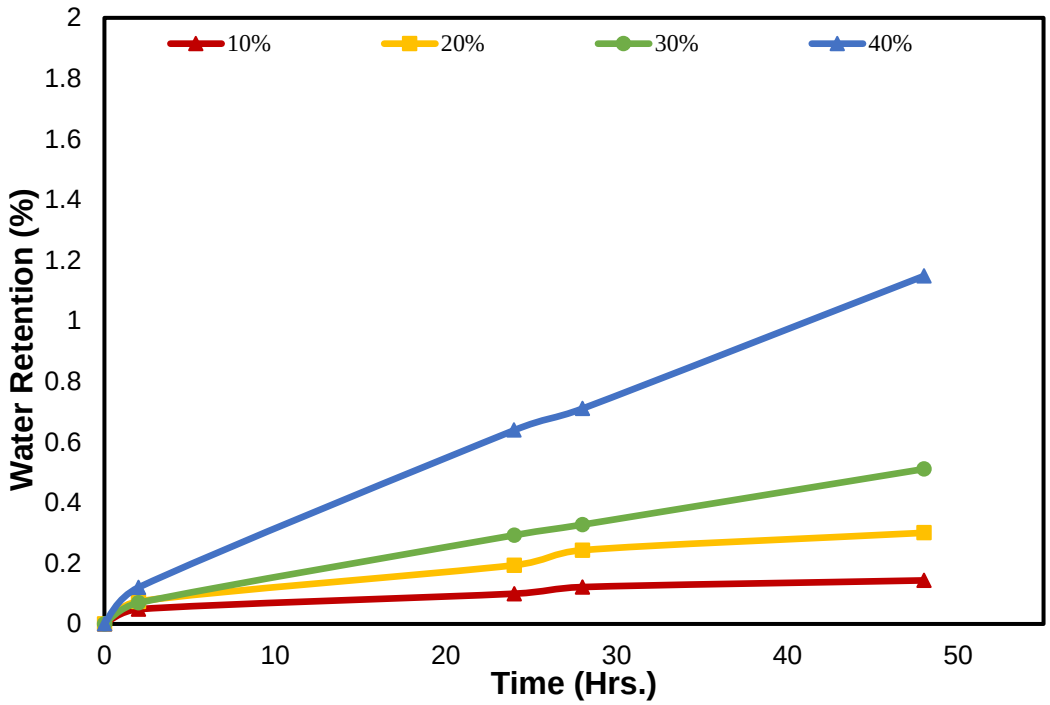

Figure 68: Cold-Water retention for 48 hours for PLA-SE

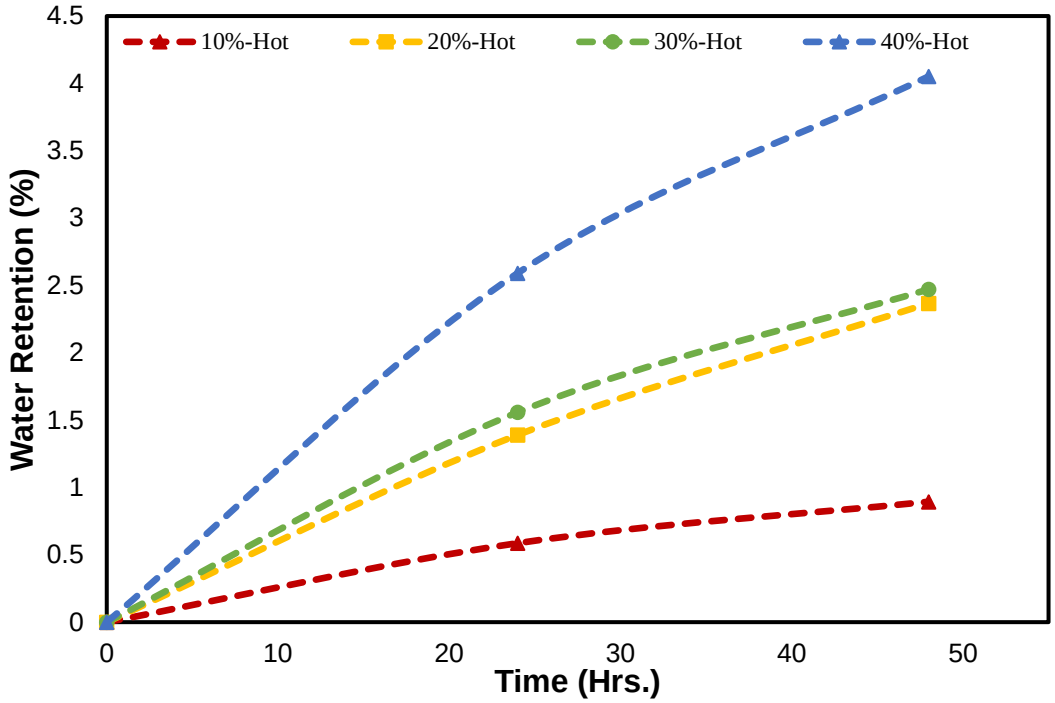

Figure 69: Hot-Water retention for 48 hours for PLA-SE

Similar behaviors were observed for the PLA-SA, and PLA-UTDPWF, which is shown in Figure 70, Figure 71, Figure 72, and Figure 73. Nevertheless, PLA-SE samples has the lowest water retention overall. It is lower than several material studied for such as clay-based unsaturated polyester [80], and polyester-rubber composites [79]. The effect of treatment on the 20 wt.% sample is shown in Figure 74.

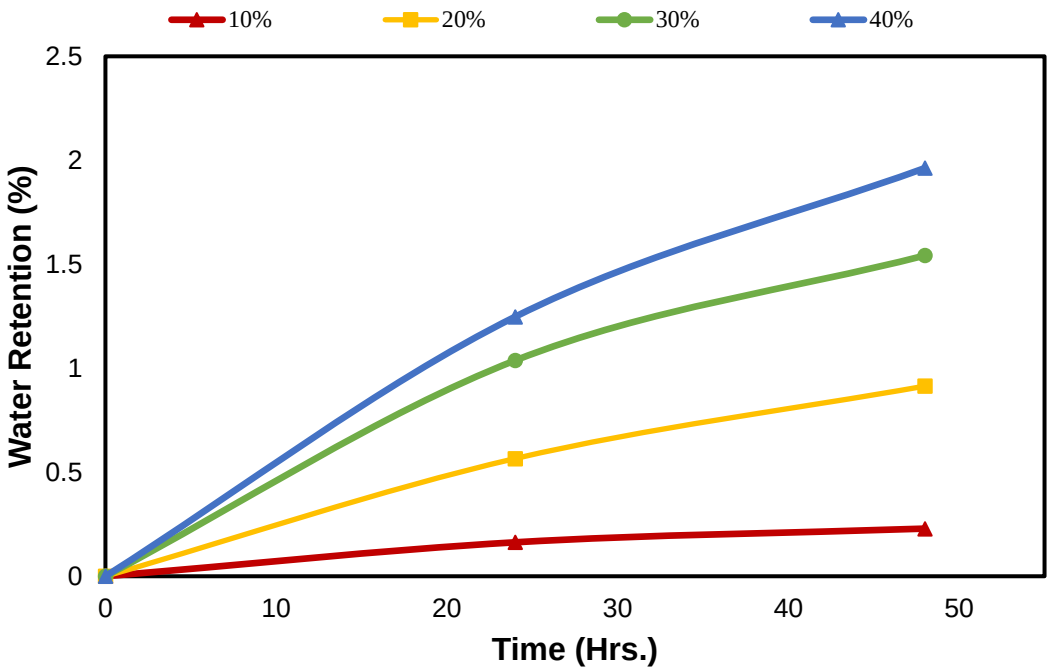

Figure 70: Cold-Water retention for 48 hours for PLA-UTDPWF system

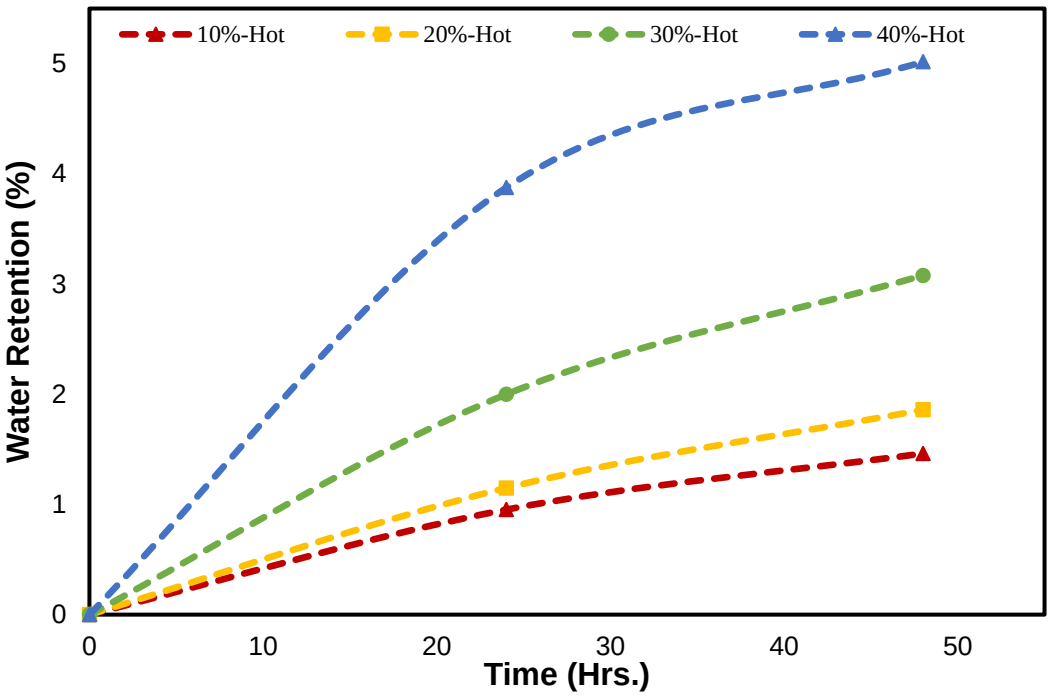

Figure 71: Hot-Water retention for 48 hours for PLA-UTDPWF system

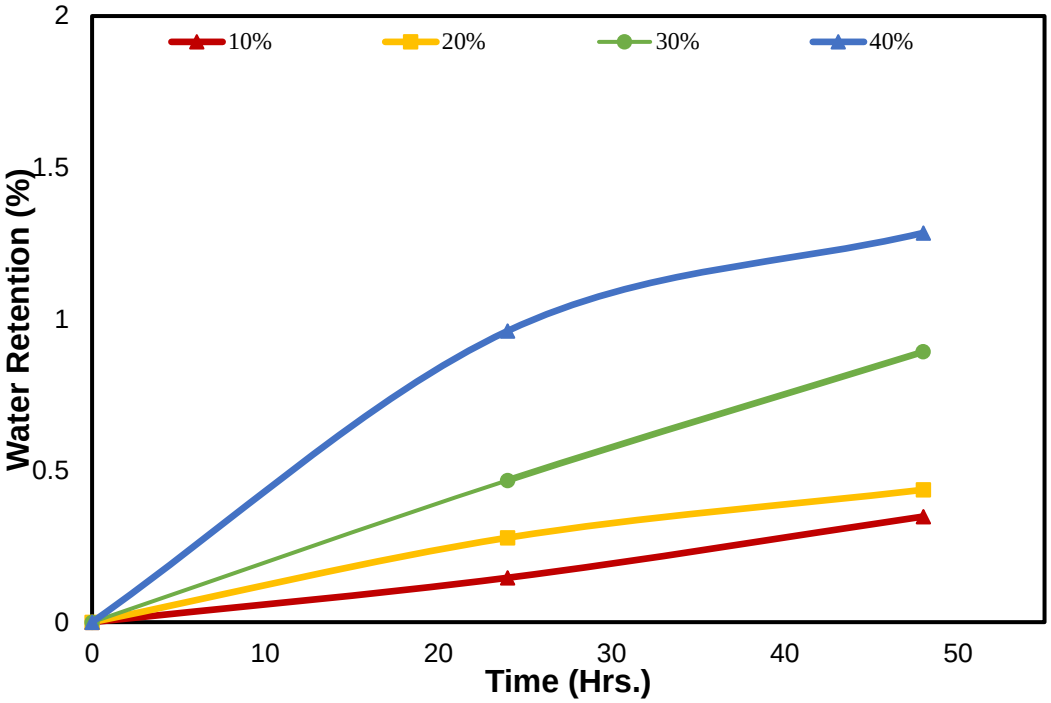

Figure 72: Cold-Water retention for 48 hours for PLA-SA system

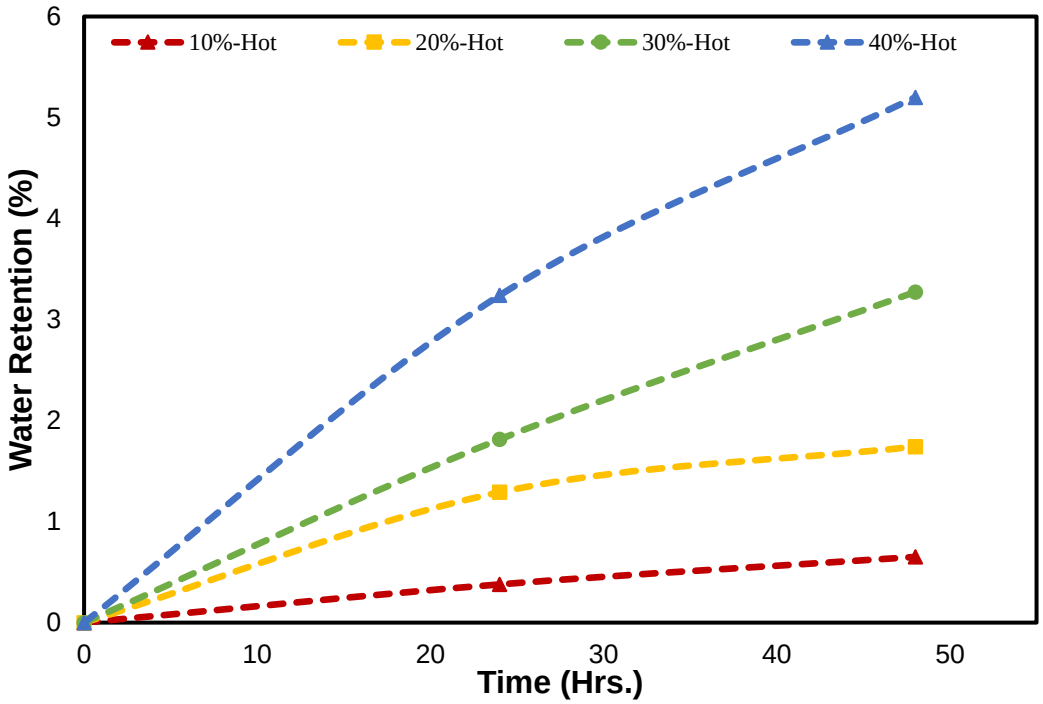

Figure 73: Hot-Water retention for 48 hours for PLA-SA system

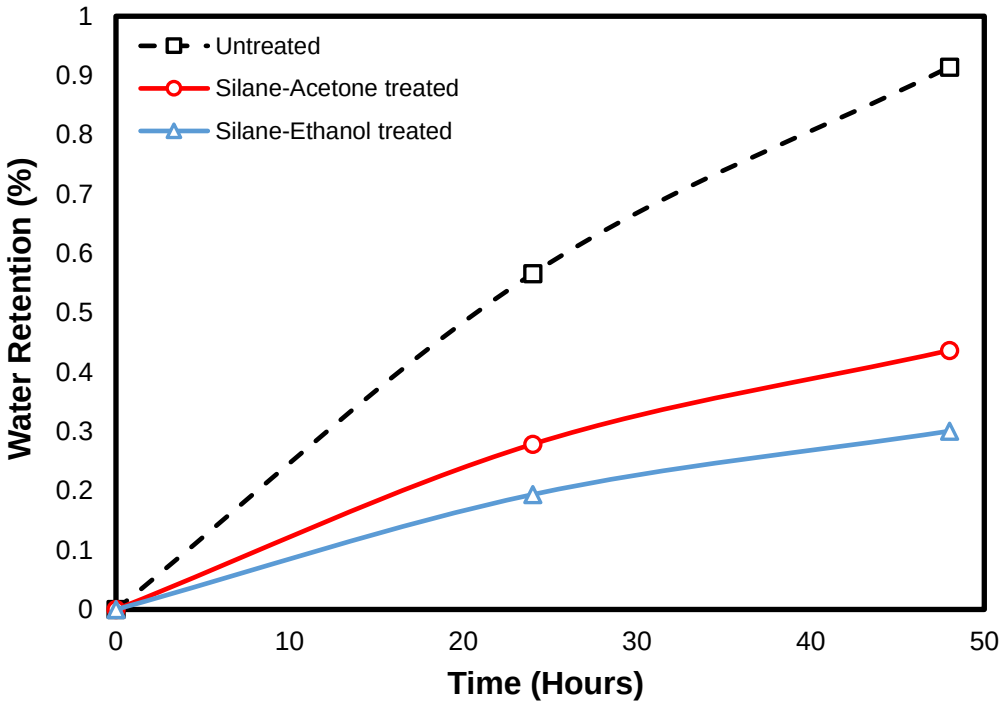

Figure 74: Effect of treatment on the 20 wt.% filler samples of the three systems

4.3 The Effect of Changing the Concentration on SE System

Silane was dissolved in a Water-Ethanol solvent with a ratio of 1:9, with two different additional concentrations, which are 1 and 2%. Tests were applied on thermal conductivity, tensile strength, and density to observe the effect of changing the concentration. Note that an equivalent amount of filler was emersed at each concentration, inside the flask. The filler percentage was fixed at 20 wt.%.

4.3.1 Thermal Conductivity

A thermal conductivity test was carried out for the 20 wt.% for the untreated, 1, 2, and 3% silane concentration. The effect of the silane concentration on the thermal conductivity is shown in Figure 75 below. We can see that the introduction of filler decreased the thermal conductivity. However, as the silane concentration increase in

the filler, the thermal conductivity increases, due to the compatibility between filler and matrix, which reduces the air voids.

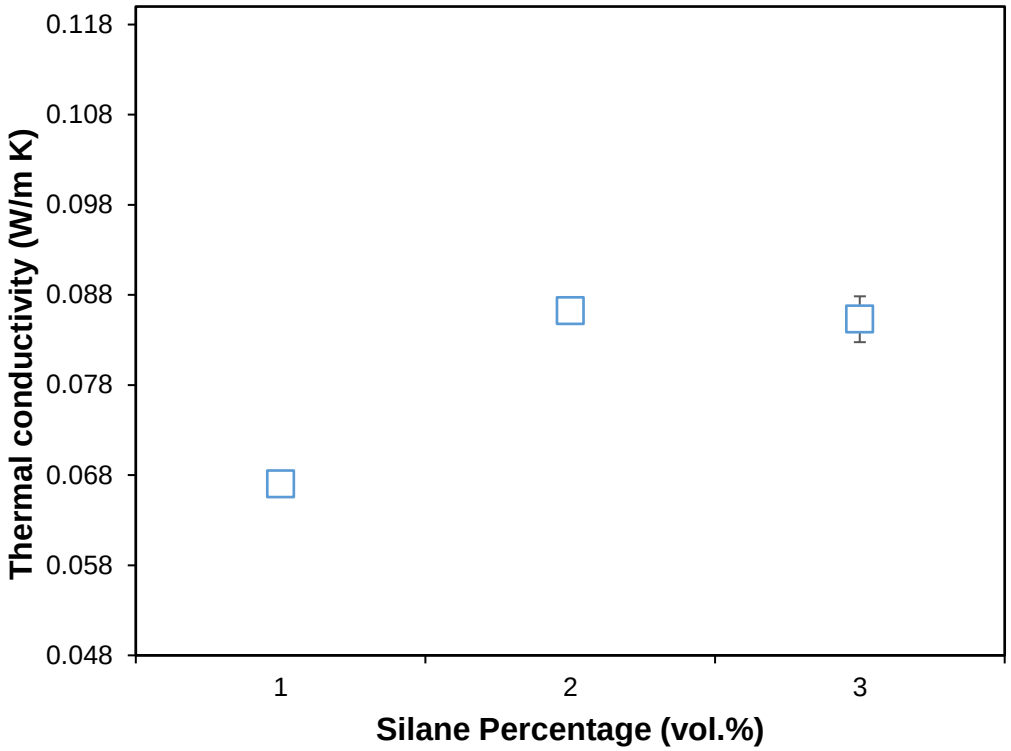

Figure 75: Thermal Conductivity values at 25°C versus the Silane Concentration in solution for 20 wt.% samples

4.3.2 Tensile Strength

It is noticeable in Figure 76 that the strength increases slightly for the 2% compared to 1%, then it drops again for the 3%. If the error margin is considered, there is no huge difference in the tensile strength increases.

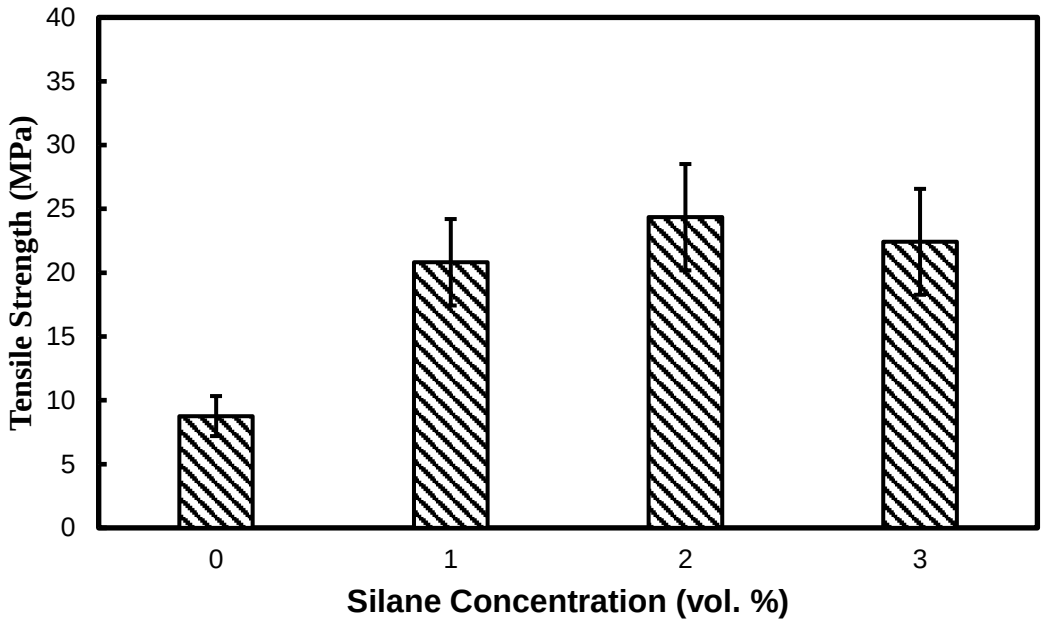

Figure 76: Tensile strength versus the Silane Concentration in solution for 20 wt.% samples

However, this is a study of trial and error to indicate what is the best concertation for silane to coat the filler. These results could change if the volume of the flask where the filler is treated was changed, or the amount of the filler was varied. A better approach is to investigate how many moles of cellulose inside the filler and matching it with the same number of moles for silanes. The challenge is this method is to find the number of moles of cellulose in the filler for each gram. A possible solution is XPS analysis. However, this machine was not available for this study. Moreover, due to the complex nature of the biomass, cellulose is not easily accessible to the silane to bind with. Thereby, the method of varying the concertation of treatment chemical agents to determine the best concentration is followed in similar works such as [77,60,78,79].

4.3.3 Density

For the density, it increased slightly for the 1% concentration of silane compared to the untreated sample (0%). Density then dropped by 2% and increased back for the 3%

sample as displayed in Figure 77 below. However, the values are relatively close, ranging from 1.34 g/cm^3 for the untreated sample, to 1.37 g/cm^3 for the 3%.

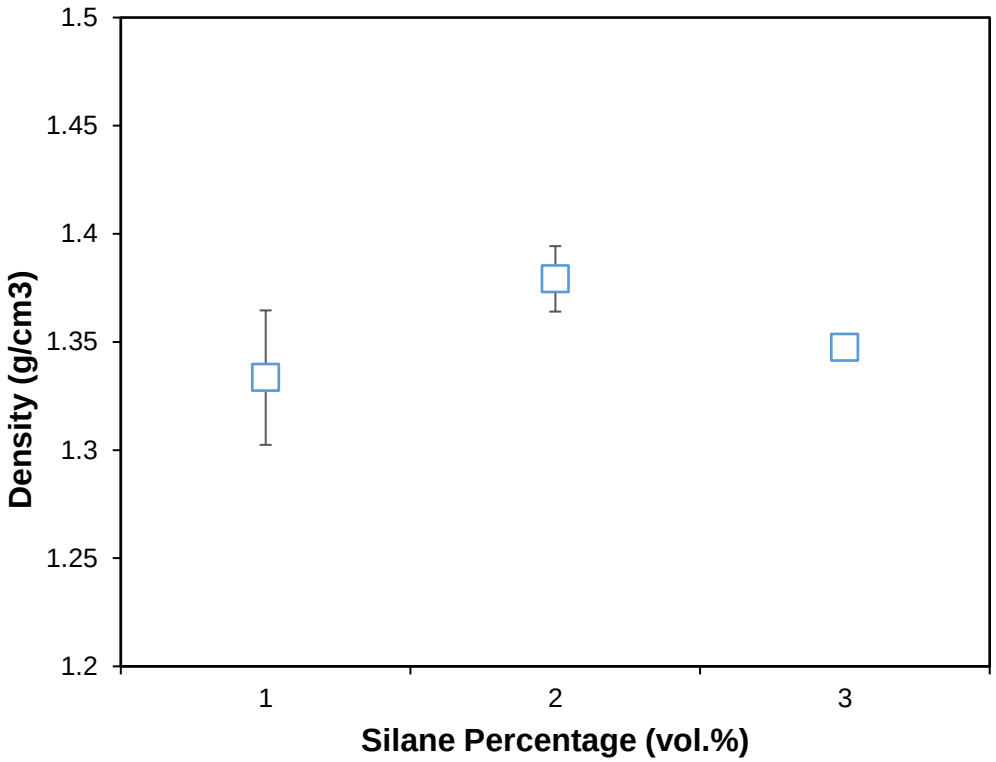

Figure 77: Density versus Silane Concentration in solution for 20 wt.% samples

4.3.4 DSC

DSC test was done on the 1 and 2% concentration samples, to investigate the change in the thermal properties, and it is presented beside the 3% results in Table 12 for comparison. The crystallinity trend corresponds to the thermal conductivity trend, in which the thermal conductivity increases as the silane concentration increase, with a negligible difference between the 2 and 3%, especially after considering the error margin.

Table 12: Results for thermal characterization for different silane concentrations

Silane vol.%	**T_g (℃)**	**T_m 1st (℃)**	**T_m 2nd (℃)**	**ΔH_m 1st (J/g)**	**ΔH_m 2nd (J/g)**	**X_c 1st (%)**	**X_c 2nd (%)**
1%	60.18	169.06	167.97	32.776	29.374	43.72465	39.18623
2%	62.67	170.84	168.97	33.054	30.27	44.09552	40.38154
3%	56.24	168.95	167.63	37.41	35.221	49.90662	46.98639

4.4 Effect of Fire Retardants

4.4.1 Fire Test ULV 94

The fire test was applied to the 20 wt.% filler samples of the PLA-SA with 3% Silane concentration, and samples that are further treated with 5, 10, and 20 wt.% ADP. The results are summarized in the table below. For the sample without the addition of fire-retardant (FR), it was completely burned, and the fire reached the clap as shown in Figure 78. For the sample treated with 5 wt.% ADP, the flame was extinguished after 4.1 seconds for the first flame exposure, and 8.53 for the second flame exposure. However, during the exposure to the flame, there was dripping of burning specimens which lead to the ignition of the cotton batting. For the 10 wt.% ADP, the flame in the sample was extinguished directly once the flame source was removed. Nevertheless, there was dripping of burning specimen, which makes it fall under the classification of V2, besides the 5 wt.% ADP. Finally, the 20 wt.% ADP samples achieved the V0 classification, with no ignition of the cotton batting. There was dripping of the specimen, but it did not cause the cotton to ignite, since it was not flaming, but the dripping was in the form of melted polymer. The ULV 94 standard is shown Table 13 and the results are presented Table 14.

Table 13: ULV 94 test criteria

Test criteria	**VTM -0**	**VTM -1**	**VTM -2**
Burning time of each individual test specimen (s) (after first and second flame applications)	≤ 10	≤ 30	≤ 30
Burning and afterglow times after second flame application (s)	≤ 30	≤ 60	≤ 60
Dripping of burning specimens (ignition of cotton batting)	no	no	yes
Combustion up to holding clamp (specimens completely burned)	no	no	no

Table 14: UL V 94 results

ADP Percentage	**T1**	**T2**	**Dripping**	**Total Combustion**	**UL-94 V**
0%			Yes	yes	Failed
5%	4.1	8.53	Yes	No	V2
10%	0	0	Yes	No	V2
20%	0	0	No	No	V0

Figure 78: Stages of complete burning for a sample without ADP treatment

4.4.2 FTIR

FTIR results for the 20 wt.% ADP sample below in Figure 79 shows a huge increase in the OH group, compared to the sample without ADP. Jong-Hyun Kim et. al. explains the mechanism of fire retardancy in their work on ADP as a fire retardant for polyester-glass fiber composites. They indicate that ADP releases water and gas that dilutes the

gases produced by the flame and thereby creates a resistant and non-flammable layer on the material surface that acts as an insulator of both heat and volatile fuels [84]. This explanation is verified in the FTIR results since the O—H peak corresponds to water release.

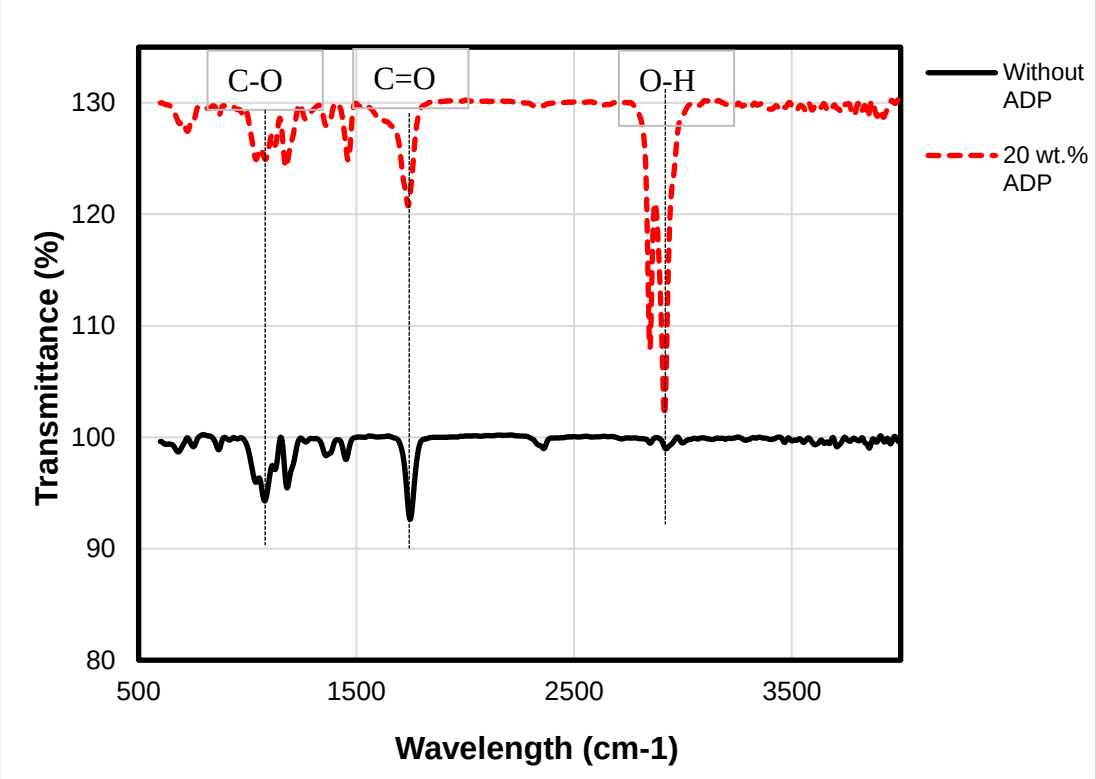

Figure 79: FTIR for sample without ADP, and with 20 wt.% ADP

4.4.3 SEM

SEM in Figure 80 below shows the change in the surface of sample after the ADP coating.

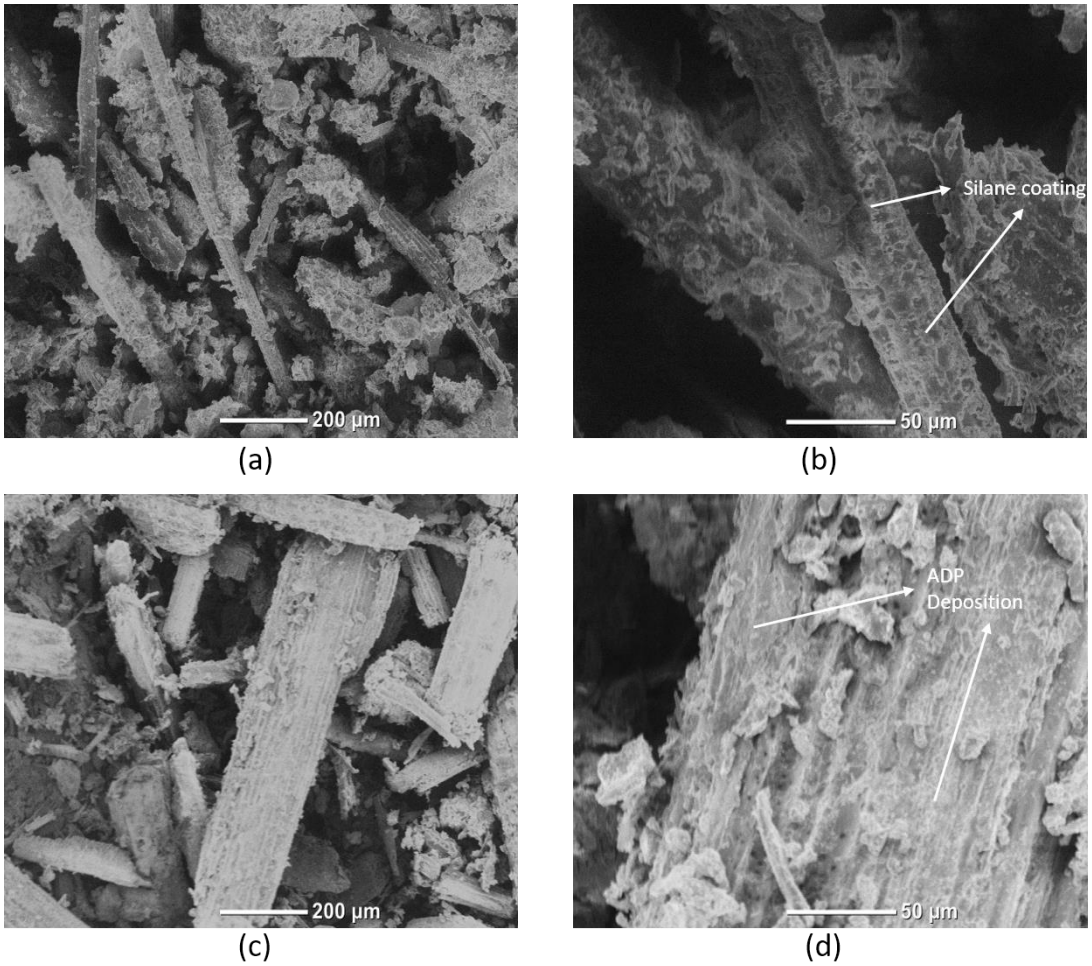

Figure 80: SEM for PLA-SE (a) and (b), PLA-SE with ADP (c) and (d)

4.4.4 Thermal Conductivity

The thermal conductivity decreased as the ADP wt.% increased, reaching a minimum value of 0.434 $\frac{W}{m.K}$ as displayed in Figure 81. The value is very suitable for heat insulation and comparable to commercial heat insulation thermal conductivity, which is around 0.05 $\frac{W}{m.K}$ for expanded and extruded polystyrene. This drop in the thermal conductivity is mostly due to the non-flammable layer mentioned by Jong-Hyun Kim et. al. that was created because of ADP deposition.

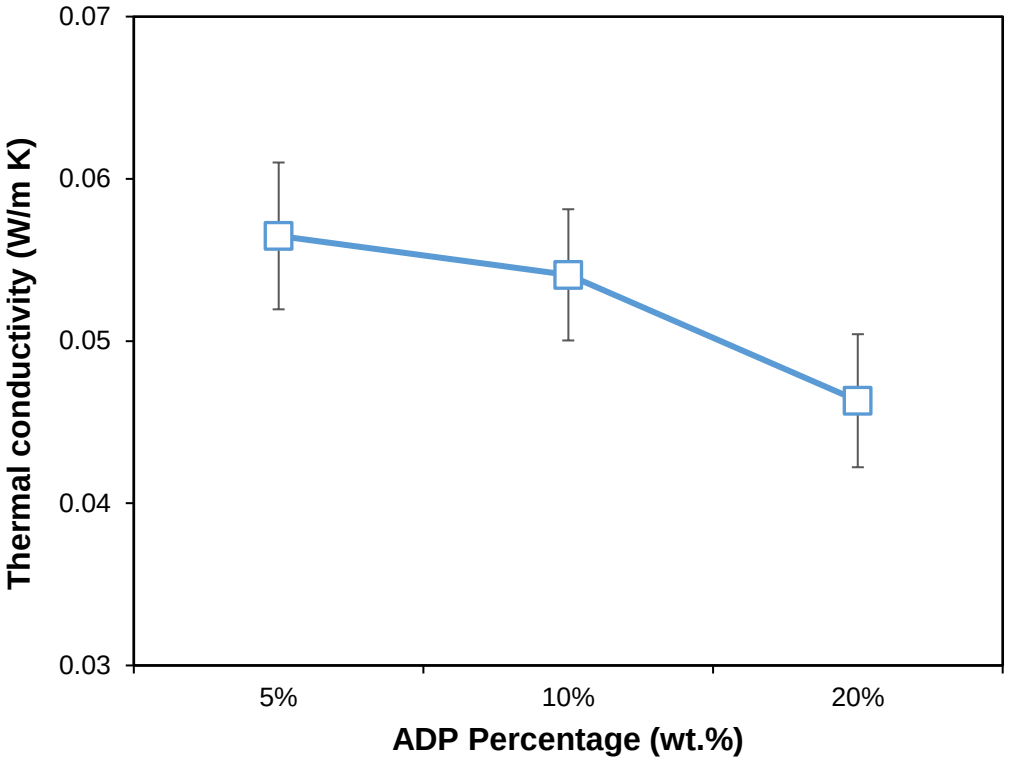

Figure 81: Thermal conductivity for samples with ADP

Taking into consideration other common heat insulators and building materials, our composite achieved relatively low thermal conductivity. The PLA-SE sample with 20 wt.% filler achieved lower thermal conductivity than concrete, brickwork, and wood fiber concrete as shown in Figure 82 [85]. Moreover, after the addition of the ADP fire retardant with 20 wt.%, the achieved thermal conductivity was lower than glass wool and stone wool, and close to commercial heat insulators such as expanded polystyrene.

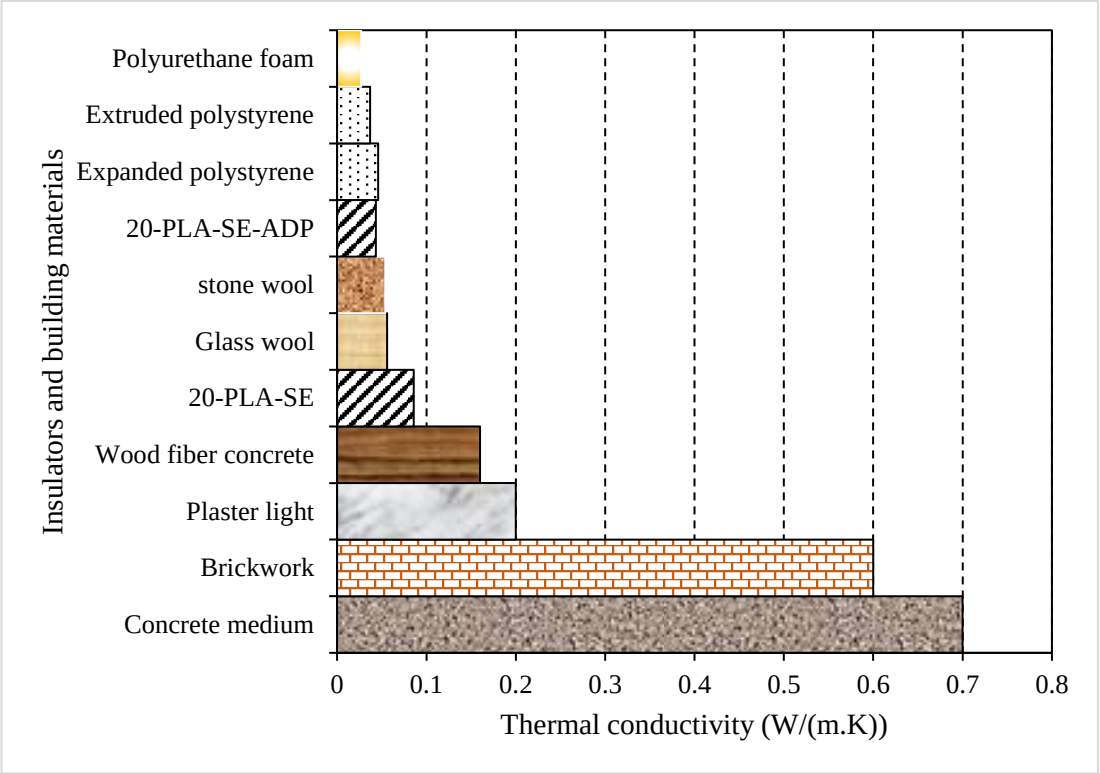

Figure 82: Comparison with common heat insulators and building materials

4.4.5 Thermal and Physical Characterization

Thermal characterization such as T_g, Tm, diffusivity, and Cp were found for the 20 wt.% ADP sample. Moreover, physical, and mechanical properties such as crystallinity, density, and compression forces were also determined. In Table 15 below, results show that the T_g decreased slightly, while Tm in the first heating cycle increased. Tm from the second heating cycle decreased, and crystallinity from both heating cycles increased.

Table 15: Results for thermal characterization of 20 wt.% ADP

sample	**T_g (°C)**	**T_m 1st (°C)**	**T_m 2nd (°C)**	**ΔH_m 1st (J/g)**	**ΔH_m 2nd (J/g)**	**X_c 1st (%)**	**X_c 2nd (%)**
0 wt. % ADP	56.24	168.95	167.63	37.41	35.22	49.90	47.0
20 wt. % ADP	54.26	169.66	166.56	37.86	37.77	50.51	50.38

The thermal conductivity was reduced to almost half of the sample without ADP addition as shown in Table 16 below, while the Cp increased. The density and the diffusivity also both decreased

Table 16: K, Cp, Density and α

Sample	**K (W/m.K)**	**Cp (J/g.K)**	**ρ (g/cm^3)**	**α (mm^2/s)**
0 wt.% ADP	0.0858	1.543	1.348	0.075
20 wt.% ADP	0.04342	2.007	1.32180172	0.028596

Finally, the mechanical properties, the sample showed excellent compression strength of 69 MPa, and a modulus of 8.05 GPa, while the strain was 2% as illustrated in Table 17.

Table 17: Compression properties

Sample	**Compression Stress (MPa)**	**Strain (%)**	**Modulus (GPa)**
20 wt.% ADP	69	2	8.05

The value of the compression stress for the final sample is relatively high when compared with other heat insulators and building materials. The PLA-SE sample with

20 wt.% filler material that is treated with 20 wt.% ADP solution has higher compression strength than concrete, brickwork sandstone and other insulators and building materials, as illustrated in Figure 83 [85,86].

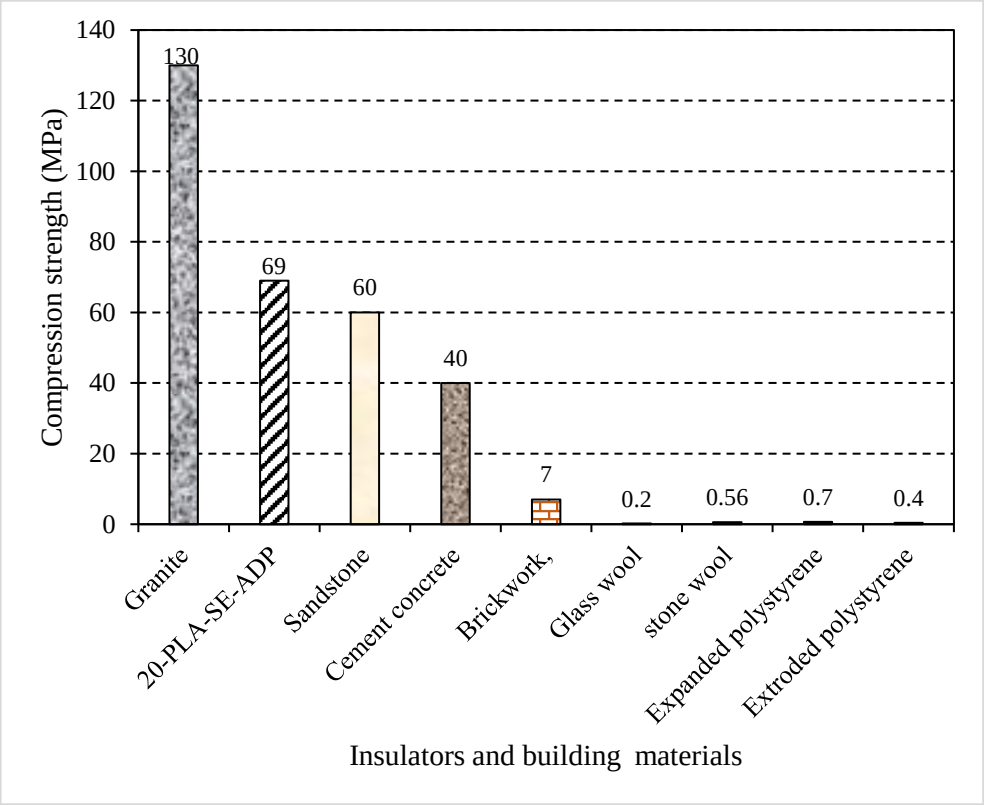

Figure 83: Comparison with compression strength of different insulators and building materials

4.4.6 Water Retention

Cold and hot water retention readings were taken for the sample with the 20 wt.% ADP and they were compared to the sample of PLA-SE, without the addition of ADP in Figure 84 and Figure 85. As expected, the addition of ADP increased the water retention, and in the cold-water retention it was significantly higher. For the hot-water

retention, after 24 hours, the 20 wt.% ADP sample had higher water intake. However, after 48 hours, the sample without ADP had a slightly higher water absorption.

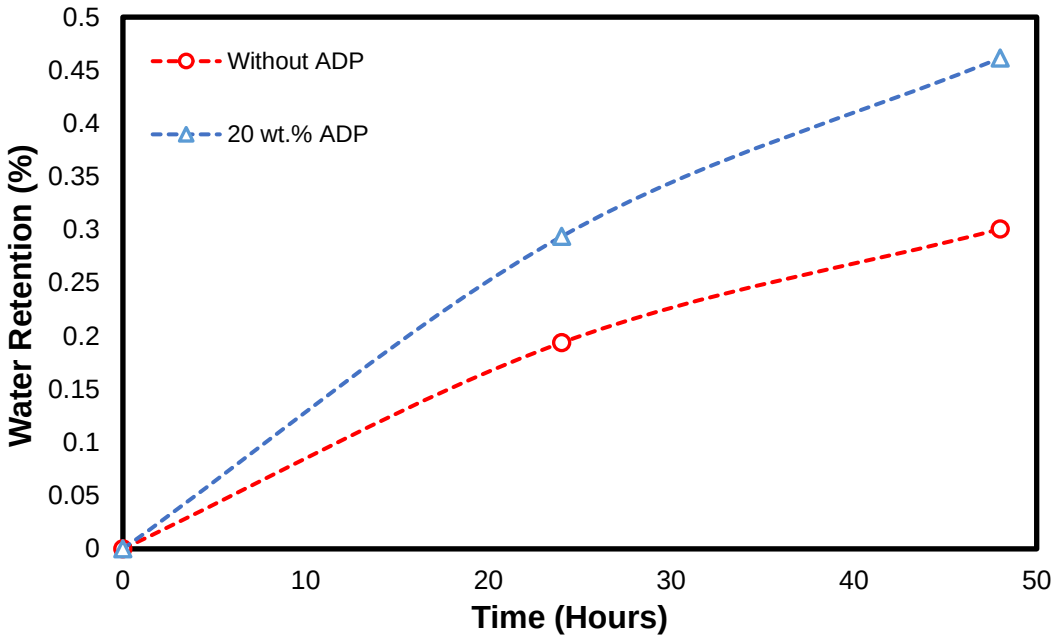

Figure 84: Cold Water retention for 20 wt.% of the PLA-SE and PLA-SE-ADP

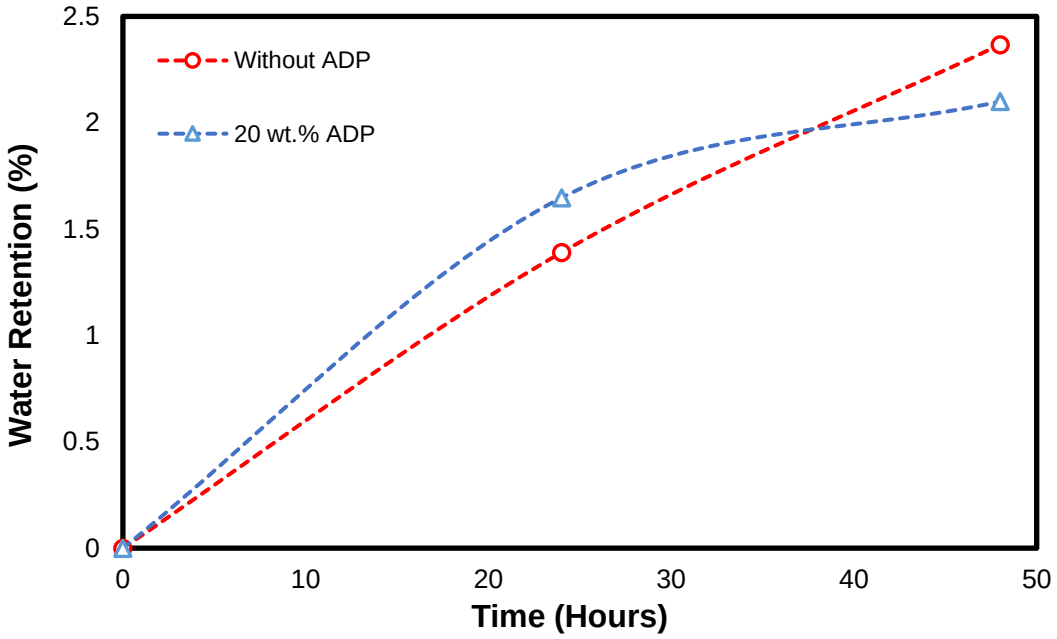

Figure 85: Hot Water retention for 20 wt.% of the PLA-SE and PLA-SE-ADP

Chapter 5: Conclusion

In this research, the potential use of PLA-Date wood fibers as a heat insulator in construction was studied. Chemical treatment and additives were studied to investigate the enhancement of the composite. The thermal conductivity values were low enough for the material to be considered as insulation since it achieved a thermal conductivity value below 0.1 $\frac{W}{m.K}$. The mechanical properties were improved, and they are much higher than common heat insulation materials. Water retention was slightly reduced after the silane treatment compared to untreated composite. The density values were higher than regular insulators. However, they are still below the value of several building and construction materials. It is concluded that the best sample was the 20 wt.% filler of the PLA-SE system, since it achieved the lowest thermal conductivity. Even though the 10 wt.% from the same system achieved higher tensile strength and lower water retention, the 20 wt.% sample still possesses good characterization. Other samples achieved lower densities than the 20 wt.%, but the difference is not very huge. ADP was added to the 20 wt.% PLA-SE sample, in 3 wt.% which are 5, 10, and 20 wt.%. The 20 wt.% ADP addition achieved the best flammability standard and reduced the thermal conductivity to commercial heat insulators level. Based on this study, incorporating palm date wood fibers into the PLA matrix is suggested as a good waste management option. The biodegradability of this composite makes it a feasible solution for the huge construction waste. Future work might include an economic study and cost analysis for the materials used in this study. The addition of other chemicals such as compatibilizer and coatings can be studied. Other biodegradable materials can be used as a matrix for natural filler, to conduct similar studies on their abilities to replace existing heat insulators.

References

[1] "Energy use per person, 2019." [Online]. Available: https://ourworldindata.org/grapher/per-capita-energy-use?region=World. [Accessed: 26-Dec-2020].

[2] "Statistics Center, Energy and Water Statistics, 2018." [Online]. Available: https://www.scad.gov.ae/Release Documents/Nov_01_Energy and Water Statistics_2018_Annual_Yearly_en.pdf. [Accessed: 26-Dec-2020].

[3] "Dubai Electiricity & Water Aauthority, Annual Statistics, 2018." [Online]. Available: https://www.dewa.gov.ae/~/media/Files/About DEWA/Annual Statistics/DEWA_Statistics Booklet_2018_Spread-Eng.ashx. [Accessed: 26-Dec-2020].

[4] "Sharjah Electricity & Water Authority, Statistical Reports, 2018." [Online]. Available: https://www.sewa.gov.ae/uploads/statspdfar/Finalbook2019.pdf. [Accessed: 26-Dec-2020].

[5] U.S. Energy Information Administration, "AEO2020 - Buildings." [Online]. Available: https://www.eia.gov/outlooks/aeo/pdf/AEO2020%20Buildings.pdf. [Accessed: 9-June-2021]

[6] B. Petter, "Traditional , state-of-the-art and future thermal building insulation materials and solutions – Properties , requirements and possibilities," *Energy and Buildings*, vol. 43, no. 7465, pp. 2549–2563, 2011.

[7] B. Abu-jdayil, A. Mourad, W. Hittini, M. Hassan, and S. Hameedi, "Traditional , state-of-the-art and renewable thermal building insulation materials : An overview," *Constr. Build. Mater.*, vol. 214, pp. 709–735, 2019.

[8] J. Zach, J. Hroudová, J. Brožovský, Z. Krejza, and A. Gailius, "Development of Thermal Insulating Materials on Natural Base for Thermal Insulation Systems," *Procedia Eng.*, vol. 57, pp. 1288–1294, 2013.

[9] W. Villasmil, L. J. Fischer, and J. Worlitschek, "A review and evaluation of thermal insulation materials and methods for thermal energy storage systems," *Renew. Sustain. Energy Rev.*, vol. 103, pp. 71–84, 2019.

[10] B. P. Jelle, A. Gustavsen, and R. Baetens, "The High Performance Thermal Building Insulation Materials and," *Proceedings of the Thermal Performance of the Exterior Envelopes of Whole Buildings XI International Conference*, Clearwater Beach, Florida, USA, 5-9 December, 2010.

[11] R. Csizmadia, G. Faludi, K. Renner, J. Móczó, and B. Pukánszky, “PLA / wood biocomposites : Improving composite strength by chemical treatment of the fibers,” *Compos. Part A*, vol. 53, pp. 46–53, 2013.

[12] D. Garlotta, “A literature review of poly(lactic acid),” *J. Polym. Environ.*, vol. 9, no. 2, pp. 63–84, 2001.

[13] “Biopolymers present new market opportunities for Biopolymers are produced from renewable resources , such as,” *Plast. Addit. Compd.*, no. June 2008, pp. 22–25, 2011.

[14] M. Savioli Lopes, A. L. Jardini, and R. Maciel Filho, “Poly (lactic acid) production for tissue engineering applications,” *Procedia Eng.*, vol. 42, no. August, pp. 1402–1413, 2012.

[15] E. Castro-Aguirre, F. Iñiguez-Franco, H. Samsudin, X. Fang, and R. Auras, “Poly(lactic acid)—Mass production, processing, industrial applications, and end of life,” *Adv. Drug Deliv. Rev.*, vol. 107, pp. 333–366, 2016.

[16] R. Auras, B. Harte, and S. Selke, “An Overview of Polylactides as Packaging Materials,” *Macromol. Biosci.*, pp. 835–864, 2004.

[17] K. Madhavan Nampoothiri, N. R. Nair, and R. P. John, “An overview of the recent developments in polylactide (PLA) research,” *Bioresource Technology*, vol. 101, no. 22. Elsevier, pp. 8493–8501, 2010.

[18] “Polylactides - Synthesis, characterization and medical application | Request PDF.” [Online]. Available: https://www.researchgate.net/publication/229898789_Polylactides_-_Synthesis_characterization_and_medical_application. [Accessed: 17-Jun-2020].

[19] R. Datta and M. Henry, “Lactic acid: Recent advances in products, processes and technologies - A review,” *Journal of Chemical Technology and Biotechnology*, vol. 81, no. 7. John Wiley & Sons, Ltd, pp. 1119–1129, 2006.

[20] A. Albertsson and I. K. Varma, “Recent Developments in Ring Opening Polymerization of Lactones for Biomedical Applications,” pp. 1466–1486, 2003.

[21] D. L. Kaplan, “Introduction to Biopolymers from Renewable Resources,” in *Biopolymers from Renewable Resources*, Springer Berlin Heidelberg, pp. 1–29, 1998.

[22] M. Jamshidian, E. A. Tehrany, M. Imran, M. Jacquot, and S. Desobry, “Poly-Lactic Acid: Production, applications, nanocomposites, and release studies,” *Compr. Rev. Food Sci. Food Saf.*, vol. 9, no. 5, pp. 552–571, 2010.

[23] L. T. Lim, R. Auras, and M. Rubino, “Processing technologies for poly(lactic acid),” *Prog. Polym. Sci.*, vol. 33, no. 8, pp. 820–852, 2008.

[24] L. Avérous, “Polylactic acid: Synthesis, properties and applications,” *Monomers, Polym. Compos. from Renew. Resour.*, pp. 433–450, 2008.

[25] F. D. Kopinke, M. Remmler, and K. Mackenzie, “Thermal decomposition of biodegradable polyesters - I: Poly(β-hydroxybutyric acid),” *Polym. Degrad. Stab.*, vol. 52, no. 1, pp. 25–38, 1996.

[26] I. C. McNeill and H. A. Leiper, “Degradation studies of some polyesters and polycarbonates-2. Polylactide: Degradation under isothermal conditions, thermal degradation mechanism and photolysis of the polymer,” *Polym. Degrad. Stab.*, vol. 11, no. 4, pp. 309–326, 1985.

[27] H. Tsuji, Y. Echizen, and Y. Nishimura, “Photodegradation of biodegradable polyesters: A comprehensive study on poly(l-lactide) and poly(ε-caprolactone),” *Polym. Degrad. Stab.*, vol. 91, no. 5, pp. 1128–1137, 2006.

[28] A. V. Janorkar, A. T. Metters, and D. E. Hirt, “Degradation of poly(L-lactide) films under ultraviolet-induced photografting and sterilization conditions,” *J. Appl. Polym. Sci.*, vol. 106, no. 2, pp. 1042–1047, 2007.

[29] D. D. Cornell, “Biopolymers in the existing postconsumer plastics recycling stream,” *J. Polym. Environ.*, vol. 15, no. 4, pp. 295–299, 2007.

[30] “NatureWorks | Incineration.” [Online]. Available: https://www.natureworksllc.com/What-is-Ingeo/Where-it-Goes/Incineration. [Accessed: 30-Jun-2020].

[31] A.-S. C. Laußmann, U. Land, B. Münster, G.H.-J. Endres, F. Hannover, G.U. Giese and A. P. Kitzler, “Disposal of bio-polymers via energy recovery,” *Bioplastics Mag.*, pp. 42–43, 2010.

[32] M. M. Kabir, H. Wang, K. T. Lau, and F. Cardona, “Composites : Part B Chemical treatments on plant-based natural fibre reinforced polymer composites : An overview,” *Compos. Part B*, vol. 43, no. 7, pp. 2883–2892, 2012.

[33] D. K. Rajak, D. D. Pagar, R. Kumar, and C. I. Pruncu, “Recent progress of reinforcement materials: A comprehensive overview of composite materials,” *J. Mater. Res. Technol.*, vol. 8, no. 6, pp. 6354–6374, 2019.

[34] D. Dai and M. Fan, *Wood fibres as reinforcements in natural fibre composites: Structure, properties, processing and applications*. Woodhead Publishing Limited, 2013.

[35] D. K. Chattopadhyay and R. V. Kothapalli, “Structural engineering of polyurethane coatings for high performance applications,” vol. *Progress in Polymer Science*, vol. 32, no. 3, pp. 352–418, 2007.

[36] M. Murariu and P. Dubois, “PLA composites: From production to properties,” *Adv. Drug Deliv. Rev.*, vol. 107, pp. 17–46, 2016.

[37] A. M. Ali, S. H. Ahmad, and M. A. Tarawneh, “Kesan penambahan nanotiub karbon berbilang dinding ke atas kekonduksian terma polilaktik asid nanokomposit,” *Malaysian J. Anal. Sci.*, vol. 20, no. 5, pp. 1084–1089, 2016.

[38] Y. Zhou, L. Lei, B. Yang, J. Li, and J. Ren, “Preparation and characterization of polylactic acid (PLA) carbon nanotube nanocomposites,” *Polym. Test.*, vol. 68, no. January, pp. 34–38, 2018.

[39] N. Gültekin, “Preparation and Characterization of Hydroxyapatite and Polymer Composite Biomaterials,” p. 128, 2002.

[40] T. Lämsä, H. Jin, J. Mikkonen, J. Laukkarinen, J. Sand, and I. Nordback, “Biocompatibility of a New Bioabsorbable Radiopaque Stent Material (Ba SO4 Containing Poly-L,D-Lactide) in the Rat Pancreas,” *Pancreatology*, vol. 6, no. 4, pp. 301–305, 2006.

[41] V. S. Sreenivasan, D. Ravindran, V. Manikandan, and R. Narayanasamy, “Influence of fibre treatments on mechanical properties of short Sansevieria cylindrica / polyester composites,” *J. Mater.*, vol. 37, pp. 111–121, 2012.

[42] E. Zini and M. Scandola, “Green Composites : An Overview,” *Polym. Compos.*, vol. 32, pp. 1905–1915, 2011.

[43] R. Siakeng, M. Jawaid, H. Ariffin, S. M. Sapuan, M. Asim, and N. Saba, “Natural fiber reinforced polylactic acid composites: A review,” *Polym. Compos.*, vol. 40, no. 2, pp. 446–463, 2019.

[44] S. A. Hinchcliffe, K. M. Hess, and W. V. Srubar, “Experimental and theoretical investigation of prestressed natural fiber-reinforced polylactic acid (PLA) composite materials,” *Compos. Part B Eng.*, vol. 95, pp. 346–354, 2016.

[45] E. Bodros, I. Pillin, N. Montrelay, and C. Baley, “Could biopolymers reinforced by randomly scattered flax fibre be used in structural applications?,” *Compos. Sci. Technol.*, vol. 67, no. 3–4, pp. 462–470, 2007.

[46] B. H. Lee, H. S. Kim, S. Lee, H. J. Kim, and J. R. Dorgan, “Bio-composites of kenaf fibers in polylactide: Role of improved interfacial adhesion in the carding process,” *Compos. Sci. Technol.*, vol. 69, no. 15–16, pp. 2573–2579, 2009.

[47] Y. Tao, H. Wang, Z. Li, P. Li, and S. Q. Shi, “Development and application ofwood flour-filled polylactic acid composite filament for 3d printing,” *Materials (Basel).*, vol. 10, no. 4, pp. 1–6, 2017.

[48] M. Avella, M. Malinconico, A. Buzarovska, A. Grozdanov, G. Gentile, and M. E. Errico, “Natural Fiber Eco-Composites,” *Polym. Compos.*, vol. 28, pp. 98–107, 2007.

[49] Y. Xie, C. A. S. Hill, Z. Xiao, H. Militz, and C. Mai, “Author ’ s personal copy Composites : Part A Silane coupling agents used for natural fiber / polymer composites : A review,” *Composites*, vol. 41A, no. 7, pp. 806–819, 2010.

[50] S. Pilla, S. Gong, E. O’Neill, L. Yang, and R. M. Rowell, “Polylactide-recycled wood fiber composites,” *J. Appl. Polym. Sci.*, vol. 111, no. 1, pp. 37–47, 2009.

[51] K. Oksman, M. Skrifvars, and J. F. Selin, “Natural fibres as reinforcement in polylactic acid (PLA) composites,” *Compos. Sci. Technol.*, vol. 63, no. 9, pp. 1317–1324, 2003.

[52] H. Zhang, Y. Cui, and Z. Zhang, “Chemical treatment of wood fiber and its reinforced unsaturated polyester composites,” *J. Vinyl Addit. Technol.*, vol. 19, no. 1, pp. 18–24, 2013.

[53] X. Li, A. Canada, L. G. Tabil, and S. Panigrahi, “Chemical Treatments of Natural Fiber for Use in Natural Fiber-Reinforced Composites : A Review Chemical Treatments of Natural Fiber for Use in Natural Fiber-Reinforced Composites : A Review,” *Journal of Polymers and the Environment*., vol. 15, no. 1, pp. 25–33, 2007.

[54] G. G. R.N.Rao, “Combined Effect of Alkali and Silane Treatments on Tensile and Impact Properties of Roystonea Regia Natural Fiber Reinforced Epoxy Composites,” *Appl. Polym. Compos.*, vol. 1, no. 3, pp. 187–196, 2013.

[55] A. Benyahi, A. Merrouche, M. Rokbi, and Z. Kouadri, “Study the effect of alkali treatment of natural fibers on the mechanical behavior of the composite unsaturated Polyester-Alfa fibers,” *Mechanics and Industry*., vol. 15, no. 1 pp. 69–73, 2013.

[56] S. Nizamuddin, A. Jadhav, S. S. Qureshi, and H. A. Baloch, “Synthesis and characterization of polylactide / rice husk hydrochar composite,” *Sci Rep*., vo;. 9, no. 5445, pp. 1–11, 2019.

[57] D. Bachtiar, S. M. Sapuan, and M. M. Hamdan, “The effect of alkaline treatment on tensile properties of sugar palm fibre reinforced epoxy composites,” *Mater. Des.*, vol. 29, no. 7, pp. 1285–1290, 2008.

[58] V. A. Alvarez, R. A. Ruscekaite, and A. Vázquez, “Mechanical properties and water absorption behavior of composites made from a biodegradable matrix and alkaline-treated sisal fibers,” *J. Compos. Mater.*, vol. 37, no. 17, pp. 1575–1588, 2003.

[59] Y. Xie, C. A. S. Hill, Z. Xiao, H. Militz, and C. Mai, “Silane coupling agents used for natural fiber/polymer composites: A review,” *Compos. Part A Appl. Sci. Manuf.*, vol. 41, no. 7, pp. 806–819, 2010.

[60] G. Cantero, A. Arbelaiz, R. Llano-Ponte, and I. Mondragon, “Effects of fibre treatment on wettability and mechanical behaviour of flax/polypropylene composites,” *Compos. Sci. Technol.*, vol. 63, no. 9, pp. 1247–1254, 2003.

[61] E. T. N. Bisanda and M. P. Ansell, “The effect of silane treatment on the mechanical and physical properties of sisal-epoxy composites,” *Compos. Sci. Technol.*, vol. 41, no. 2, pp. 165–178, 1991.

[62] “IR Spectrum Table & Chart | Sigma-Aldrich.” [Online]. Available: https://www.sigmaaldrich.com/technical-documents/articles/biology/ir-spectrum-table.html. [Accessed: 07-Dec-2020].

[63] G. Siqueira, J. Bras, and A. Dufresne, “Cellulosic Bionanocomposites: A Review of Preparation, Properties and Applications,” no. i, pp. 728–765, 2010.

[64] Q. Yao *et al.*, “One-step solvothermal deposition of ZnO nanorod arrays on a wood surface for robust superamphiphobic performance and superior ultraviolet resistance,” *Sci. Rep.*, vol. 6, no. October, pp. 1–11, 2016.

[65] H. Wang *et al.*, “A simple, one-step hydrothermal approach to durable and robust superparamagnetic, superhydrophobic and electromagnetic wave-absorbing wood,” *Sci. Rep.*, vol. 6, no. July, pp. 2–11, 2016.

[66] R. Osugi, H. Takagi, K. Liu, and Y. Gennai, “Thermal Conductivity Behavior of Natural Fiber-Reinforced Composites,” *Asian Pacific Conf. Mater. Mech. 2009 Yokohama, Japan, Novemb. 13-16*, pp. 2–4, 2009.

[67] M. Borhani zarandi, H. Amrollahi Bioki, Z. alsadat Mirbagheri, F. Tabbakh, and G. Mirjalili, “Effect of crystallinity and irradiation on thermal properties and specific heat capacity of LDPE & LDPE/EVA,” *Appl. Radiat. Isot.*, vol. 70, no. 1, pp. 1–5, 2012.

[68] O. P. Balogun, J. A. Omotoyinbo, K. K. Alaneme, and I. O. Oladele, “The Effect Of Chemical Treatment On Tensile Properties Of Soil Retted Entada Mannii Fibres,” *American Journal of Engineering Research (AJER)*., vol. 4, no. 9, pp. 168–175, 2015.

[69] R. Guo, Z. Ren, H. Bi, M. Xu, and L. Cai, “Electrical and thermal conductivity of polylactic Acid (PLA)-based biocomposites by incorporation of nano-graphite fabricated with fused deposition modeling,” *Polymers (Basel).*, vol. 11, no. 3, 2019.

[70] T. Kemala, E. Budianto, and B. Soegiyono, “Preparation and characterization of microspheres based on blend of poly(lactic acid) and poly(ε-caprolactone) with poly(vinyl alcohol) as emulsifier,” *Arab. J. Chem.*, vol. 5, no. 1, pp. 103–108, 2012.

[71] A. N. Frone, S. Berlioz, J.-F. Chailan, D. M. Panaitescu, and D. Donescu, “Cellulose fiber-reinforced polylactic acid,” *Polym. Compos.*, vol. 32, no. 6, pp. 976–985, 2011.

[72] R. Tiskatine et al., “Thermo-physical analysis of low-cost ecological composites for building construction,” *J. Build. Eng.*, vol. 20, pp. 762–775, 2018.

[73] M. S. Barkhad, B. Abu-jdayil, A. H. I. Mourad, and M. Z. Iqbal, “Thermal Insulation and Mechanical Properties of Polylactic Acid (PLA) at Different Processing Conditions,” vol. 12, no. 9, pp. 1–16, 2020.

[74] H. Takagi, S. Kako, K. Kusano, and A. Ousaka, “Thermal conductivity of PLA-bamboo fiber composites,” *Adv. Compos. Mater. Off. J. Japan Soc. Compos. Mater.*, vol. 16, no. 4, pp. 377–384, 2007.

[75] M. S. Barkhad, B. Abu-Jdayil, M. Z. Iqbal, and A. H. I. Mourad, “Thermal insulation using biodegradable poly(lactic acid)/date pit composites,” *Constr. Build. Mater.*, vol. 261, p. 120533, 2020.

[76] W. Hittini, B. Abu-Jdayil, and A. H. Mourad, “Development of date pit–polystyrene thermoplastic heat insulator material: Mechanical properties,” *J. Thermoplast. Compos. Mater.*, pp. 1–18, 2019.

[77] “Thermal insulation materials, technical characteristics and selection criteria.” [Online]. Available: http://www.fao.org/3/y5013e/y5013e08.htm. [Accessed: 11-Oct-2020].

[78] L. Di Landro, G. Sala, and D. Olivieri, “Deformation mechanisms and energy absorption of polystyrene foams for protective helmets,” *Polym. Test.*, vol. 21, no. 2, pp. 217–228, 2002.

[79] B. Abu-Jdayil, A. H. Mourad, and A. Hussain, “Thermal and physical characteristics of polyester-scrap tire composites,” *Constr. Build. Mater.*, vol. 105, pp. 472–479, 2016.

[80] K. Al-Malah and B. Abu-Jdayil, “Clay-based heat insulator composites: Thermal and water retention properties,” *Appl. Clay Sci.*, vol. 37, no. 1–2, pp. 90–96, 2007.

[81] J. G. Gwon, S. Y. Lee, S. J. Chun, G. H. Doh, and J. H. Kim, “Effects of chemical treatments of hybrid fillers on the physical and thermal properties of wood plastic composites,” *Compos. Part A Appl. Sci. Manuf.*, vol. 41, no. 10, pp. 1491–1497, 2010.

[82] O. M. L. Asumani, R. G. Reid, and R. Paskaramoorthy, “The effects of alkali-silane treatment on the tensile and flexural properties of short fibre non-woven kenaf reinforced polypropylene composites,” *Compos. Part A Appl. Sci. Manuf.*, vol. 43, no. 9, pp. 1431–1440, 2012.

[83] I. Van de Weyenberg, J. Ivens, A. De Coster, B. Kino, E. Baetens, and I. Verpoest, “Influence of processing and chemical treatment of flax fibres on their composites,” *Compos. Sci. Technol.*, vol. 63, no. 9, pp. 1241–1246, 2003.

[84] J. H. Kim et al., “The evaluation of the interfacial and flame retardant properties of glass fiber/unsaturated polyester composites with ammonium dihydrogen phosphate,” *Compos. Part B Eng.*, vol. 167, no. December 2018, pp. 221–230, 2019.

[85] “Thermal Conductivity of some selected Materials and Gases.” [Online]. Available: https://www.engineeringtoolbox.com/thermal-conductivity-d_429.html. [Accessed: 05-May-2021].

[86] “Compression and Tension Strength of some common Materials.” [Online]. Available: https://www.engineeringtoolbox.com/compression-tension-strength-d_1352.html. [Accessed: 05-May-2021].

[87] “Concrete Properties.” [Online]. Available: https://www.engineeringtoolbox.com/concrete-properties-d_1223.html. [Accessed: 05-May-2021].

جامعة الإمارات العربية المتحدة
United Arab Emirates University
UAEU
UAEU Libraries
DigitizationDepatment
United Arab Emirates

Digitally signed by Shrieen
DN: cn=Shrieen, o=United Arab Emirates University, ou=UAEU Library Digitizatio, email=shrieen@uaeu.ac.ae, c=AE
Date: 2021.08.24 14:22:20 +04'00'